
Electronic Thesis and Dissertation Repository

11-29-2021 2:30 PM

Effects of the soil spatial variability on pipelines

Jose Luis Espinosa Mendez, *The University of Western Ontario*

Supervisor: Wenxing Zhou, *The University of Western Ontario*

A thesis submitted in partial fulfillment of the requirements for the Doctor of Philosophy degree
in Civil and Environmental Engineering

© Jose Luis Espinosa Mendez 2021

Follow this and additional works at: <https://ir.lib.uwo.ca/etd>



Part of the [Structural Engineering Commons](#)

Recommended Citation

Espinosa Mendez, Jose Luis, "Effects of the soil spatial variability on pipelines" (2021). *Electronic Thesis and Dissertation Repository*. 8348.

<https://ir.lib.uwo.ca/etd/8348>

This Dissertation/Thesis is brought to you for free and open access by Scholarship@Western. It has been accepted for inclusion in Electronic Thesis and Dissertation Repository by an authorized administrator of Scholarship@Western. For more information, please contact wlsadmin@uwo.ca.

Abstract

Pipelines are the safest and most efficient way to transport large volumes of oil and gas from extraction fields, to refineries, industry and home consumption. Extensively used to transport fluids over long distances, pipelines may pass through terrain features exposed to geohazards. The performance of buried pipelines in areas subjected to ground displacements constitute a criterion for the design, assessment and management of gas pipelines to ensure public, environment and property safety in a cost-effective manner. Modern surveying and sampling techniques allow for better geotechnical characterization of ground movements and variability of the soil properties with confidence. The statistical data enables reliable models to correlate the inspection measurements with the overall safety of the buried pipelines.

Random field theory is widely used to model the spatial variability of soil properties that affect the probability of failure of pipelines. A limit state for onshore gas pipelines laid down over hill-type features is the Upheaval Buckling (UHB). In this study, the spatial variability of the soil properties is considered in a simplified manner. First, the soil properties are modeled as an Expansion Optimal Linear Estimation (EOLE) of the random field. Further, the soil correlation structure is idealized as a multivariable cross-correlated Gaussian random field, approximated with Statistical Preconditioning. A parametric example illustrates the impact of the spatiality variability of the soil on the failure probability due to UHB and the applicability of simple empirical equations to account for the spatial variability of soil. The analysis results suggest that accounting for the soil spatial variability of the soil may lead to less conservative estimations of the failure probability due to the UHB.

A practical approach to analyze probability of failure of pipelines susceptible to landslides is also presented in the thesis. Soil displacements can impose significant loads on pipelines and may result in the failure of pipelines along unstable slopes. A simple procedure to estimate the probabilities of tensile rupture and compressive local buckling is presented. The soil is characterized as a random field. The probability of failure is obtained by numerical simulation, extending the Generalized Slice Method. A particular Critical Slip Surface is found for each random field realization.

Keywords: Critical Slip Surface, Cross-Correlation, Expansion Optimal Linear Estimation, Generalized Slice Method, Upheaval Buckling, Slope Stability, Statistical Preconditioning.

Summary for Lay Audience

Pipelines are considered the safest and most efficient way to transport large volumes of oil and gas from extraction fields to refineries, industry and home consumption. Thus, pipelines are critical infrastructure and have been used extensively. Buried gas pipelines usually transport fluid at elevated temperatures to optimize the productivity of the wells. Due to these conditions, an overall compressive force is induced along the pipes. This compression, may cause the pipeline to buckle upward or even break out of the ground if the soil cover or restraining measures are not sufficient.

Additionally, out-of-straightness imperfections or geometric features along the pipeline topography can further reduce the buckling resistance of the pipeline. Trenched or buried pipelines are designed to protect the pipe from external actions and ensure structural stability. The current state of the art allows for estimations of the critical axial buckling force considering different types of soil, pipe materials and the pipeline geometric conditions.

Different from engineering materials, natural soil deposits have mechanical properties that vary orders of magnitude more. This uncertainty has to be taken into account to assess the optimal operation of pipelines in a safe and efficient manner. The main objective of this research is to investigate the effects of the soil inherent variability on the stability of buried pipelines.

Acknowledgement

This research was carried out during the Doctoral studies of the author at the Department of Civil & Environmental Engineering, University of Western Ontario, London, Ontario.

First of all, I would express all my gratitude and appreciation to my supervisor Dr. Wenxing Zhou, for his continuous support and patient guidance throughout this study. His expertise and academic excellence always encouraged me to persevere during the fulfillment of this Thesis. It has been my honour to pursue Doctoral research under his supervision.

I greatly appreciate Dr. Hanping Hong for generously sharing his scholar advice and life philosophy.

I am thankful to my committee members, Dr. Hanping Hong, Dr. Ayman El Ansary, Dr. Jiang Liying, and Dr. Yong Li for their insight, advice and critical assessment of my dissertation.

The research in this dissertation was, in part, jointly supported by The Ontario Council on Graduate Studies of Canada (OCGS) and The National Council of Science and Technology of the United Mexican States (CONACYT)

Lastly, I would like to thank my colleagues and the people I know for accompanying me through this endeavor at the University of Western Ontario. I appreciate everyone I met here and cherish the experience with each of you.

Dedication

To my beloved parents

List of Tables

Table 2.1 Material Data and Ramberg-Osgood Parameters.	34
Table 2.2 Cases considering different mean values for the soil parameters. The imperfection Sharpness is measured as the angle θ in Fig. 2.4. For a base case comparison, the same pipe was used for all 18 cases. X65 pipe with good hardening; weight 1.741 (kN/m), $\sigma_y = 448$ MPa (60), $D/t = 60$, $D = 609.6$ mm (24 inches), and ratio between hoop stress due to internal pressure and yield strength is (0.6)	38
Table 2.3 Random Field domain discretization, for each region shown in Fig. 2.4.	44
Table 2.4 Commonly observed values of PSI for the soil cover.	46
Table 2.5 Normal to Lognormal parameters from Eq. 2.40 and Eq. 2.41	47
Table 2.6 Results of Case 3 from Table 2.2 after 1000 random field realizations	58
Table 3.1 Comparison of FE and Calculated Values for Effective Force for a pipeline that weights 1.741 (kN/m), material grade (448 MPa), D/t ratio (60), diameter (24 inches), and ratio between hoop stress and yield strength is (0.6).....	84
Table 3.2 Largest error cases in empirical Eq. 3.10 vs FE analysis.	90
Table 3.3 Comparison of Q_{eff} considering the soil spatial variability from FE models vs the empirical values.	92
Table 5.1 A simple approach to assess the probability of failure of pipeline due to land slide.	144
Table 5.2 Soil Statistical properties	154
Table 5.3 Iterative algorithm for calculating F_s and λ	163
Table 5.4 Material Data and Ramberg-Osgood Parameters. σ_{el} is the elastic limit.....	169

List of Figures

Figure 2.1 Pipe, Caped and Pinned at both ends, under Axial Load and Pressure differential. (b)	
Differential equilibrium of a pipe wall section.	24
Figure 2.2 Upheaval Buckling Phenom diagram, Pipeline breaking through the ground	27
Figure 2.3 Cold formed bends diagram. Pipeline over a Hill-Type imperfection. θ is the bending angle of the pipe joint at the top. R is radius of the pipe bend at the top of the imperfection.	31
Figure 2.4 Diagram of burried pipeline over a Hill-Crest imperfection ^[2]	32
Figure 2.5 Diagram of FE model, pipeline over a Hill-Crest imperfection	33
Figure 2.6 Axial Force-Displacement Relationship	35
Figure 2.7 Force-displacement diagram for the soil model in the vertical direction ^[14]	37
Figure 2.8 correlation functions, and Triangular bound	45
Figure 2.9 Upper and lower strain response due to upheaval buckling. After 1000 RF realizations. Considering different stochastic models of friction angle φ . Case 1 from Table 2.2. Smooth imperfection	52
Figure 2.10 Upper and lower strain response due to upheaval buckling. After 1000 RF realizations. Considering different stochastic models of friction angle φ . Case 3 from Table 2.2. Sharp imperfection	52
Figure 2.11 Mean value of Q_{eff} vs Maximum and minimum values of Q_{eff} after random field realizations. Case 1 from Table 2.2 Smooth imperfection	53
Figure 2.12 Mean value of Q_{eff} .vs Maximum and minimum values of Q_{eff} after random field realizations. Case 3 from Table 2.2 Sharp imperfection	53

Figure 2.13 Mean value of Q_{eff} vs Maximum and minimum values of Q_{eff} after random field realizations. Case 9. From Table 2.2 Strong soil condition.	55
Figure 2.14 Mean value of Q_{eff} vs Maximum and minimum values of Q_{eff} after random field realizations. Case 15. From Table 2.2 Weak soil condition.	55
Figure 2.15 Mean value of Q_{eff} vs Maximum and minimum values of Q_{eff} after random field realizations. Case 4. From Table 2.2 Smooth imperfection shape.....	56
Figure 2.16 Mean value of Q_{eff} vs Maximum and minimum values of Q_{eff} after random field realizations. Case 5. From Table 2.2 regular imperfection size.....	56
Figure 2.17 Mean value of Q_{eff} vs Maximum and minimum values of Q_{eff} after random field realizations. Case 6. From Table 2.2 Sharp imperfection size.....	57
Figure 2.18 Mean value of Q_{eff} vs Maximum and minimum values of Q_{eff} after random field realizations. Case 18. From Table 2.2 Sharp imperfection size.....	57
Figure 2.19 Q_{eff} Case 18. Maximum and minimum response after 1000 realizations with scale of fluctuation of $L_h = 10$	58
Figure 2.20 Case 18 Maximum and minimum variability while using Bessel Second kind type of correlation.	59
Figure 3.1 Most common imperfection idealization types; (a) hill imperfection, (b) partially restrained, (c) lay-down straight, (d) prop imperfection.....	72
Figure 3.2 Cold formed bends over a hill (Source: Argonne National Laboratory) ^[4]	73
Figure 3.3 critical applied axial force Q_{app} , function of the acting or effective compressive force.	76
Figure 3.4 Diagram of burried pipeline over a Hill-Crest imperfection ^[2] $L_b = 100\text{m}$, and the Total Length is 300m.	79

Figure 3.5 Effective Force Q_{eff_base} , Bend Angle. Case number for Q_{eff_base} obtained from the Empirical Eq 2.6, Q_{eff_base} obtained from FE Parametric analys.	83
Figure 3.6 The best fitting Model error B	89
Figure 3.7 Empirical model of Q_{eff} , by maximum likelihood estimator Eq. 3.10. Case 1	90
Figure 3.8 Variability comparison between, the empirical Q_{eff} vs FE Q_{eff} Case 3	91
Figure 5.1 Axial Force-Displacement Relationship f soil axial friction per unit length, δ soil displacement.....	147
Figure 5.2 Force-displacement diagram for the soil model in the vertical direction; Q_u soil bearing capacity at the bottom of trench, q_s static soil download, q_d dynamic soil download, δ_{vs} static limit displacement and δ_v fully mobilized displacement ^[11]	150
Figure 5.3 Uplift mechanisms of buried pipes in sand: (a) Problem geometry; (b) sliding block with vertical slip surfaces; (c) sliding block with inclined slip surfaces; and (d) flow around the pipe ^[26]	151
Figure 5.4 limit equilibrium methods of slices. (a) Sliding soil mass, where; A and B, are sliding soil mass boundary points, P_i is interslice force at the i th slide, n is the total number slides. (b) Typical slice forces, where; α_i is inclination angle, h_i is height, b_i is width.....	158
Figure 5.5 FE model; $\theta = 30^\circ$, bending radius is 80m, Slope is 180m long, Toe and Crown are 60m long.	166
Figure 5.6 Master node, pipeline and soil profile. Direction of imposed displacements.	168
Figure 5.7 Idealization of FE model with soil-pipe, force displacement relationships	170
Figure 5.8 Failure surface bounds from geotechnical survey $30 \leq \text{Failure length} \leq 90$	173
Figure 5.9 Failure probability for an increasing soil displacement	174

List of symbols

a	constant for correlation function.
a_n	amplitude constant.
$a(x)$	linear function
A	Fig. 5.4 Boundary for Generalized Limit Equilibrium method.
A	area
b	constant for correlation function.
$b(x)$	linear function
B	model error.
B	Fig. 5.4 Boundary for Generalized Limit Equilibrium method.
c	soil cohesion
cov[.]	covariance
cr	meaning critical, as subindex
C_s	undrained shear strength
C	Fig. 2.1 Thermally induced compression.
C_{ij}	cross-correlation
d_i	separation length
D	outer pipe diameter
e	meaning external, as subindex
E[.]	mean as expected value
E	Young's modulus of elasticity
E_i	horizontal force
f	soil axial friction force
f_c	coating dependent pipe-soil friction factor.
f_0	assumed function for Generalized Limit Equilibrium method
F_{app}	ratio between the applied force to effective force.

F_{dia}	Pipe outside diameter correction factor.
F_{Dt}	Diameter to wall thickness correction factor.
F_{hs}	hoop stress correction factor, hoop stress to internal pressure ratio.
F_{ys}	material grade correction factor.
F_s	factor of safety
$F\gamma$	soil density factor
$F_{\sigma_\phi^2}$	variance reduction factor due to friction angle.
$F_{\sigma_I^2}$	variance reduction factor due to imperfection shape.
g	gravitational acceleration constant
h	random field variable
h_i	high of a discrete slice in Fig. 5.4 for Generalized Limit Equilibrium method.
H	burial depth of the pipeline
$H(x)$	spatial random field
i	iteration constant
I	moment of inertia
j	iteration constant
J_α	Bessel function First kind
k	iteration constant
K_0	coefficient of pressure at rest
K_α	Modified Bessel function Second kind
l	separation length
$l(\theta; \xi)$	logarithm or maximum likelihood as PDF fitting criteria.
L	Fig. 2.1 pipe length.
L_b	Fig. 2.4 Length between bends
L_h	horizontal fluctuation of the soil
$\text{Log } L(.)$	log likelihood operator
$\mathbf{M}(\mathbf{h} \mathbf{v}, \alpha)$	Matérn covariance, field parameter h , given \mathbf{v}, α Bessel function parameters.

M	Fig. 2.1 bending moment.
M	Truncated modes, for spectral decomposition.
n	iteration number
n	Ramberg-Osgood exponent
N_{cv}	vertical uplift factor for clay
N_f	frequencies for spectral decomposition
N_i	normal force
N_{qv}	vertical uplift factor for sand
p	Fig. 2.1 pressure
P	operating pressure
q	iteration number
$q(x)$	distributed load function.
$q_h(x)$	transverse distributed load function.
q_d	dynamic component of the soil model.
q_s	static download of the soil model.
Q	Fig. 2.1 Shear force
Q_{eff}	maximum compressive load at the middle of the buckling pipe.
Q_{eff_base}	base case effective force
Q_{crit}	Critical Upheaval Buckling Force
Q_P	pressure induced axial load
Q_T	temperature induced axial load
Q_u	soil bearing capacity
r	Fig. 2.1 pipe radius.
R	Fig. 2.4 pipeline bending radius.
$R(.)$	auto-correlation function.
s	nodal value of a cross-correlated multivariate random field.
S_i	mobilized shear resistance

t	wall thickness.
T	operating temperature.
T	period, as in spectral decomposition.
U	elastic energy.
v	Fig. 2.1 Shear force.
$\text{var}[\cdot]$	variance
$\sigma^2(\mathbf{x})$	variance at locations
\mathbf{V}	block matrix for the co-variogram of multidimensional random field.
V	potential energy.
W_i	self-weight of a soil slice.
w_{pipe}	pipe weight per unit length
w_{tot}	total vertical resistance per unit length (soil resistance plus pipe weight).
W_p	weight of the pipe per meter of length.
$Y(\mathbf{x})$	multivariate random field
z	vertical distances Fig. 5.4 Generalized Limit Equilibrium method.
Z	covariance matrix for simple cross-correlated random fields.
α_i	slope of the failure surface
α	Ramberg-Osgood linear parameter.
α_T	coefficient of thermal expansion.
γ	bulk density of the soil.
$\bar{\gamma}$	the unit weight of soil
δ	variational operator.
δ	displacement limit.
δ_v	soil mobilization displacement for the vertical soil model.
δ_{vs}	displacement static limit for the vertical soil model.
ϵ	strain.
ϵ_x	axial pipe strain.

ε_{xx}	axial strain.
$\varepsilon_{(.)}$	model error for soil factors
θ	Fig. 2.4 Imperfection angle.
θ_i	eigenvalues
ϕ_i	eigenvectors
λ	scale factor for horizontal forces in the Generalized Limit Equilibrium method.
μ	soil-pipe axial friction coefficient.
$\mu(.)$	mean value
ν	Poisson's ratio.
$\nu(x)$	transversal displacement function.
$\tilde{\nu}(x)$	approximate transversal displacement function.
ξ	independent normal standard random variables
π	pi, as geometric constant.
ρ	correlation
σ	Engineering stress.
σ_y	yield strength.
τ	Euclidian distance between points
φ	soil friction angle.
χ	vector containing discrete random field values
ψ	orthogonal function
ω	circular frequency
Γ	Legendre Gamma function
Δ	axial displacement at the far end of the pipe model.
Δt	frequency increment
Λ	Diagonal matrix.
Σ	auto-correlation matrix

Contents

Abstract.....	i
Summary for Lay Audience.....	iii
Acknowledgement	iv
Dedication	v
List of Tables	vi
List of Figures	vii
List of symbols.....	x
1 Introduction	1
1.1 Background, Upheaval Buckling	2
1.1.1 Upheaval Buckling accidents.....	5
1.2 Background, Landslides	5
1.3 Background, Spatial Variability of Soil Geotechnical Properties.....	9
1.4 Objectives of the thesis	12
1.5 Motivation	13
1.6 Thesis outline	14
1.7 Scope of the thesis.....	16
1.8 References	18
2 Upheaval buckling of onshore pipelines considering soil spatial variability	23
2.1 Motivation	29

2.2	Methodology	31
2.2.1	Finite Element Modelling	32
2.2.2	Pipeline Material	34
2.2.3	Soil Axial Friction.....	35
2.2.4	Soil Downward Load	36
2.2.5	Soil Bearing Capacity	37
2.2.6	Applied Loads	38
2.2.7	EOLE Method	40
2.2.8	Random Field domain discretization	42
2.3	Results	48
2.3.1	Effects of spatial variability of the soil	49
2.3.2	Effects of correlation length.....	58
2.3.3	Effects of the correlation type.....	59
2.4	Conclusions	60
2.5	References	62
3	An Empirical Equation for Upheaval buckling Capacity Considering Soil Spatial Variability.	70
3.1	Motivation	73
3.2	Methodology	75
3.2.1	Finite Element Modelling	79

3.2.2	Soil Model.....	80
3.2.3	Empirical Critical Upheaval Buckling Force Function.	81
3.2.4	Variance Reduction Empirical Equations.....	86
3.3	Results	88
3.3.1	Empirical equation.....	89
3.4	Conclusions	92
3.5	References	94
4	Upheaval buckling of onshore pipelines considering spatial cross correlation of the soil properties.....	99
4.1	Motivation	103
4.2	Methodology	106
4.2.1	Tri-variate Friction Angle/Cohesion/Density spatial random field.	109
4.2.2	Simplified cross correlation model	117
4.2.3	Random Field Model Characterization.....	125
4.3	Results	128
4.4	Conclusion.....	136
4.5	References	137
5	Reliability of Pressurised Pipelines along Unstable Slopes	141
5.1	Motivation	141
5.2	Methodology	143

5.2.1	Soil domain	145
5.2.2	Random Field Realizations	157
5.2.3	Finite Element Modelling	164
5.2.4	Assessment of probability of failure	171
5.3	Numerical example	172
5.4	Conclusion.....	174
5.5	References	176
6	Conclusion	184
	Curriculum Vitae	191

1 Introduction

Pipeline networks are critical infrastructure. It is the safest and most efficient means of transport for large volumes of oil or gas, according to the Canadian Transportation Safety Board statistics. Extensively used in transmission lines, from the production wells to points of distribution and consumption, pipelines cross through diverse terrain features, in offshore and onshore environments. The design and operation of pipelines are regulated by design standards to ensure protections for the environment and public health while maintaining adequate efficiency.

The U.S. Pipeline and Hazardous Materials Safety Administration (PHMSA) and the Canadian Pipeline transportation safety investigations and reports indicate that the main risk for the pipeline integrity is third party damage due to careless ground excavations. Excluding all man-made risk sources, the corrosion and degradation of old pipelines is the main risk. Considering only natural incidents (ground movements, heavy rains, floods, and severe temperature fluctuations), ground movements are the main cause of failure, accounting for about 50% of all-natural force-related incidents and about 10% of the overall failure accidents in pipelines.

Ground movements often occur due to external actions (earthquake, subsidence, freeze and thaw processes, etc.). Whatever the cause, an unstable soil mass poses risk to pipelines because it may induce failure loads. Further, almost every pipeline that traverse areas in mountainous terrain has some vulnerability to ground instability. The uncertainty involved in the assessment of pipelines due to soil movements is usually approached in a conservative way by considering the large inherent variability of the soil properties.

A different limit state of pressurized pipelines, involving ground stability, is related to operating conditions. Efficient pipelines usually transport oil or gas at elevated temperatures and pressure. Such conditions induce axial compressive loads on the pipelines that may cause the pipelines to buckle globally. The capacity or critical buckling force of a particular pipeline depends on several key parameters that are random in nature.

1.1 Background, Upheaval Buckling

Oil or gas pipelines operate at high temperatures to reduce the pumping energy lost due to fluid viscosity, and facilitating high pressure flow. The design and operation of pipelines optimises the cost, subjected to an acceptable safety risk. Due to these operating conditions, an overall compressive force is induced along the pipes, as the soil partially constrains the axial expansion of pipelines. Excessive compression may cause the pipeline to buckle upward or even break out of the ground if the soil cover or restraining measures are not sufficient. Usually, buried pipelines under axial loading are more likely to buckle upwards because the bottom and lateral wall of the trench are more resistant against pipe movements. This instability mechanism is generally known as the upheaval buckling or overbend instability for onshore pipelines.

In addition to the compressive forces, out-of-straightness imperfections or features along the line topography can further reduce the buckling capacity of the pipeline. Upheaval buckling in itself is not an ultimate limit state but it can lead to considerable deformations, expensive remediation measures needed to avoid high cycle fatigue or leaks. The critical forces at which upheaval

buckling occurs for pipe laydown over hill-crest type imperfections along the line cannot be readily predicted using analytical methods.

Since 1980, analytical models have been developed to investigate the upheaval buckling behaviour in order to predict the pipeline integrity and reliability. Upheaval buckling according to Hobbs ^[1] and Boer et al. ^[2] imply perfectly straight pipelines laydown over rigid soil with a uniform elastic soil cover. Analogous to the vertical stability of railway tracks. Taylor et al. ^[3] and Richards ^[4] proposed models to account for initial out-of-straightness imperfections over rigid soil with a uniform elastic soil cover.

Ju et al. ^[5] developed a model that considers the pipeline as a long beam resting on a rigid foundation with an imperfection characterized by shape functions. The axial soil resistance is linear elastic. The vertical soil resistance is lumped as a constant value equal to the sum of the soil resistance and weight of the soil and contents of the pipeline. This model adopts the Ramberg-Osgood stress-strain relationship for the pipe steel. Pederson et al. ^[6] formulated a similar model to Ju et al.'s model but considered a variable distance of the liftoff point, defined as the vertical displacement of the uplifted part of the pipeline, as the the thermally induced axial load increases. This semi-analytical, linearized model accounts for the gradual upward movement of the pipe due to the pressure and temperature induced axial forces.

In general, semi-analytical models to define upheaval rely on numerical computation to satisfy compatibility of axial displacement from the equilibrium equations. Their main limitations are:

1.- They do not provide a conservative estimation of the critical load for all soil and imperfection shape cases because the soil vertical resistance will degrade considerably long before the breakthrough condition is reached.

2.- The initial uplift displacements of the pipeline are likely to artificially vary depending on the function chosen to approximate the shape of the imperfection. Although one particular function may conform well to a realistic pipeline geometry, the degree or type of function used may yield different curvature near the center of the buckling pipe, leading to different vertical displacement rates for the same increment of axial loading depending purely on the function chosen.

3.- Considering the mechanical stability of the pipe-soil system, one can see that the semi-analytical models only yield equilibrium solutions with a simple stability structure. In a more realistic model, it is possible that subsequent equilibrium solutions exist after the initial instability or bifurcation point (e.g., some pipelines may become stable again after buckling, with enough capacity to operate at even higher pressure and temperature without keep moving upwards).

In the present, an upheaval buckling model is proposed from empirical equations, derived from parametric analyses of numerical pipe-soil models ^[7]. In order to overcome the limitations of semi-analytical models and to account for more commonly design parameters found on onshore gas pipelines (i.e., hill type imperfections and cold formed bends pipe joints). This approach also allows to consider: load path dependency, non-linear soil and pipe material properties and second order effects.

1.1.1 Upheaval Buckling accidents

UHB or overbend instability reports of large diameter distribution pipelines can be found in publications as early as 1967. A 1.02 m diameter pipeline, operating at 48°C buckled. Protruding for 65m in length and 3m high out of the ground. A combination of soil cover erosion and cold winter, triggered the excessive displacement on a section of the pipeline that was laydown onshore over a natural hill in Western Siberia, Russia ^[8,9].

A notorious UHB accident was published by Nielsen et al. in 1990 ^[10]. After an offshore pipeline was brought into service in the North Sea, it suddenly buckled with a maximum vertical displacement of 1.1 m above the seabed. Given the cost associated of remedial measures and the risk involved in this particular case gather, it gathered academic interest in subsequent years. Nevertheless, more UHB cases occurred after in other pipelines around the world.

More recently, in Canada, a UHB driven failure of a pipeline at the Nexen Long Lake facility near Anzac, Alberta, happened in 2016 ^[11].

1.2 Background, Landslides

Pipelines routes often are designed through diverse geological and topographic features. Due to the environmental and public safety concerns or constraints imposed by the land use, the lines are sometimes placed in rough terrains or even over previous unforeseen unstable soil conditions. Despite extensive surveys during the planning and design of the optimal route, some unstable soil

mechanisms remain underestimated since the soil resistance can be affected by highly uncertain parameters (e.g., unusual rainfall, change in vegetation that modifies water infiltration, change of water currents, additional surcharge introduced by careless constructions processes, etc.). The soil may become unstable many years after the pipeline construction.

Landslides are rarely a sudden phenomenon. Earlier soil instability evidence can be detected during monitoring and inspection, which allows time to assess and develop maintenance strategies. Overly conservative risk estimations may lead to premature actions, generating unnecessary maintenance costs. On the other hand, relative movements between the moving soil mass and the stable part of the line can exert significant loads to the pipe joints and even failure of the pipeline. In spite of modern design practices and maintenance strategies, ground movements such as slope instability have been reported. In the US, Canada, and Europe ^[12] about 10% of all gas pipeline incidents are related to ground movements.

Forces induced by soil movements have a direct relationship with the soil-pipe mechanical interaction. However, the occurrence of the landslide is random itself and the relationship between the peak induced load and the corresponding pipe displacement as well as the determination of the corresponding structural stresses are also uncertain, as a result of the inherent variability of the soil properties. In a sense, the probability of failure due to landslides can be understood as the probability of the landslide happening multiplied by the probability of failure of the pipeline buried in a random media given the landslide event.

The stability of slopes is usually analyzed by methods of the limit equilibrium, and finite-element analyses. Force limit equilibrium is achieved between rigid body discrete partitions of the soil domain. The outcome is a ratio between the soil resistance capacity and the sum of the soil weight plus external forces. This ratio is only a factor of safety and no deformation or displacements can be predicted from it. Finite element analysis provides information about the magnitude of displacements of the soil mass but does not provide a direct measure of the stability that is equivalent to the factor of safety.

From a geotechnical perspective, the forces of each element or slice in the limit equilibrium method can be calculated from the effective stress or total stress parameters. In effective stress analyses, the shear strength of the soil is related to the effective normal stress along the potential slip surface. The water pore pressure is a parameter in the effective stress shear strength. In the total stress analyses, the shear strength of the soil depends on the total normal stress on the potential slip surface. This total shear strength is measured at undrained and representative stress conditions to obtain a direct relationship to total stresses without the need to consider the undrained excess pore pressures.

Total stress procedures for analysis of undrained conditions can provide a straightforward method to account for the uncertainty in the soil properties, rather than characterizing the stochastic properties of the undrained excess pore pressures for use in effective stress analyses of undrained conditions. Well known force equilibrium methods were the one developed by Janbu in 1968, generalized procedure of slices, Morgenstern and Price's method in 1965 and Spencer's method in 1967. The main criticism of the force equilibrium methods is that the horizontal forces between

the slices ignore elastic effects, and its distribution may be unrealistic and has some consequences for the equilibrium.

Finite-element or deformation analysis can predict stresses and movements in slopes by considering more realistic soil behaviour. The main advantages are: (1) no assumption needs to be made in advance about the shape or location of the failure surface; (2) deformation and stress results can be obtained from the elastic properties of the soil; thus, it is very useful for monitoring the progressive mechanical behaviour of the slope, and (3) it allows to consider complex soil behaviour such as compressibility and pressure dependent material relationships.

For a safe design and assessment of pipelines buried in slopes, the simplicity of the force limit equilibrium methods could be useful to investigate all the slope features along the pipeline with a high degree of uncertainty. FE methods are generally more time-consuming than slope stability analyses, and they require more detailed data. They may be valuable in planning instrumentation, to identify the location and magnitude of the most critical displacements. They also provide more complete results, useful to plan remedial actions.

When the ground movement spans a wide area, the vulnerable regions are initially identified from on a regional-level pipeline risk assessment. This is followed by detailed macro-level pipe-soil interaction analysis on pipe segments identified from the regional-level assessment ^[13]. In section level analysis, the basic pipe loading mechanisms can be modeled to assess the pipeline safety due to landslide.

In this thesis, a concise procedure to account for the inherent soil spatial variability of the soil is proposed in Chapter 5, as an alternative to assess all the slopes along the pipeline in a section level analysis. The procedure considers soil stochastic characteristics that can be quantified with modern survey equipment such as monitoring of ground movements and its variations over time, with reasonable confidence.

1.3 Background, Spatial Variability of Soil Geotechnical Properties

The inherent spatial variability of soil properties has been identified as one of the major sources of uncertainty in geotechnical properties. The uncertainty involved in natural soils may be orders of magnitude more significant than the uncertainty involved in the geotechnical models to predict soil behaviour.

Several methods to study stochastic mechanical systems have been developed since the 1960s. Buried pipelines can be idealized as very long structure (i.e., hundreds of meters to model a large pipe diameter upheaval buckling problem or landslide), surrounded by a random media and likely to resist plastic deformation before failure. These characteristics can be considered in a simple manner by adopting an adequate stochastic method.

Perturbation methods, to estimate the first two statistical moments of the response (e.g., finite element-based reliability analysis such as First Order Reliability Method (FORM), Second Order (SORM)) are inefficient if a large number of variables involved in the soil discrete locations are correlated. Stochastic finite element or series expansion methods are cumbersome to implement in

this particular type of model, because it requires manipulation of the global stiffness matrix, dealing with the plastic deformation of the pipe and soil material, and the step loading nature of the stability problem for the upheaval buckling models. Thus, the most straightforward method is a reliability method based directly on the simple Monte Carlo simulation from a set of random field realizations.

Theoretical functions are used to approximate the variability of geotechnical properties along the soil domain. Single exponential, squared exponential or other valid decrement functions are commonly fitted to capture the correlation structure of soil properties ^[13-18] as a function of the distance between measurement points.

A spatial random field is called univariate or multivariate depending on whether the parameter associated to a location point in space is a variable or a vector. The values of the parameter along all the points in the domain are random but always maintains a correlation structure, and it can be fitted to match the stochastic properties observed by measurements taken from a real random media. This mathematical representation is useful to model mechanical systems that are random in nature, like the soil layers in an earth embankment or a natural slope.

Different techniques have been proposed to estimate random field realizations. A random field can be discretized as: (1) a grid of spatial locations or points, (2) as a mesh or spatial areas, or (3) a series involving random variables operating on deterministic spatial functions ^[18]. A brief reference of discretization methods is given:

The point discretization methods include the Optimal Linear Estimation Method proposed by Der Kiureghian and Ke in 1988 ^[19], Shape Function method by Liu et al. 1986 ^[20], and Integration Point method by Matthies et al. ^[21] in 1997. The Midpoint methods have questionable accuracy according to a comparison presented by Li and Der Kiureghian ^[19]. The Optimal Linear Estimation is the most accurate among the Midpoint methods. Nonetheless, it always underestimates the variance of the original or target random field.

Average discretization methods include the Spatial Average method proposed by Vanmarke and Grigoriu in 1983 ^[22], and Weighted Integral method by Deodatis and Shinozuka in 1990 ^[23]. It has been shown that the variance of the spatial average over an element under-represents the local variance of the random field by Der Kiureghian and Ke, 1988. The spatial average method is limited to the Gaussian correlation type according to Matthies et al. 1997. The Weighted Integral method is actually mesh-dependent as pointed out by Matthies et al. in 1997.

Series expansion methods include the Karhunen-Loève expansion method in 1977 ^[24], Orthogonal series expansion method proposed by Zhang and Ellingwood in 1994 ^[25], and Expansion Optimal Linear Estimation (EOLE) method by Li and Der Kiureghian in 1993 ^[26]. The Karhunen-Loève expansion, is the most accurate method for Gaussian correlation structure in terms of variance estimation and using all the orthogonal values. The EOLE method is the second most accurate.

For the upheaval buckling problem, the EOLE method seems to be the most convenient method. Because all the orthogonal values can be used for minimum error without increasing the computational time (in comparison with each FE analysis of the Upheaval Buckling model).

Further, all the error in variance seems to be concentrated at the boundaries of the soil domain. For the Upheaval Buckling problem and the Slope Stability, the variability of the soil properties at end of the pipeline, faraway from the instable mechanism, have a negligible impact on the variability of the response. Thus, the marginal improvement on accuracy of using the Karhunen-Loève expansion is not noticed for these FE models.

1.4 Objectives of the thesis

This thesis describes research aimed at addressing the effects of soil spatial variability on the reliability assessment of pipelines. Two concerning soil mechanics are considered: Upheaval buckling and land slides through parametric numerical analysis. The objectives are categorised into four technical chapters, with the primary objectives of each outlined as follows:

Propose a simple approach to assess the UHB of pipelines laydown over hill type imperfections by considering the effects of the spatial variability of the soil properties. By analyzing the most basic case, i.e., a dry granular soil, the soil is defined as a unidimensional random field with the aim of clearly identifying the isolated effects and influence of the spatial variability of a single dominant mechanical property to assess the UHB variability.

Develop a deterministic empirical equation to predict the UHB of pipelines laydown over hill type imperfections built with cold-formed bends. The work is intended to account for the structural parameters involved in the thermal buckling mechanism and to examine the influence of soil resistance generally, as well as provide a practical expression to assess pipelines.

Quantify the influence of the cross-correlation among the soil mechanical properties to assess the UHB behavior. Present a collection of cross-correlated random field discretization methods capable of modeling particular soil conditions that do not follow a commonly used correlation structure and distributions.

Present a practical example of the use of random field discretization methods combined with the limit equilibrium methods to assess the safety of pipelines subjected to landslides by accounting for potential failure surfaces consistent with the soil random characteristics.

1.5 Motivation

Recent advances in survey technology allow for the acquisition of extensive site data in a cost-effective manner. The Airborne Light Detection and Ranging (LiDAR) can be used to track the ground movements and its variations over time, along entire sections of a pipeline with reasonable accuracy. Also, versatile sampling mobile rigs can efficiently complete geotechnical investigations, reducing the need for heavy equipment. This availability of measurements can be used to characterize stochastic mechanical models and treat the natural uncertainty involved in the assessment of pipelines in risk of ground movements more accurately.

Life time management of pipelines is needed to ensure safe and economic transportation of hydrocarbons. Accurate estimations of the probability of failure due to ground movement will allow timely and effective mitigation measures, ultimately reducing preventable accidents without increasing the maintenance and monitoring cost.

The soil spatial variability, in particular the horizontal plane of the soil properties, may be significant to the reliability assessments of pipelines. Because of the limited width and small average burial depth in comparison with the total length of a pipeline, the influence of the soil spatial variability has been found relevant in previous studies for long structures such as strip and pile foundations and retaining walls. Thus, a clear understanding of the influence the spatial variability of the soil properties has on the overall variability of the pipeline response is highly valuable to evaluate the relevance of considering more refined stochastic models.

Once the relevance of soil stochastic parameters is established, a procedure to implement stochastic models in a reliability-based design and assessment framework is relevant and useful for practical application. The main motivation of this work is to contribute to better assessing the risk of pipeline failure due to soil unstable conditions through better representation of the inherent variability of the soil properties during structural analysis. This study helps to reduce the number of accidents, improving public and environmental safety.

1.6 Thesis outline

This thesis represents an effort to further understand the effects of soil spatial variability on the reliability assessment of pipelines. The contents are organized in six chapters as follows:

Chapter 1, the Introduction, contains a brief historical review and basic definitions for each research topic, as well as the motivation and research objectives.

Chapter 2 explores the effects of the soil friction angle modeled as a univariate random field on the Upheaval Buckling variability for onshore pipelines laydown over hill-type imperfections and constructed with cold formed joints. The direct Monte Carlo simulation and the EOLE method are employed in the investigation.

Chapter 3 proposes an empirical equation to estimate the Upheaval Buckling resistance for onshore pipelines laydown over hill-type imperfections and constructed with cold formed joints. The empirical equation was fitted from a FE parametric analysis, using commonly observed values for pressurized transmission gas pipelines.

Chapter 4 contains a review of selected mathematical models that can be used to include the most specific statistical data in the assessment of pipelines against Upheaval Buckling. It also, shows the effects of considering a cross-correlated, multivariate (i.e., the friction angle, cohesion factor and density) random field by adopting a simple cross-correlated random field discretization method.

Chapter 5 presents a practical example of investigating the reliability of pressurised pipelines along unstable slopes by accounting for potential failure surfaces given the soil random characteristics. The limit equilibrium methods of slices are performed for each random field realization of the soil properties to identify particular failure surfaces. A uniform displacement is applied parallel to failure surface in a FE model. The response is compared to the capacity of the pipe section

Chapter 6: The overall conclusions are presented with significant contributions and key findings summarized.

1.7 Scope of the thesis

In Chapter 2, the pipeline is model as a Timoshenko beam, including temperature as a body load, and equivalent section forces to account for the internal pressure through the hoop stress relationship. The pipe steel material is characterized using the Ramberg-Osgood stress-strain relationship. All manufacturing residual stresses in the pipe wall are ignored. The FE analyses are carried out using commercial software ABAQUS. The soil-pipe forces are model as multi-linear springs to represent the frictional force at the pipe and the soil cover resistances, similar to ASCE (1984) and ALA (2001).

A parametric analysis was conducted to investigate the effects of the soil spatial variability on the UHB phenomena. The studied parameters are pipe diameter, steel grade, imperfection size, operating internal pressure and soil resistance.

The soil friction angle is model as univariate random field, representing the soil friction angle with a lognormal distribution. Several valid correlation structures and correlation lengths were studied. The random field discretization was performed with the EOLE series expansion method. The applicability of the conclusion obtained are valid for cases inside the parametric range.

Chapter 3 is based on the deterministic analysis performed in Chapter 1. After the parametric analysis, a result matrix is formed to fit an empirical equation to estimate the critical UHB load. The model error is calibrated using the Maximum Likelihood criteria. The scope of the parametric analysis includes 252 parametric cases.

Additionally, the Monte Carlo simulation is performed using the empirical equation in comparison with the statistics obtained in Chapter 1. The empirical equation is a function of random variables in a reliability analysis. To account for the effects of the soil spatial variability within the range of the parametric analysis, two empirical variance reduction factors for the critical UHB force distribution are proposed.

In chapter 4, a more robust approach to generate valid cross-correlated structures is presented. This approach is based on the Matérn correlation type to deal with empirical correlation structures. In this method, the discretization of the random field is possible for soil variables with modified Bessel second kind probability density functions. The random field discretization is achieved by linear coregionalization following loglikelihood approximations of the Bessel function parameters. Additionally, a basic example is presented using statistical preconditioning to characterize a simple cross-correlated tri-variate random field. This method was developed by Shinozuka in 1990 [27], and improved by Vořechovský in 2008 []. The cross-correlation structure of the field, seems to be of marginal relevance, for the cases studied assuming the soil properties to have lognormal PDF, and normal correlation, and correlation structure. But it is clear that this may be not the case for different soil stochastic properties.

In chapter 5, a simple cross-correlated tri-variate random field discretization method is incorporated in a reliability analysis involving a limit equilibrium method (generalized Morgenstern–Price). The limit equilibrium method of slices is performed for each random field realization of the soil properties to identify particular failure surfaces. A particular failure surface is found for each random field realization. This failure surface is imported on a FE model to obtain the maximum compressive and tensile strain in the pile wall and construct a cumulative distribution function. This approach may be useful as a coarse assessment of all slopes in a pipeline, due to its simplicity. Leaving more refined analysis for the most critical cases.

1.8 References

1. Hobbs, R.E., 1984. “In-service buckling of heated pipelines”. *Journal of Transportation Engineering*, 110(2), pp.175-189.
2. Boer, S., Hulsbergen, C.H., Richards, D.M., Klok, A. and Biaggi, J.P., 1986. “Buckling considerations in the design of the gravel cover for a high-temperature oil line”. In *Offshore Technology Conference*. OnePetro.
3. Taylor, N. and Gan, A.B., 1986. “Submarine pipeline buckling—imperfection studies”. *Thin-Walled Structures*, 4(4), pp.295-323.
4. Richards, D.M., 1990. “The effect of imperfection shape on upheaval buckling behaviour”. In *Advances in subsea pipeline engineering and technology* (pp. 51-66). Springer, Dordrecht.

5. Ju, G.T. and Kyriakides, S., 1988. "Thermal buckling of offshore pipelines". ASME. J. Offshore Mech. Arct. Eng. November 1988; 110(4): 355–364.
6. P.Pedersen and J.Jensen, 1988. "Upheaval creep imperfections of buried heated pipelines". Marine Structures, 1, pp 11-22.
7. Matheson, I., Zhou, W., Zhou, J. and Gailing, R., 2008, January. "An upheaval buckling limit state function for onshore natural gas pipelines". In International Pipeline Conference (Vol. 48593, pp. 781-791).
8. Luscher, U., Thomas, H.P. and Maple, J.A., 1979. "Pipe-Soil Interaction, Trans-Alaska Pipeline". In Pipelines in Adverse Environments: A State of the Art (pp. 486-502). ASCE.
9. Spiridonov, V. et al., 1967 "Stability Provisions for Gas Pipelines in the North and in Central Asia". Translated from Stroitelstvo truboprovodov, No.6, and given in A Survey of Soviet Pipeline Construction Techniques and Related Activities in Western Siberia, Williams Brothers Company, Tulsa, Oklahoma.
10. Nielsen, N.J., Lyngberg, B. and Pedersen, P.T., 1990. "Upheaval buckling failures of insulated buried pipelines: a case story". In Offshore Technology Conference. OnePetro.

11. McMurray, A. B., et al. "Annex J1: Recent pipeline accidents involving crude oil in Canada and the United States." Guidance for the Environmental Public Health Management of Crude Oil Incidents (2018): 131.
12. Wu, J., Zhou, R., Xu, S. and Wu, Z., 2017. "Probabilistic analysis of natural gas pipeline network accident based on Bayesian network". Journal of Loss Prevention in the Process Industries, 46, pp.126-136.
13. Wijewickreme, D., Honegger, D., Mitchell, A. and Fitzell, T., 2005. "Seismic vulnerability assessment and retrofit of a major natural gas pipeline system: a case history". Earthquake spectra, 21(2), pp.539-567.
14. Phoon, K.K., Kulhawy, F.H., 1999. "Characterization of geotechnical variability". Can. Geotech. J. 36 (4), 612–624.
15. Cho, S.E., 2007. "Effects of spatial variability of soil properties on slope stability". Eng. Geol. 92 (3–4), 97–109.
16. Cho, S.E., 2010. "Probabilistic assessment of slope stability that considers the spatial variability of soil properties". J. Geotech. Geoenviron. 136 (7), 975–984.
17. Cho, S.E., 2012. "Probabilistic analysis of seepage that considers the spatial variability of permeability for an embankment on soil foundation". Eng. Geol. 133–134, 30–39.

18. Vanmarcke, E.H., 2010. Random Fields: Analysis and Synthesis (revised and expanded). New ed. World Scientific Publishing Co. Pte. Ltd., Singapore.
19. Der Kiureghian, A. and Ke, J.-B., 1988, “The stochastic finite element method in structural reliability”, Prob. Eng. Mech., 3, 2, 83-91.
20. Liu, P.-L. and Der Kiureghian, A., 1986, “Multivariate distribution models with prescribed marginals and covariances”, Prob. Eng. Mech., 1, 2, 105-112.
21. Matthies, G., Brenner, C., Bucher, C., and Guedes Soares, C., 1997, “Uncertainties in probabilistic numerical analysis of structures and solids - stochastic finite elements”, Struct. Safety, 19, 3, 283-336.
22. Vanmarcke, E.-H. and Grigoriu, M., 1983, “Stochastic finite element analysis of simple beams”, J. Eng. Mech., ASCE, 109, 5, 1203-1214.
23. Deodatis, G. and Shinozuka, M., 1991, “The weighted integral method, II: response variability and reliability”, J. Eng. Mech., 117, 8, 1865-1877.
24. Loève, M., 1977, “Probability theory”, Springer Verlag, New-York, 4th ed.

25. Zhang, J. and Ellingwood, B., 1994, "Orthogonal series expansion of random fields in reliability analysis", J. Eng. Mech., ASCE, 120, 12, 2660-2677.
26. Li, C.-C. and Der Kiureghian, A., 1993, "Optimal discretization of random fields", J. Eng. Mech., 119, 6, 1136-1154.
27. Yamazaki, F. and Shinozuka, M., 1990. "Simulation of stochastic fields by statistical preconditioning". Journal of Engineering Mechanics, 116(2), pp.268-287.
28. Vořechovský, M., 2008. "Simulation of simply cross correlated random fields by series expansion methods". Structural safety, 30(4), pp.337-363.

2 Upheaval buckling of onshore pipelines considering soil spatial variability

Pipelines are considered the safest and most efficient way to transport large volumes of oil and gas from extraction fields to refineries, industry and home consumption. Thus, pipelines are critical infrastructure and have been used extensively since 1970. The high efficiency of pipelines can be explained by the low energy cost of pumping pressurized fluids with reduced viscosity at high temperatures over long distances. Maximum values of the operation pressure are about 70 MPa and the maximum operation temperature can reach over 100 °C ^[1].

The high operating pressure and temperature require adequate restraint measures along the pipelines as the weight of the pipe and the soil friction against the pipe wall are likely to be insufficient to avoid excessive movements during operation as a result of the global Euler buckling of the pipeline. A similar problem was studied as early as 1939 to investigate the lateral and vertical buckling of railway lay-down on a rigid base due to thermal expansion ^[2].

This earlier analysis assumes that a buckle has already formed, to estimate the initial conditions that yields a particular buckling displacement ^[3]. In 1984, the approach for analyzing the buckling of railroad was extended to analyze the problem of buckling pipelines in the vertical or horizontal direction ^[4] considering the qualitative effects of imperfections of a pipeline. In ^[4], an asymptotic relationship is demonstrated between the buckling length and the buckling amplitude for the stable and unstable buckled behavior of pipelines at different temperature changes ^[4].

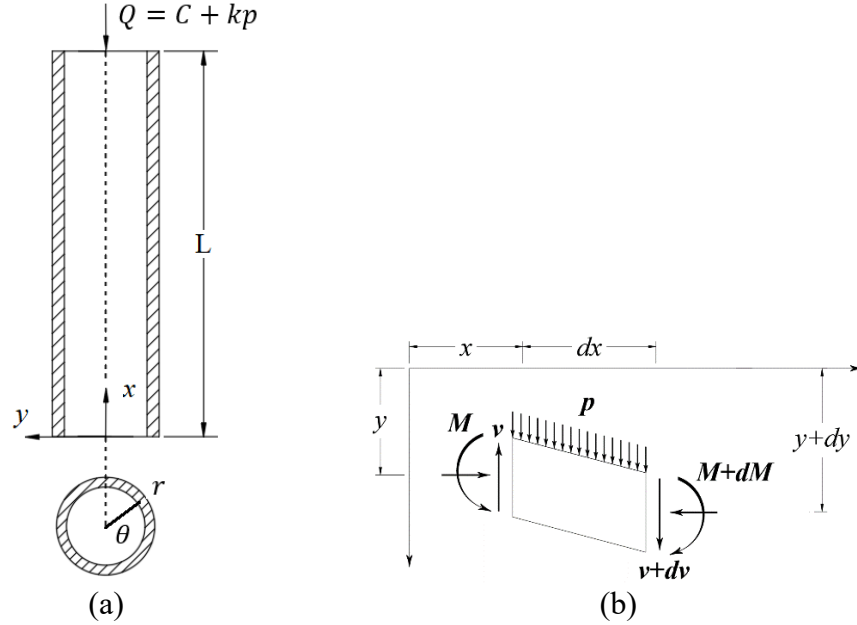


Figure 2.1 Pipe, Capped and Pinned at both ends, under Axial Load and Pressure differential.
(b) Differential equilibrium of a pipe wall section.

A perfectly straight slender pipe as shown in Fig. 2.1 is used to illustrate the fundamental actions induced on the pipe by the operating conditions. In the figure, Q denotes the total axial compressive load; C accounts for temperature induced compression along the length L , which results from the restrained thermal expansion; p is the internal pressure, and k is a constant to account for the boundary condition of the pressure (i.e., capped ends, open ends). The displacement along y axis is given by $v(x)$ and the axial strain is ^[5]

$$\varepsilon_{xx} = -v''(x)r \cos \theta \quad (2.1)$$

On a differential pipe length, the resultant pressure force due to the pipe bending $q(x)$ is normal to the bent axis direction. The force due to pipe bending is

$$q(x)dx = 2 \int_0^\pi p \cos \theta (1 + \varepsilon_{xx}) r d\theta dx \quad (2.2)$$

$$q(x) = -p\pi r^2 v''(x) \quad (2.3)$$

Where the horizontal and vertical components are:

$$q_h(x) = q(x)\cos[v'(x)] ; \quad q_v(x) = q(x)\sin[v'(x)] \quad (2.4)$$

By series expansion and simplifying the higher order terms:

$$q_h(x) = -p\pi r^2 v''(x) ; \quad q_v(x) = 0 \quad (2.5)$$

Using the Principle of Minimum Potential Energy; U is elastic energy stored in the pipe material,

V is potential of the external conservative loads:

$$\delta(U - V) - \int_0^L q_h \delta v(x) dx = 0$$

$$U = \frac{EI}{2} \int_0^L [v''(x)]^2 dx \quad (2.6)$$

$$V = \frac{Q}{2} \int_0^L [v'(x)]^2 dx$$

$$\int_0^L q_h \delta v(x) dx = \int_0^L -p\pi r^2 v''(x) \delta v(x) dx$$

$$\delta \left[\frac{EI}{2} \int_0^L [v''(x)]^2 dx - \frac{Q}{2} \int_0^L [v'(x)]^2 dx \right] + p\pi r^2 \int_0^L v''(x) \delta v(x) dx \quad (2.7)$$

where a Rayleigh-Ritz ^[6] approximate solution is given by;

$$\tilde{v}(x) = \sum_n a_n \sin \frac{n\pi x}{L} \quad (2.8)$$

$$\left[\frac{EIn^4\pi^4}{L^3} - \frac{Qn^2\pi^2}{L} - p\pi^3r^2 \frac{n^2}{L} \right] a_n = 0 \quad (2.9)$$

$$\left[\frac{EIn^4\pi^4}{L^3} - \frac{Qn^2\pi^2}{L} - p\pi^3r^2\frac{n^2}{L} \right] = 0; \text{ } n \text{ buckling mode}$$

$a_n = 0$ if the pipe is straight

The critical load is given by the possible solutions

$$Q_{cr} + p_{cr}\pi r^2 = \frac{EIn^2\pi^2}{L^2} \quad (2.10)$$

$$C_{cr} + kp_{cr} + p_{cr}\pi r = \frac{EIn^2\pi^2}{L^2}$$

$$p_{cr} = \frac{EI\pi}{L^2r^2} \quad (2.11)$$

And for the external pressure

$$Q_{cr} - p_{ecr}\pi r^2 = \frac{EIn^2\pi^2}{L^2} \quad (2.12)$$

$$C_{cr} + kp_{ecr} - p_{ecr}\pi r = \frac{EIn^2\pi^2}{L^2}$$

$$p_{ecr} = \frac{EI\pi}{L^2(r_e^2 - r^2)} \quad (2.13)$$

p_{ecr} external pressure, r_e external radius of the pipe section. Eq. 2.10 to Eq. 2.12 predict that there is a critical external pressure p_{cr} to buckle the pipe even without the temperate-induced compression, when $C_{cr} = 0$ or even with some negative $C_{cr} < 0$, i.e., tension acting on the pipe. The fundamental actions induced on the pipeline by the operating conditions can be summarized as follows:

1.-The temperature differential between the operating and tie-in temperatures will induce a compressive axial force if the pipe is restrained in the longitudinal direction by the surrounding

soils. The tie-in temperature is the temperature at which the pipeline is initially constructed and connected, typically marked lower than the operating temperature. There is a thermally induced critical load. 2.- There is a critical internal pressure that can buckle the pipe, even if there some additional axial tension acting. 3.- The external pressure has a stabilizing effect on the pipelines [5].

Approximate expressions for the critical global buckling force due to internal pressure were proposed based on experimental results in [7]. To prevent the pipelines from buckling, adequate supports must be designed to ensure the pipeline's stability including partial or complete restrains in the lateral, vertical and axial directions. If the pipelines are buried, a fully restrained condition in the axial direction can be achieved. The restrained pipelines inside trenches have competing global buckling modes in the horizontal and vertical directions, respectively. If the pipe weigh per unit length is greater than the lateral resistance of the soil, then lateral buckling may occur. Pipelines with sufficient lateral restrain can only buckle upwards, where the soil cover, the weight and the bending stiffness of the pipe are not sufficient to prevent the buckling movement. This vertical or upward buckling mode is known as the upheaval buckling (UHB) [7], or overbend instability for onshore pipelines [8]. Fig. 2.2 depicts a pipeline that has undergone upheaval buckling.

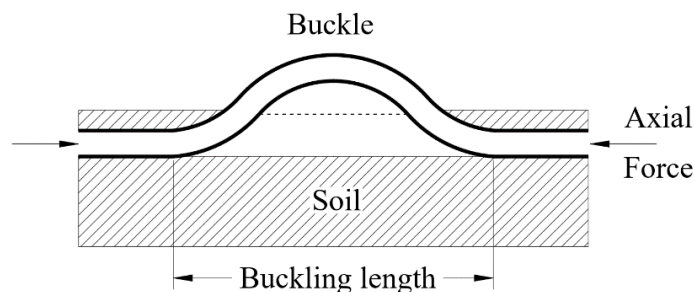


Figure 2.2 Upheaval Buckling Phenom diagram, Pipeline breaking through the ground

The UHB phenomenon is dependent on the internal pressure, difference between the operating and tie-in temperatures, soil properties, pipe burial depth, construction initial stresses, and geometry of the trench or line base. Once the global vertical buckling deformation exceeds a critical value, local buckling (i.e., wrinkling) of the pipe cross section may occur, resulting in large plastic strains, rupture or low-cycle fatigue failure due to cyclic nature of the pipe operating pressure [7].

Substantial theoretical and experimental research efforts were made to understand and model the mechanism leading to UHB [7-10] between 1990 and 2005. From 2000 to date, research has been conducted to improve earlier simple models to account for the pipe-soil interaction and the in-situ geometric conditions [11]. The resulting nonlinear boundary problems can be solved with numerical methods overcoming the simplicity of the closed form solutions. More recent studies have been focused on the improvement of the soil-pipe interaction models [11] and finite element analysis (FE) model of UHB [12].

The geotechnical research of soil-pipe models in the context of UHB is focused on identifying the parameters of the uplift resistance mechanism of soil; from its initial configuration to the break-through ground condition [11], the fully mobilized soil resistance, the post-peak softening of soil, and their dependency on the soil density and confining stress, and the evolution of the angle of the slip planes between the moving soil mass and the static soil in the trench wall [13]. The UHB has been investigated using sophisticated FE [15-17]. However, such analyses are mainly limited to research applications due to the computational demand and the extensive data required to fully

characterize the parameters involved in the analysis. Thus, it is valuable to develop simplified yet robust, practical FE models that can be used in practical engineering applications ^[12].

2.1 Motivation

Life time management of pipelines is required to ensure safe and economic transportation of hydrocarbons. The reliability-based design and assessment (RBDA) methodology is recognized as a powerful decision-making tool for maintenance and operation of pipelines. RBDA has been included in the Canadian pipeline standard, CSA Z662-19 ^[14], as a viable alternative for the design and assessment of onshore natural gas pipelines in Canada ^[14]. Accurate estimations of the probability of UHB will allow timely effective mitigation measures to be carried out to stabilize pipelines with a high probability of UHB.

Although UHB is usually not considered an ultimate limit state condition, it can lead to high strains if local buckling occurs ^[15]. It is assumed that the soil cover can only sustain a certain amount of vertical displacement before local shear failure in the soil layer occurs. The failure criterion is based on the total maximum uplift resistance

UHB is a multivariable phenomenon. A series of studies have been conducted to investigate the relevance of such parameters to the overall buckling behavior of pressurized pipelines. ^[21-31]. Most recent efforts have been made to predict the soil capacity, highlighting shortcomings of design guidelines ^[31] as well as the sources of variability and uncertainty in the pipe-soil interaction (PSI) parameters ^[22]. Because of these complex interactions, there is no single conservative value of soil

resistance to assess the competing limit state conditions of the pipeline structural system. Instead, it is necessary to determine the potential range of end expansions and the strains in the buckles by considering friction factors that have been calculated using the full range of relevant pipeline and soil input properties that may occur over the entire UHB mechanism domain. This results in low estimate (LE), best estimate (BE), and high estimate (HE) design values of each PSI parameter, which can be utilized to develop statistical distributions ^[30].

The relevance of the inherent variability involved in the geotechnical PSI parameters is recognized from previous studies ^[29]. Probabilistic and numerical analysis are useful to examine the performance of pipelines under UHB ^[21] However, previous studies are limited by treating the overall uncertainty of each PSI parameter as a single random variable ^[24]. Thus, ignoring the effects of spatial variability of the soil on the overall UHB phenomena.

The soil spatial variability, in particular the horizontal inherent fluctuation of the soil properties ^[33] may be significant to the reliability assessments of pipelines. Because of the limited width and small average burial depth in comparison with the total length of a pipeline, the influence of the soil spatial variability has been found relevant in previous studies for long structures such as strip and pile foundations ^[19-21] and retaining walls ^[22]. Thus, the main objective of the present work is to investigate the influence of the spatial variability of the soil mechanical properties on the UHB behavior, and the relevance of specific stochastic characteristics of the soil properties including the correlation length and correlation structure.

2.2 Methodology

A parametric nonlinear FEA is carried out to investigate the effect of the soil spatial variability on UHB. The analysis cases considered in the present study are similar to those considered in [20]. In this study a pipeline is assumed to be laid over a hill-crest imperfection as illustrated in Fig. 2.3 subjected to a constant internal pressure and increasing thermal loading until UHB occurs. The critical UHB force at the onset of upheaval buckling is defined as the maximum compressive force reached at the crown of the buckling pipe as the thermal load increases. The friction angle φ of the soil is characterized from a lognormal distribution. The expansion optimal linear estimation (EOLE) method proposed in [28] is adopted to represent the random field. For comparison, the friction angle is also assumed to be represented by a single random variable (i.e., a random field with an infinitely long correlation length), and a random field with independent, identically distributed (iid) random variables at every node (i.e., a random field with a zero-correlation length). For the random model of the soil property, selected analysis cases are used to investigate the effects of the correlation length, commonly used correlation structures and the inherent variability of common geotechnical properties [18] on the analysis results.

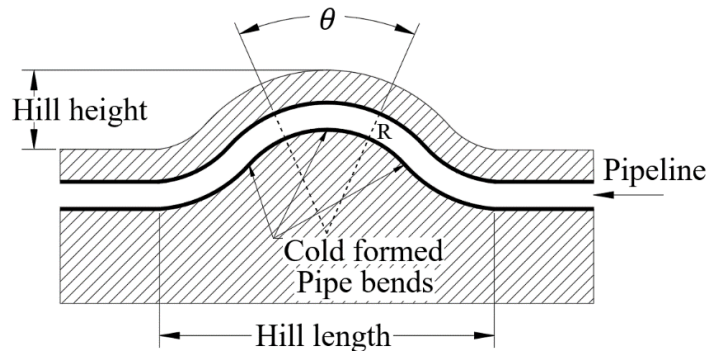


Figure 2.3 Cold formed bends diagram. Pipeline over a Hill-Type imperfection. θ is the bending angle of the pipe joint at the top. R is radius of the pipe bend at the top of the imperfection.

2.2.1 Finite Element Modelling

The commercial software ABAQUS is employed to carry out the parametric analysis. The pipeline is depicted in Figure 1.4, with symmetric geometry. However, the symmetry in geometry is not being utilized in FEA because of the random field-based characterization of the soil property.

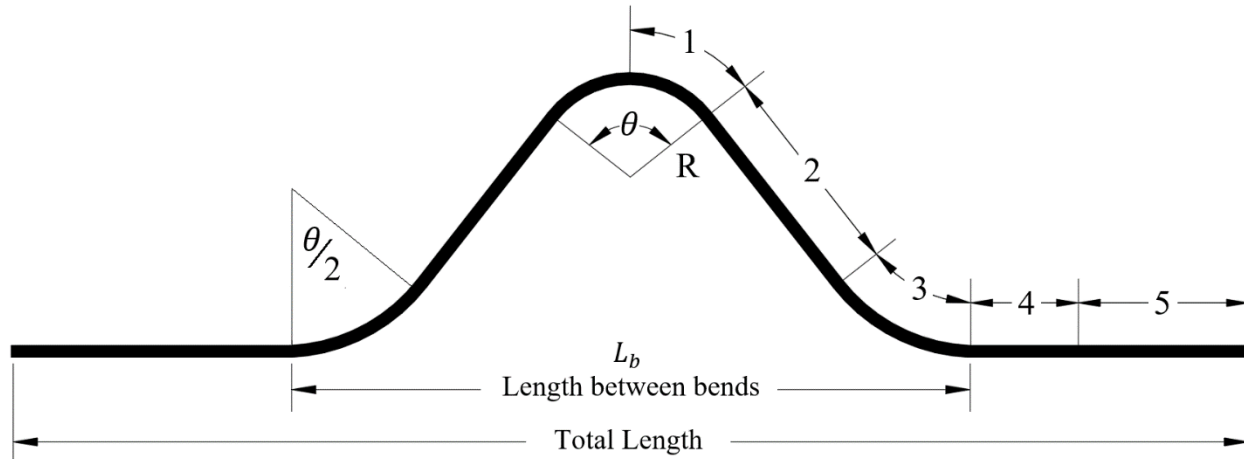


Figure 2.4 Diagram of buried pipeline over a Hill-Crest imperfection ^[2]

The pipeline is modeled using the ABAQUS elastic-plastic pipe elements PIPE31 as Timoshenko beams. The total length of the pipeline is about 300 m, depending on the parametric case. The element length in zone 1 is 0.1 m within 20 m of the hill crest and zone 3 within the lower bend. The elements length in zone 2 is increased to 0.25 m between these two zones and for 20 m beyond the bottom bend in zone 4. The remaining 80 m of pipeline is modeled with elements of 2.0 m length in zone 5. For simplicity, the residual stresses at the cold-formed bends are ignored. The pipe-soil interaction (PSI elements) is represented by force-displacement relationship acting on PIPE31 elements, as overbend soil resistance in the vertical direction and soil friction in the horizontal direction. The model incorporates one spring at each far end of pipeline to allow for the feed-in to the buckling. This was done to model the axial stiffness of the pipeline restrained by

the soil at the far end condition. The spring is characterized from the contribution of the soil at each random realization in the parametric analysis following the original formulation^[20] Consider Q as the total axial force due to internal pressure and temperature. At some point, far away from the hill imperfection, there is an axial force Q_0 that is fully constrained by the soil friction per unit length f given displacement x :

$$Q = Q_0 - f \cdot x \quad (2.14)$$

the axial stain in the pipe is

$$\varepsilon_x = \frac{Q_0 - Q}{EA} = \frac{f \cdot x}{EA} \quad (2.15)$$

A force-displacement is given by Eq.2.16, at the end of the feed-in, as function of Q as the total axial force due to internal pressure and temperature, where E denotes, Young's modulus of the pipe steel; A denotes the pipe cross-sectional area; f denotes the soil friction per unit length; Δ is the axial displacement at the end of the feed-in, and L_s is between the end of the model and where the virtual anchor would occur:

$$\Delta = \frac{(Q_0 - Q)^2}{2EA \cdot f} \quad (2.16)$$

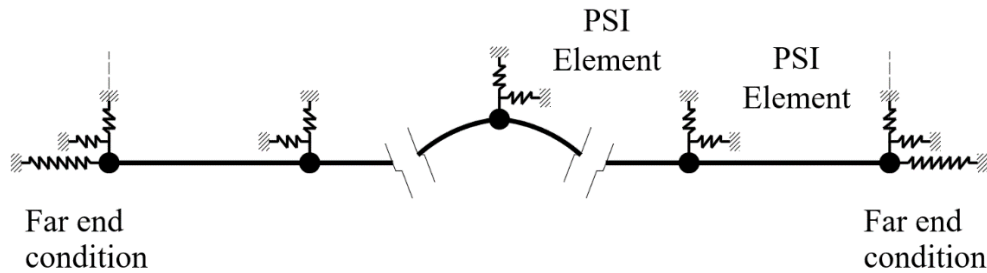


Figure 2.5 Diagram of FE model, pipeline over a Hill-Crest imperfection

2.2.2 Pipeline Material

Three steel grades were considered, X52, X65 and X80, to quantify the effects of the yield strength. The Ramberg-Osgood stress-strain relationship, Eq. 2.17, is assumed to model the elastic and plastic responses. The yield strength is assumed to equal the specified minimum yield strength (SMYS) of the steel grade, i.e., 359, 448 and 550 MPa for X52, X65 and X80, respectively. The hardening was characterized by modifying the plastic curve of the X65 steel. As show on Table 2.1, the value of the strain hardening exponent, n , is assigned to be consistent with the general strain hardening characteristics of different steel grades. For X65 steel, two values of n are considered, $n = 22.5$ and 45, representing strong and weak hardening, respectively.

$$\varepsilon = \frac{\sigma}{E} + \frac{\alpha \sigma_y}{E} \left(\frac{\sigma}{\sigma_y} \right)^n \quad (2.17)$$

where: ε strain
 σ stress
 E elastic modulus = 205,000 MPa
 σ_y yield strength
 α, n Ramberg-Osgood parameters

Grade	Hardening	σ_y (MPa)	σ_{el} (MPa)	E (MPa)	Ramberg-Osgood parameters	
					α	n
X80	Good	551	468.4	205,000	1.13	27.1
X65	Good	448	380.8	205,000	1.29	22.5
X65	Low	448	380.8	205,000	1.29	45.0
X52	Good	358	304.3	205,000	1.86	15.4

Table 2.1 Material Data and Ramberg-Osgood Parameters.

2.2.3 Soil Axial Friction

The axial soil resistance was modeled as a bilinear force-displacement relationship (Fig. 2.6), where the mobilization displacement was assumed as 0.0015m ^[17,26] and the fully mobilized friction force is given as:

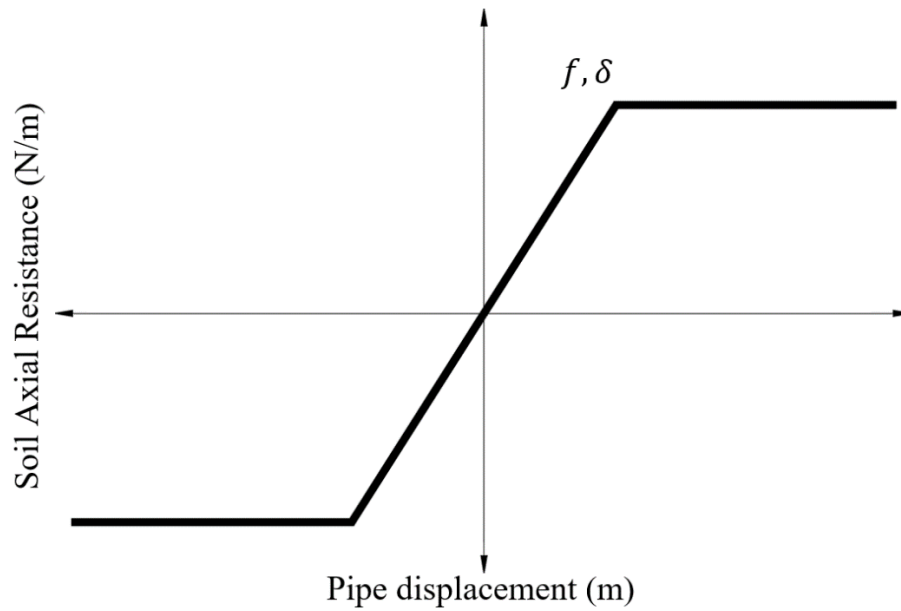


Figure 2.6 Axial Force-Displacement Relationship

$$f = \mu \left[\left(\frac{\pi}{2} \gamma g \left(H + \frac{D}{2} \right) D (1 + (1 - \sin \varphi)) \right) + W_p - \gamma g \frac{\pi}{4} D^2 \right] \quad (2.18)$$

- Where:
- D outer diameter of the pipe (m)
 - g gravitational constant = 9.81 m/s²
 - H burial depth of the pipeline, assumed to equal 0.7 m
 - W_p weight of the pipe per meter of length (kN/m)
 - φ soil friction angle (degree)
 - μ soil-pipe axial friction coefficient, assumed to equal 0.5
 - γ bulk density of the soil (kN/m³)
 - δ displacement limit

2.2.4 Soil Downward Load

The soil download is modeled with the same parameters as in Matheson et al ^[20]. The force-displacement relationship of the soil download (Fig. 2.7) includes a linear static component (or the weight of the soil above the pipe), a linear dynamic component according to the pipe-soil response models from the Oil and Gas Pipeline System (CSA-2019) ^[14] and a linear decrement to account for the breakthrough condition that happens once the displacement is equal to the burial depth. The static download, q_s , is the weight of the soil above the pipe as:

$$q_s = \gamma H D \quad (2.19)$$

The dynamic component q_d according to ALA ^[6] is given by:

$$q_d = N_{cv} c D + N_{qv} \gamma H D \quad (2.20)$$

Where:

- N_{cv} vertical uplift factor for clay (0 for $c = 0$)
- c backfill soil cohesion (Pa)
- N_{qv} vertical uplift factor for sand (0 for $\phi = 0^\circ$)
- ϕ backfill friction angle (degree)
- $N_{cv} = 2 \frac{H}{D} \leq 10$, applicable for $\frac{H}{D} \leq 10$
- $N_{qv} = \frac{\phi H}{44D} \leq N_q$ where $N_q = \exp(\pi \tan \phi) \tan^2 \left(45 + \frac{\phi}{2} \right)$
- δ_{vs} displacement static limit = 1.5 mm

Two soil mobilization displacements were considered: $\delta_v = 10\text{mm}$ and $\delta_v = 40\text{mm}$. N_{cv} , N_{qv} and N_q are dimensionless fitting parameters in Eq. 2.20 ^[32].

2.2.5 Soil Bearing Capacity

The maximum resistance of the soil was calculated by determining bearing capacity factors, N_c and N_q , according to the formulae of Prandtl-Reissner ^[27]. The limit displacement is taken as upper bound, being 10% of the pipe diameter. Illustrated in Fig. 2.3.

$$Q_u = C_s N_c D \quad (2.21)$$

Where: C_s undrained shear strength
 N_c $(N_q)/\tan\phi$
 N_q $e^{\pi \tan\phi} \tan^2 \left(45 + \frac{\phi}{2} \right)$
 ϕ soil friction angle (degree)

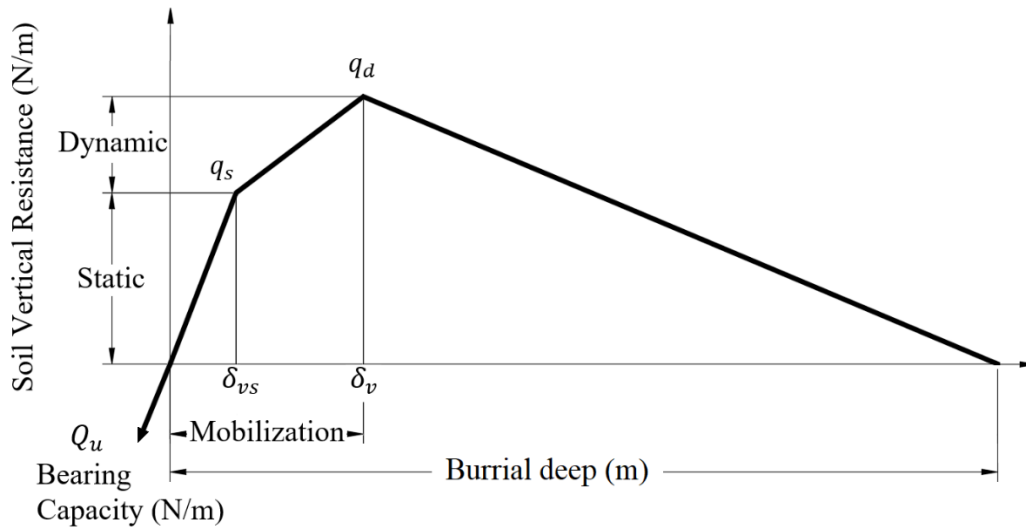


Figure 2.7 Force-displacement diagram for the soil model in the vertical direction ^[14]

Case number	Imperfection Sharpness (degrees)	q_s (kN/m)	q_d (kN/m)	w_{tot} (kN/m)
1	38.2	7.32	6	15.06
2	19.1	7.32	6	15.06
3	9.6	7.32	6	15.06
4	38.2	7.32	2	11.06
5	19.1	7.32	2	11.06
6	9.6	7.32	2	11.06
7	38.2	7.32	9	18.06
8	19.1	7.32	9	18.06
9	9.6	7.32	9	18.06
10	38.2	3.05	6	10.79
11	19.1	3.05	6	10.79
12	9.6	3.05	6	10.79
13	38.2	3.05	2	6.79
14	19.1	3.05	2	6.79
15	9.6	3.05	2	6.79
16	38.2	3.05	9	13.79
17	19.1	3.05	9	13.79
18	9.6	3.05	9	13.79

Table 2.2 Cases considering different mean values for the soil parameters. The imperfection Sharpness is measured as the angle θ in Fig. 2.4. For a base case comparison, the same pipe was used for all 18 cases. X65 pipe with good hardening; weight 1.741 (kN/m), $\sigma_y = 448$ MPa (60), $D/t=60$, $D = 609.6$ mm (24 inches), and ratio between hoop stress due to internal pressure and yield strength is (0.6)

2.2.6 Applied Loads

The UHB is a load-path dependent problem. The pipeline can only deform vertically, once the combined pressure and temperature effects overcome the pipe self-weight. Additionally, the pressure and temperature are likely to occur at slightly different time. When the internal fluid reaches a pressure peak, the induced hoop stress is almost instantaneous. Whereas, if the fluid

temperature increases, the heat still has to be conducted through the thickness of the pipe wall. Also, the operating internal temperature and pressure are more or less stable but the external temperature may change leading to a greater temperature differential, acting as last effect. Furthermore, as a stability problem, if the loading path is not realistic, previous loading can precondition the model into a non-linear configuration, yielding unrealistic results. A high pressure, low internal temperature condition is not realistic for oil and gas pipelines.

The external loads on the pipeline are applied in three step load cases: Step 1, the self-weight of pipe is applied. Step 2, the internal pressure is applied as a distributed load along the pipeline according to Eq. 2.22. The corresponding equilibrium load at the far end, is applied as the same rate, as a fully constrained condition (axial loading applied at both ends of the pipeline). Step 3, the thermal expansion is applied incrementally as a body force on the pipe elements. A constrained thermal axial load is applied at the far ends, at the same rate as the thermal expansion from Eq. 2.23. The increments are 0.5°C up to the final load, corresponding to a differential of 100 °C.

$$Q_P = \left(1 - \frac{2\nu(D - t)}{(D - 2t)}\right) \frac{\pi(D - 2t)^2}{4} P \quad (2.22)$$

$$Q_T = E\alpha_T(T_2 - T_1)\pi(D - t)t \quad (2.23)$$

where: Q_P pressure induced force (positive for compression), Q_T temperature induced force (positive for compression), E Young's modulus, α_T thermal expansion coefficient for steel (11.7×10^{-6} °C), T_2 operating temperature, T_1 tie-in temperature, t wall thickness, ν Poisson's ratio and P operating pressure.

2.2.7 EOLE Method

Although different methods have been proposed to discretize random fields such as the K-L expansion and polynomial chaos expansion, the EOLE method ^[35] is advantageous for large random fields due to its computational efficiency. It was developed for efficient FE analysis involving random media properties. A brief description of the EOLE method is presented below.

A random field $\mathbf{H}(\mathbf{x})$ can be approximated as $\hat{\mathbf{H}}(\mathbf{x})$ from a linear function of target nodal values

$\boldsymbol{\chi} = \{\mathbf{H}(x_1), \dots, \mathbf{H}(x_q)\}^T$, where \mathbf{x} represents a vector of spatial coordinate:

$$\hat{\mathbf{H}}(\mathbf{x}) = a(\mathbf{x}) + \sum_{i=1}^q b_i(\mathbf{x})\chi_i = a(\mathbf{x}) + \mathbf{b}^T(\mathbf{x}) \cdot \boldsymbol{\chi} \quad (2.24)$$

where: $a(\mathbf{x}), b_i(\mathbf{x})$ linear functions, to be optimized

q number of nodal points involved in the approximation

The optimization of $a(\mathbf{x}), b_i(\mathbf{x})$ is obtained by minimizing the difference or error in variance for all points in the domain, $\text{var}[\mathbf{H}(\mathbf{x}) - \hat{\mathbf{H}}(\mathbf{x})]$. This optimization is constrained or subjected to zero difference in the mean value of the field properties, $\mathbb{E}[\mathbf{H}(\mathbf{x}) - \hat{\mathbf{H}}(\mathbf{x})] = 0$.

$$\forall \mathbf{x} \in \Omega, \quad \arg \min \text{var}[\mathbf{H}(\mathbf{x}) - \hat{\mathbf{H}}(\mathbf{x})] \quad \text{subject to} \quad \mathbb{E}[\mathbf{H}(\mathbf{x}) - \hat{\mathbf{H}}(\mathbf{x})] = 0$$

The variance error is:

$$\begin{aligned} \text{var}[\mathbf{H}(\mathbf{x}) - \hat{\mathbf{H}}(\mathbf{x})] &= \mathbb{E} \left[\left(\mathbf{H}(\mathbf{x}) - \hat{\mathbf{H}}(\mathbf{x}) \right)^2 \right] = \\ &= \sigma^2(\mathbf{x}) - 2 \sum_{i=1}^q b_i(\mathbf{x}) \text{cov}[\mathbf{H}(\mathbf{x}), \chi_i] + \sum_{j=1}^q \sum_{i=1}^q b_i(\mathbf{x}) \cdot b_j(\mathbf{x}) \cdot \text{cov}[\chi_i, \chi_j] \end{aligned} \quad (2.25)$$

The minimization requires a discrete partial differential with respect to $b_j(\mathbf{x})$ of the variance error and solved when equal to zero.

$$\forall_i = 1, \dots, q \quad -\text{Cov}[\mathbf{H}(\mathbf{x}), \chi_i] + \sum_{j=1}^q b_j(\mathbf{x}) \text{Cov}[\chi_i, \chi_j] = 0 \quad (2.26)$$

Let $\mathbf{\Sigma}$, denote a covariance matrix, and Eq. 2.26 can be written as:

$$-\mathbf{\Sigma}_{\mathbf{H}(\mathbf{x})\chi} + \mathbf{\Sigma}_{\chi\chi} \cdot \mathbf{b}(\mathbf{x}) = 0 \quad (2.27)$$

Let μ denote the mean value at each nodal point. Then, the optimal linear estimator ^[8] is:

$$\hat{\mathbf{H}}(\mathbf{x}) = \mu(\mathbf{x}) + \mathbf{\Sigma}_{\mathbf{H}(\mathbf{x})\chi} + \mathbf{\Sigma}_{\chi\chi}^{-1} \cdot (\chi - \mu_\chi) \quad (2.28)$$

$$\hat{\mathbf{H}}(\mathbf{x}) = [\mu(\mathbf{x}) + \mathbf{\Sigma}_{\mathbf{H}(\mathbf{x})\chi}^T + \mathbf{\Sigma}_{\chi\chi}^{-1} \cdot \mu_\chi] + \sum_{i=1}^q \chi_i (\mathbf{\Sigma}_{\chi\chi}^{-1} \cdot \mathbf{\Sigma}_{\mathbf{H}(\mathbf{x})\chi})_i \quad (2.29)$$

Note that $\mathbf{\Sigma}_{\mathbf{H}(\mathbf{x})\chi}$ is a q -dimensional vector containing the covariances of $\mathbf{H}(\mathbf{x})$ with the elements of χ , $a(\mathbf{x})$, and $b_i(\mathbf{x})$ solved as:

$$a(\mathbf{x}) = \mu(\mathbf{x}) - \mathbf{b}^T(\mathbf{x})\mu \quad (2.30)$$

$$\mathbf{b}(\mathbf{x}) = \mathbf{\Sigma}_{\chi\chi}^{-1} \mathbf{\Sigma}_{\mathbf{H}(\mathbf{x})\chi} \quad (2.31)$$

$$\chi = \mu_\chi + \sum_{i=1}^q \xi_i \sqrt{\theta_i} \phi_i \quad (2.32)$$

where: ξ_i independent normal standard random variables
 θ_i, ϕ_i eigenvalues and eigenvectors of $\mathbf{\Sigma}_{\chi\chi} \phi_i = \theta_i \phi_i$ from its orthogonal decomposition

An appealing characteristic for using this method arises from its formulation^[8]. The error is simply the difference between the variances of $\mathbf{H}(\mathbf{x})$ and $\hat{\mathbf{H}}(\mathbf{x})$. Since the error variance is always positive, it follows that $\hat{\mathbf{H}}(\mathbf{x})$ always will be a numerical underestimation of the variance of the objective random field $\mathbf{H}(\mathbf{x})$.

2.2.8 Random Field domain discretization

An adequate resolution for the domain discretization is important to develop accurate numerical models. The elements sizes are established to represent deterministic and stochastic mechanical properties in an efficient manner. The upheaval buckling mechanism was modeled as a continuous beam uniformly confined by the soil, along an idealized pipeline profile. The geometric conditions, and the soil and pipe properties are the main variables of interest in the UHB analysis. Thus, a fine discretization or mesh size is chosen to model the cold-formed bends in the crown of imperfection and two shoulders. In general, a fine mesh size was chosen around the region of hill-type imperfection and coarser mesh sizes farther way from the buckling length (Fig. 2.3). A total of five resolutions were selected for each symmetric part of the UHB model. These regions are uniform for the soil and pipe elements.

The geometry of the pipeline is fully defined by assuming the bending angle of the lower parts as $\theta/2$ and a constant distance of $L_b = 50$ m, between lower bends (Fig. 2.4). Deterministic FE analyses indicate that the critical UHB forces are not sensitive to the horizontal distance between the lower bends. As the L_b varies from 40m to 150m with all the other parameters being the same, the critical UHB force varies by less than 4%, corresponding to less than 1°C in terms of the

temperature differential. Therefore, the distance between the lower bends is fixed at 50 m for the parametric analysis. The points of interest in the stochastic domain are discrete locations in the FE model deterministic model. However, the size and resolution of the random field discretization depends on the inherent variability of the soil. The scale of fluctuation is a very useful parameter to characterize the spatial variability and adequate discretize the random field. Statistical information about common soil common soil properties ^[7] is available from previous studies, including the scale of fluctuation. Most of the geotechnical data in the literature is sufficient to characterize general soil properties.

Assuming the soil property to be a homogenous Gaussian random field appears to be reasonable to investigate the general effects of the soil spatial variability on UHB. Scale of fluctuation of a random field ^[35], L_h , is a characterizing parameter for the correlation between points inside the domain (i.e., if the separation is less than L_h , then properties at those points are correlated; otherwise, the correlation is negligible). Given the correlation function $\rho(l)$, where l is the separation length, one can establish [29]:

$$L_h = 2 \int_0^{\infty} \rho(l) dl \quad (2.33)$$

Depending on the soil parameter's scale of fluctuation, the optimal scheme of a random field discretization can be obtained. In this study, an element size was chosen according to Table 2.3. This is many times the recommended threshold to warranty convergence in variance. The average scale of fluctuation is about 50 m for the soil properties in this study. One order of magnitude less than the scale of fluctuation seems to be a conventional approach to select an appropriated size for the random field mesh ^[34].

Region	Length of region	Mesh resolution
1	20m	0.1m
2	Variable	0.25m
3	Variable	0.1m
4	20m	0.25m
5	80m	2m

Table 2.3 Random Field domain discretization, for each region shown in Fig. 2.4.

However, to ensure a good characterization of soil variability for all the parameters and the FE mesh, the random field discretization of Table 2.3 was chosen instead. There are gaps between the resolution of the properties in the EF model mesh and the random field discretization. This was sorted out by means of EOLE method to simulate random fields. The former criterion, was used for all parametric cases for consistency and it was verified for 1000 Monte Carlo simulations for each case. The effects of using five different correlation structures were studied. For a lower bound, a type V Triangular expression was use. The upper bound was set as a type IV Bessel, second kind, correlation, as show in Fig 2.8.

$$\rho_I(x_i, x_j) = \exp(-a \cdot \tau) \quad (2.34)$$

Where:

τ Euclidian distance between points

a π / L_h

$$\rho_{II}(x_i, x_j) = \exp(-a \cdot \tau) \cdot \cos(b \cdot \tau) \quad (2.35)$$

b $1 / L_h$

$$\rho_{III}(x_i, x_j) = \exp(-a \cdot \tau) \cdot J_\alpha(b \cdot \tau) \quad (2.36)$$

J_α Bessel function First kind

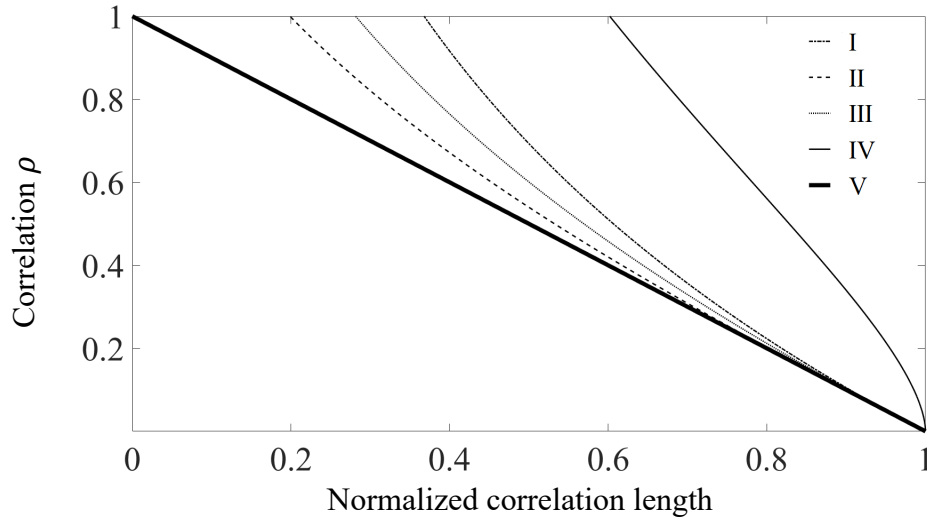
$$\rho_{IV}(x_i, x_j) = \frac{(-c \cdot \tau)^d \cdot K_{L_h}(c \cdot \tau)}{(5^{d-1} \Gamma(L_h))} \quad (2.37)$$

c 1

K_α Modified Bessel function Second kind

Γ Legendre Gamma function

$$\rho_V(x_i, x_j) = 1 - \frac{\tau}{L_h} \quad (2.38)$$



Normalized correlation types: I Exponential, II, Cos-Exponential, III Bessel, First kind order 0, IV Modified Bessel Second kind and V Triangular.

Figure 2.8 correlation functions, and Triangular bound

A literature review concerning the scale of fluctuation was used to establish the inherent variability of the soil geotechnical properties along natural deposits. The amount of information in the literature related to the soil spatial variability is adequate to establish base case scenarios in a realistic manner. For the horizontal fluctuation of the soil, the most common values of L_h [37-40] are between 40 and 60 m [38]. Three values of L_h are considered in the present study: 10, 50 and 90 m, where 50 m is the base case with the other two values being the sensitivity cases. The effect of the vertical scale of fluctuation on UHB is ignored in the present study due to the fact that most pipelines are buried at the same depth on average.

Negligible effects were observed by changing the correction functions for $L_h = 90$. The effects of correlation structure functions ρ were studied by a comparison of the maximum and minimum values of the critical buckling force. The relevance of the correction function on the upheaval

buckling problem, becomes more relevant for smaller values of L_h . Being less than 10% between the lower and upper bounds for $L_h = 10$, after 1000 simulations of the cases detailed on Table 2.2. Only an exponential auto-correlation structure was considered in subsequent analysis.

In order to match realistic force-displacement PSI relationships used in the analysis, as shown in Table 2.3, the mean values of geotechnical properties: the soil density γ and the cohesion of the soil c were adjusted accordingly to match experimental values of q_s and q_d [45]. The parameter q_d , depends on the friction angle, so as the angle is simulated randomly in the analysis, the value of q_d will also vary randomly. In a simplified manner, the soil $c = 75\text{kPa}$ was kept constant to study the effect of the soil friction angle φ variability alone. whereas, γ was made linearly dependent on φ according to Eq. 2.39 [38-45].

Property	
Static soil q_s	5kN/m ² , 12kN/m ²
Dynamic soil q_d	2kN/m, 6kN/m, 9kN/m
Mobilization displacement δ_v	10mm, 40mm

Table 2.4 Commonly observed values of PSI for the soil cover.

The soil friction angle is assumed to be represented by a homogeneous random field, having lognormal distribution with a mean value of 30° , a coefficient of variation (COV) of 30% [38] and a scale of fluctuation of 50 m [38]. The lognormal values can be easily mapped to Gaussian space, by means of Eq. 2.40 to Eq. 2.42. The relationship between the means, COVs and correlation coefficients associated with these two random values are summarized in Table 2.5.

Property	Lognormal-value	Lognormal
$\mu(\varphi)$	3.358	30
cov	0.0874	0.3
L_h	50	50

Table 2.5 Normal to Lognormal parameters from Eq. 2.40 and Eq. 2.41

A density factor $F\gamma$ was introduced to account for the relationship between φ and the characteristic void ratio of the backfill material ^[42]. The current soil model, is a homogenous random field with simple mechanical properties, derived from Mohr's Circle failure criterion. Thus, the soil mechanical properties are fully defined by c, γ, φ , the pipeline geometry and the pipe-soil friction coefficient μ from Eq. 2.18. As such, this soil model is only applicable for deposits with similar mineralogical composition in which variations on void ratio have a considerable effect on the soil friction angle ^[42-44]. Further, by considering γ dependent on φ , the variability of q_s and q_d increases, yielding conservative results. Realistic values for γ can be close to 0 in swamp areas or as high as 20kN/m³ for soils with high content of gravel or rocks. In this study, a linear expression for γ is adopted to match the values of q_s detailed on Table 2.4. as function of φ .

This means, a 10% density variation for 10 degrees of φ . Eq. 2.39 is applied at each random field location of φ . The factor $F\gamma$ is applied to γ , in the PSI Eq. 2.40, 2.41 and 2.42. If the friction angle is $\mu(\varphi) = 30^\circ$, a density $\gamma = 17.15 \text{ kN/m}^3$, corresponds to a realistic value of $q_s = 7.32 \text{ kN/m}$, with a factor $F\gamma = 1$ for a 24" outside diameter pipe as show in Table 2.2. The assumption being; c , the pipeline geometry and μ are to remain constant along the domain for each random field realization. γ is fully correlated to φ . The effects of the correlation structure of φ can be observed in a conservative approximation.

$$F\gamma = \frac{3\varphi}{200} + \frac{11}{20} \quad (2.39)$$

The properties of φ were treated as Gaussian random field^[35] by converting the lognormal random field into the normal space

$$\mu(\varphi) = \ln(\bar{\varphi}) \frac{\ln(1 + \text{cov}^2)}{2} \quad (2.40)$$

$$\sigma^2(\varphi) = \frac{\sqrt{\ln(1 + \text{cov}^2)}}{\mu(\varphi)} \quad (2.41)$$

$$\Sigma_{\varphi\varphi} = \sigma^2(\varphi) \frac{\ln(1 + \rho_{\varphi\varphi} \cdot \text{cov}^2)}{\ln(1 + \text{cov}^2)} \quad (2.42)$$

2.3 Results

A parametric nonlinear FEA is carried out to investigate the effect of the soil spatial variability φ on the UHB of pipelines laid down over a hill-crest imperfection as illustrated in Fig. 2.3. The geometry, burial deep and all parameters other than the friction angle φ and γ are considered as deterministic quantities in the analysis. γ is fully correlated or dependent on the value of φ for each RF realization, to consider the natural dependency of φ on the void ratio of the backfill material.

The acting forces; self-weight, internal pressure, and temperature are also model as deterministic. Upward displacements are restrained by the self-weight of the pipe and the soil cover. Accordingly, the first load step is self-weight in the FE model, follow by the internal pressure. To

identify the effects φ as random field, an incremental thermal load is added after the self-weight and internal pressure. The increment size is equivalent to 1°C of thermal expansion, until UHB occurs. The critical UHB force at the onset of instability is defined as the maximum compressive force in the pipe section, reached at the crown of the buckling pipe as the thermal load increases. In Fig1.5, region 1 there are pipe joints in which the maximum compression occurs. As the soil is model as RF, the maximum compression is not always at the geometric symmetry point in the model. The results are presented as the maximum compressive force among the FE pipe sections inside region 1.

The friction angle φ of the soil is characterized from a set experimental data, presented by Phoon, et al ^[38]. Stochastic characteristics are defined in Table 2.5, lognormal distribution and correlation length. Each RF realization is obtained by means of EOLE method. The soil mechanical properties are fully defined by c, γ, φ , the pipe section geometry and the pipe-soil friction coefficient μ . Only φ is studied in this chapter as RF, γ is model as fully dependent on φ and all the other parameters in the study are deterministic.

2.3.1 Effects of spatial variability of the soil

UHB can lead to significant compressive strains in the middle of buckling bend. This compressive strain is induced by the internal pressure, temperature differential and the partial soil restraint. The combined effects of pressure and temperature differential constitute the driving force of the UHB phenomenon. The total driving forces are referred as the applied axial load in this model.

As a result of the applied axial load, there is a maximum compressive strain along the pipeline undergoing UHB at the lower part of the pipe cross section due to the upward bending, herein called the effective compressive strain. A relationship between the applied axial load and the resulting effective compressive strain is presented in Figures 6 and 7.

For each parametric case, there is a critical applied axial load that leads to UHB. The critical point can be determined by finding the maximum compressive force at the buckle crown in region 1 of Fig 2.4. This total section force at the middle of the buckling bend is identified as the effective load Q_{eff} .

The effects of the spatial variability of φ on the UHB can be analyzed by observing the variability of the effective compressive strain for a given applied axial load, considering different stochastic models. Further validation can be established by studying the variability of Q_{eff} for a robust comparison against the conclusions obtained by studying the variability of the effective compressive strain as show in Fig 2.9 and 2.10.

The EOLE method was implemented to perform 1000 random field simulations to investigate the effects of the φ spatial variability on the UHB phenomenon. The correlation structure is assumed to be the Type I exponential.

$$\rho_I(x_i, x_j) = \exp(-a \cdot \tau)$$

Where:

τ	Euclidian distance between points
a	π / L_h

Simulations were performed for the parametric cases from Table 2.2 to identify the maximum variability between different stochastic soil models (i.e., perfect random, random field and perfect homogenous). In Figures 1.9 and 1.16, 1000 simulations were performed for each soil idealization. The mean response is obtained by setting the soil parameters equal to the mean value for all FE points in the soil domain and it is shown as a solid line in middle. The average response, obtained from each stochastic soil models, correspond to the deterministic soil line in all cases. These response values are due to thermal axial loading.

The lines with different styles are an envelope of the results from 1000 simulations for each stochastic soil model. In Figures 1.9 and 1.10, dash lines represent perfect random (iid case, or perfect random), dot lines are obtained from model with correlation structure (RF case), marker lines are the most conservative soil model (fully correlated or perfect homogenous). Every soil stochastic soil model follows the same lognormal distribution from Table 2.5.

The iid case implies a fully independent random variable φ at each location of the FE soil domain. The random field case involves an exponential correlation structure among all the φ point values. The perfect correlation case is equivalent to having a single random value of φ for all domain points at each simulation. Lines with the same style in the figure represent the maximum and minimum observed responses over 1000 simulation trials, respectively.

Slight variations can be observed the origin, corresponding to the random response of different soil models, due to self-weight and internal pressure. The self-weight and internal pressure response, represents a base point for the thermal load case.

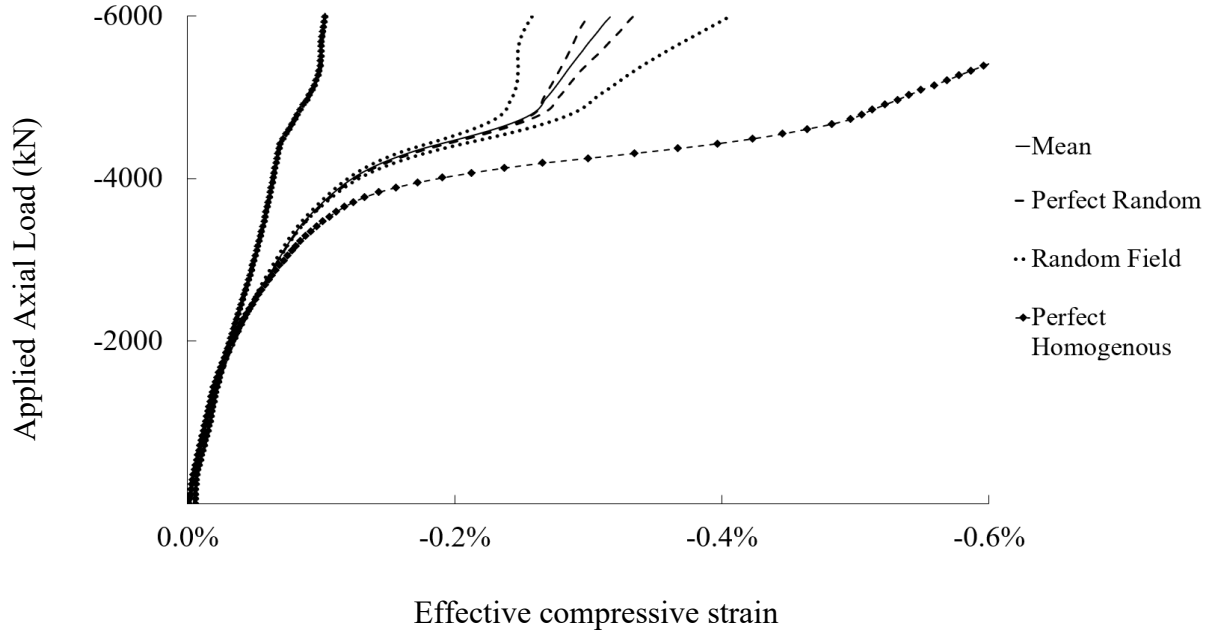


Figure 2.9 Upper and lower strain response due to upheaval buckling. After 1000 RF realizations. Considering different stochastic models of friction angle φ . Case 1 from Table 2.2.
Smooth imperfection

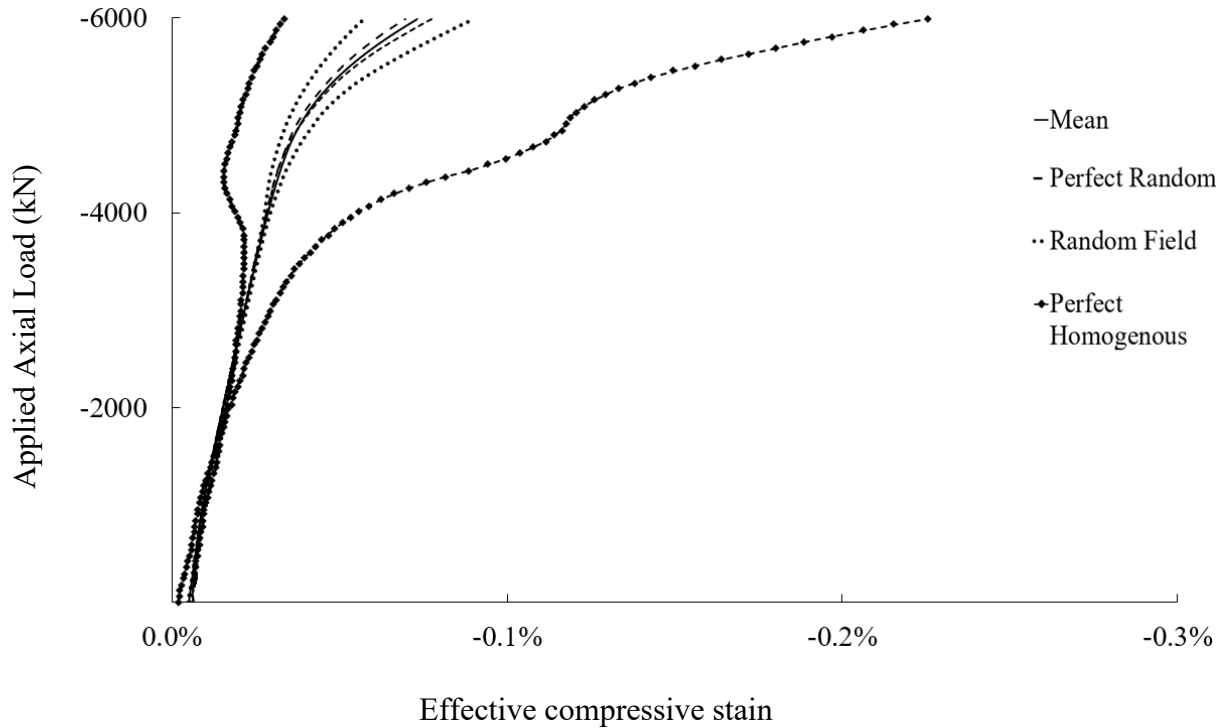


Figure 2.10 Upper and lower strain response due to upheaval buckling. After 1000 RF realizations. Considering different stochastic models of friction angle φ . Case 3 from Table 2.2.
Sharp imperfection

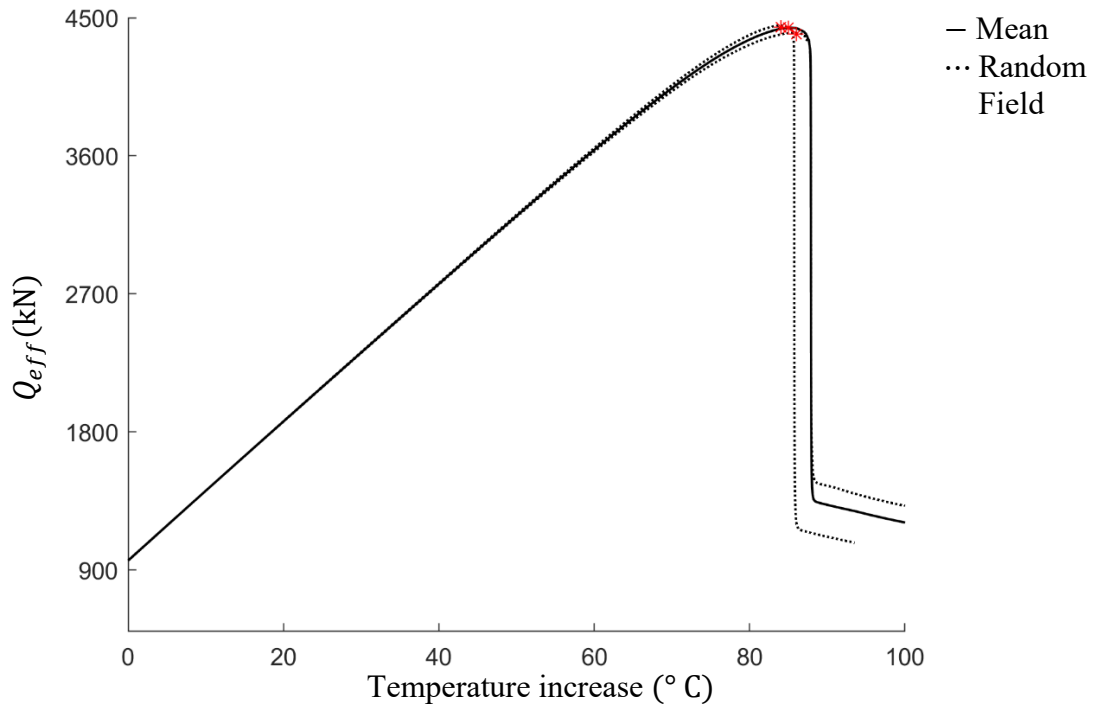


Figure 2.11 Mean value of Q_{eff} vs Maximum and minimum values of Q_{eff} after random field realizations. Case 1 from Table 2.2 Smooth imperfection

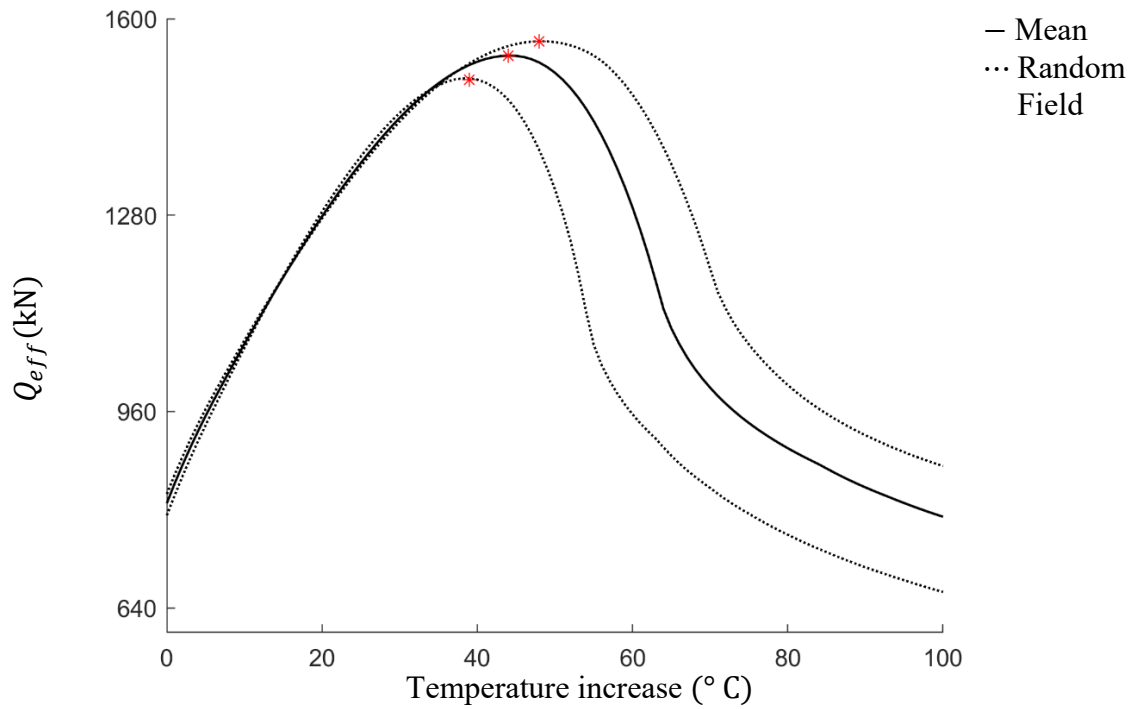


Figure 2.12 Mean value of Q_{eff} vs Maximum and minimum values of Q_{eff} after random field realizations. Case 3 from Table 2.2 Sharp imperfection

The effects of the spatial variability of φ on the UHB are more relevant for pipe lines laid down over narrow hills, or sharp imperfections. In Fig. 2.15, a marginal difference between the maximum observed value of Q_{eff} and the minimum can be explained in terms of the imperfection angle θ . If the arc length of pipe bend at the crown of the hill is large enough, given by $\theta=38.2^\circ$ the total resistance against the upward displacement is provided by a wider soil mass. As the available resistance is more distributed along the total arc length of the pipe the effects of the spatial variability of φ are less relevant. This behaviour holds for all the parametric cases, due the fact the UHB location is still dominated by the imperfection size and shape. In Fig. 2.17 the arc length of the pipe bend is given by $\theta=9.6^\circ$, thus the available soil resistance is dependent on a smaller soil mass and the effects of spatial variability of φ are significant.

Q_{eff} varies, considering different soil conditions. The effects of including the soil spatial variability are compared using the same pipe properties, and same imperfection shape. In Fig. 2.13 a sharp imperfection is represents a strong soil condition, case 9 of Table 2.2. $w_{tot} = 18.06$ kN/m. Whereas, a weak soil condition for the same sharp imperfection is presented in Fig. 2.14, case 15 of Table 2.2. $w_{tot} = 6.79$ kN/m. In both cases the effects of spatial variability of φ are significant.

For pipelines constructed on soils with a dominant static component $q_s=7.32$ kN/m and minimal dynamic component $q_d= 2$ kN/m, Fig. 2.17, case 6 from Table 2.2. The effects of the spatial variability of φ are more significant that those build with soil dominated by Its dynamic component, $q_s=3.05$ kN/m and $q_d=9$ kN/m, Fig. 2.18, case 18 from Table 2.2.

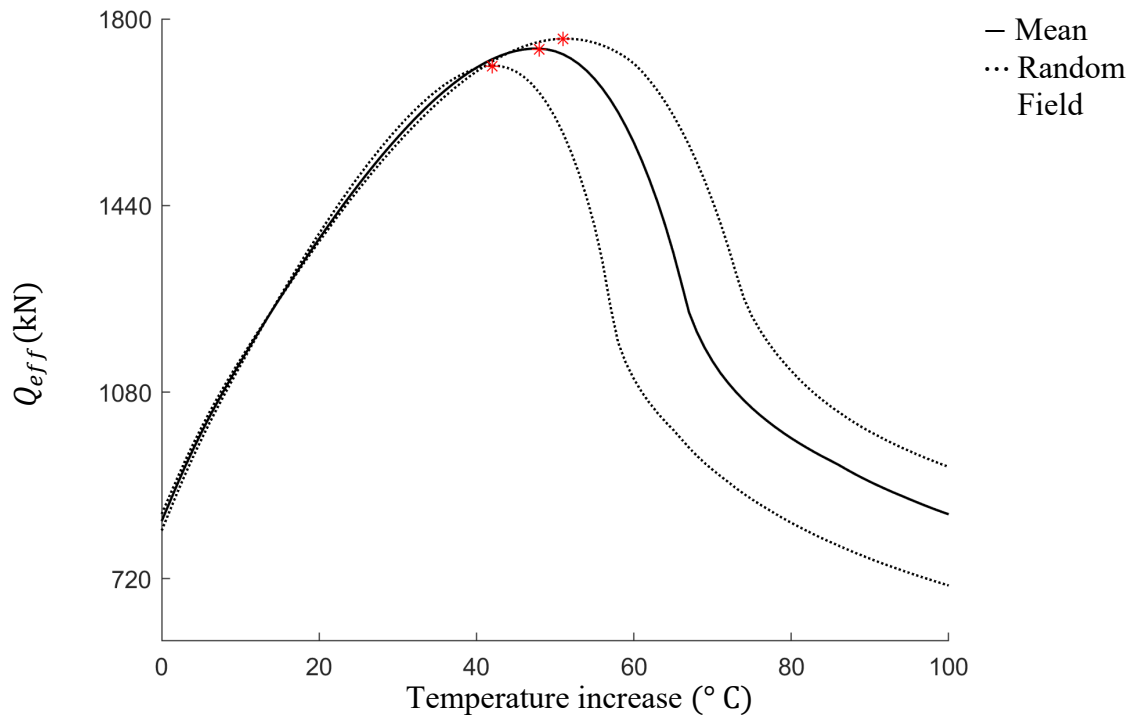


Figure 2.13 Mean value of Q_{eff} vs Maximum and minimum values of Q_{eff} after random field realizations. Case 9. From Table 2.2 Strong soil condition.

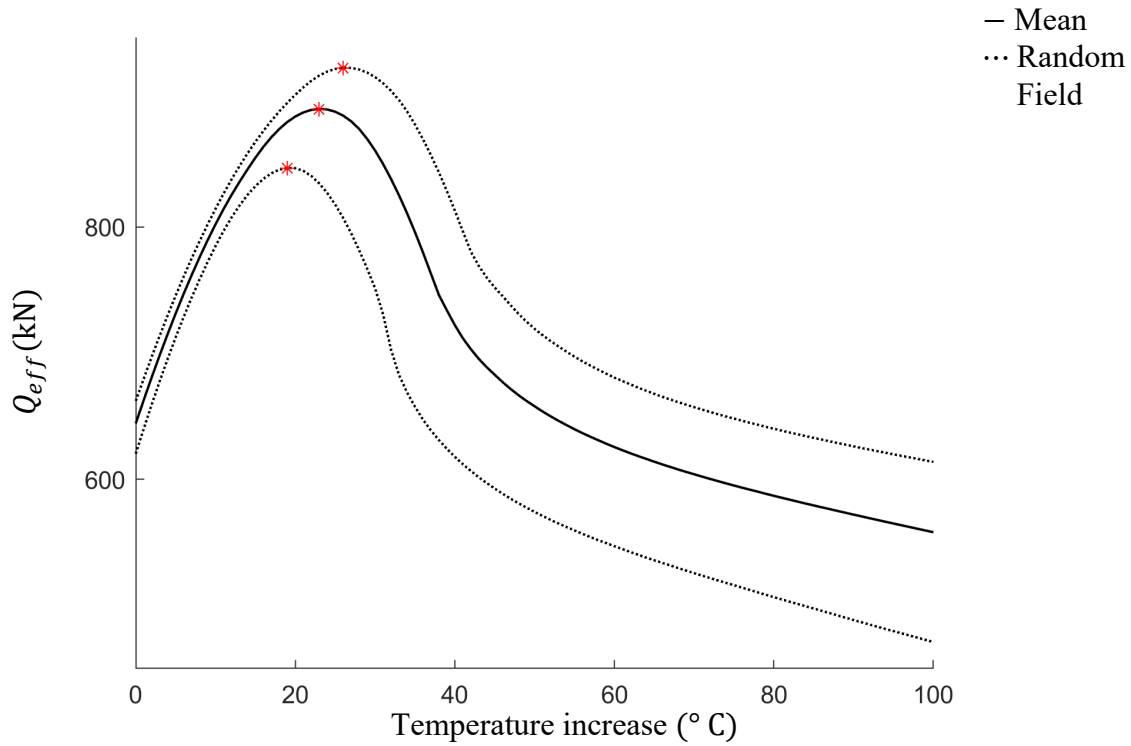


Figure 2.14 Mean value of Q_{eff} vs Maximum and minimum values of Q_{eff} after random field realizations. Case 15. From Table 2.2 Weak soil condition.

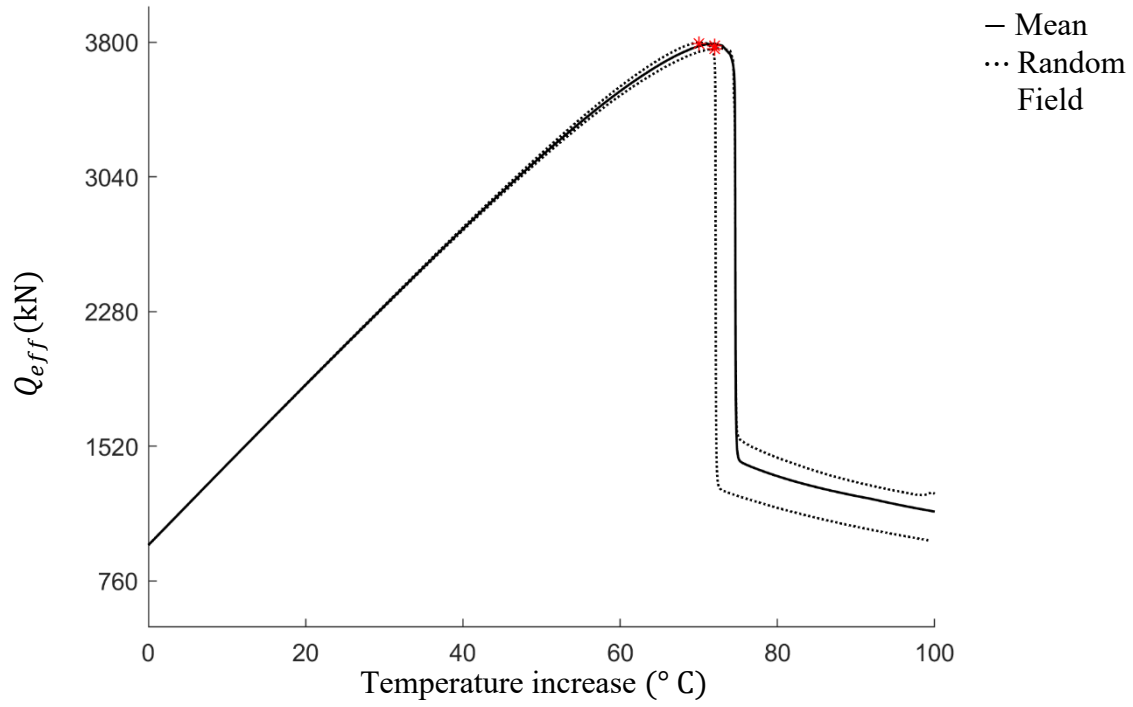


Figure 2.15 Mean value of Q_{eff} vs Maximum and minimum values of Q_{eff} after random field realizations. Case 4. From Table 2.2
Smooth imperfection shape

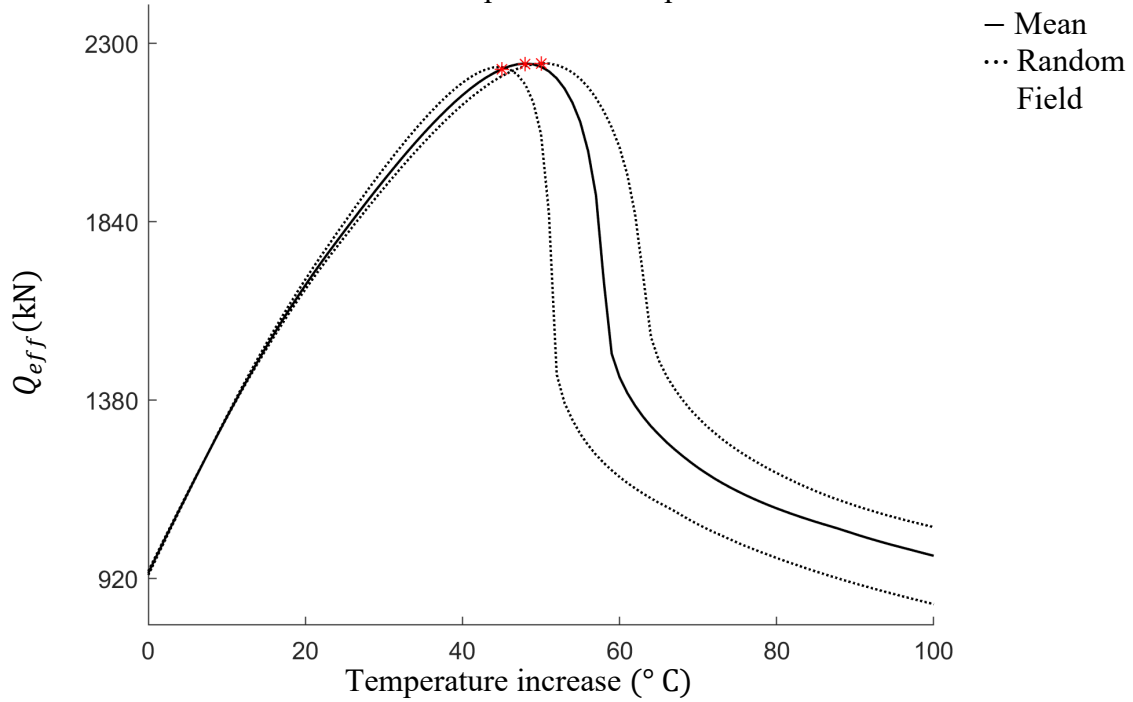


Figure 2.16 Mean value of Q_{eff} vs Maximum and minimum values of Q_{eff} after random field realizations. Case 5. From Table 2.2 regular imperfection size

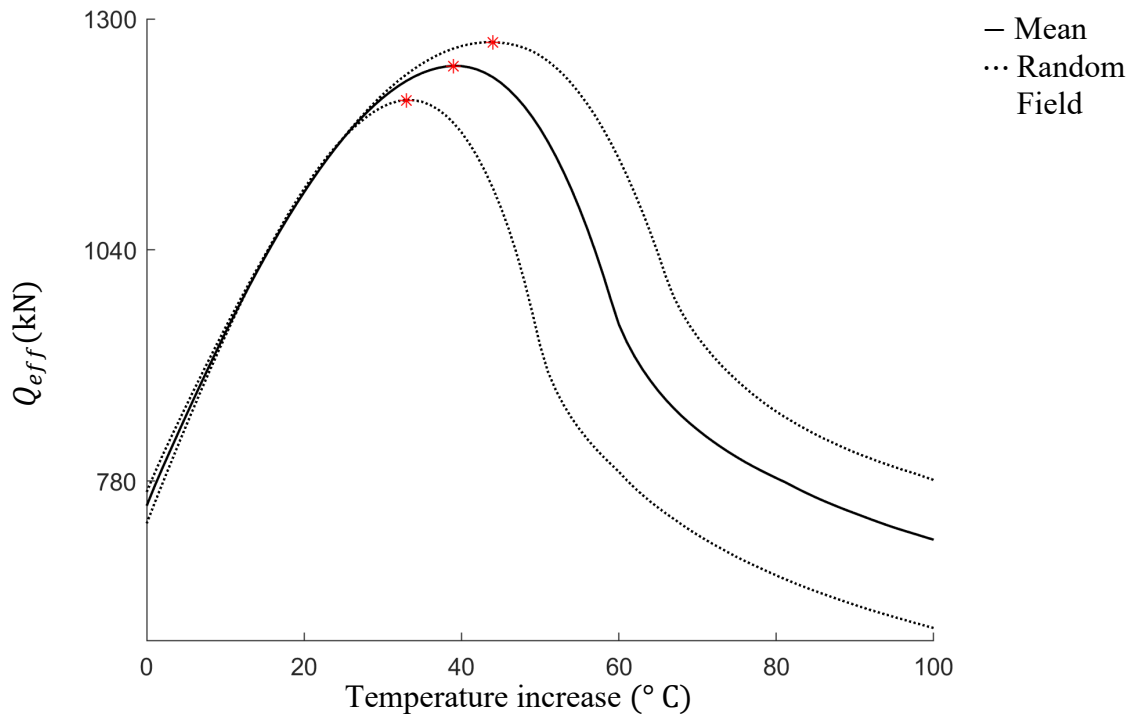


Figure 2.17 Mean value of Q_{eff} vs Maximum and minimum values of Q_{eff} after random field realizations. Case 6. From Table 2.2 Sharp imperfection size

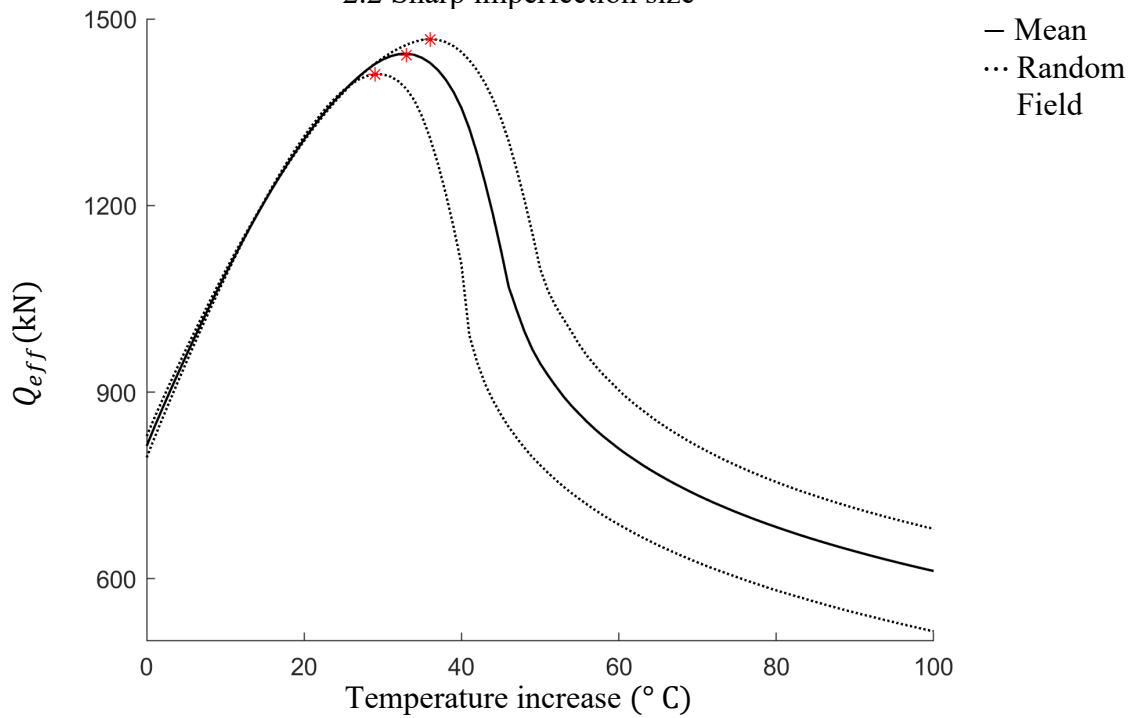


Figure 2.18 Mean value of Q_{eff} vs Maximum and minimum values of Q_{eff} after random field realizations. Case 18. From Table 2.2 Sharp imperfection size

2.3.2 Effects of correlation length

Case 18 from Table 2.2 was selected as the most sensitive case to study the effect of the correlation length. It was found that the UHB buckling phenomena is almost insensitive to the soil scales of fluctuations larger than the size of the imperfection for the cases studied. If the scale of fluctuation is less than size width base of the imperfection it has some influence on the variability of the Q_{eff} although $L_h = 10$ represents a less common case ^[38].

Q_{eff} (kN/m)							
case	Mean Q_{eff}	scale of fluctuation $L_h = 10$		scale of fluctuation $L_h = 50$		scale of fluctuation $L_h = 90$	
		Q_{eff} max	Q_{eff} min	Q_{eff} max	Q_{eff} min	Q_{eff} max	Q_{eff} min
18	-1448	1580	1375	1510	1408	1502	1443

Table 2.6 Results of Case 3 from Table 2.2 after 1000 random field realizations

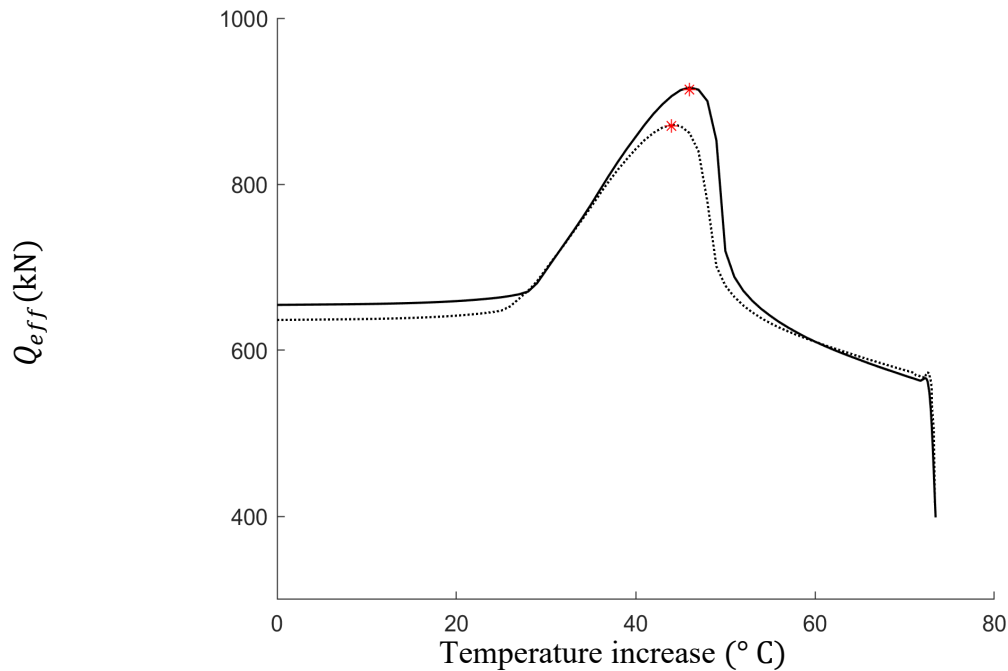


Figure 2.19 Q_{eff} Case 18. Maximum and minimum response after 1000 realizations with scale of fluctuation of $L_h = 10$

2.3.3 Effects of the correlation type

Effects of correlation structure are negligible. The type of correlation studied were bounded by the Triangular type and the Bessel Second kind. Case 18 was analyzed as the most sensitive case by exploring the correlation structures as shown in Figure 1.20. The effects of the correlation length are not significant in the range of study for L_h 40-80m.

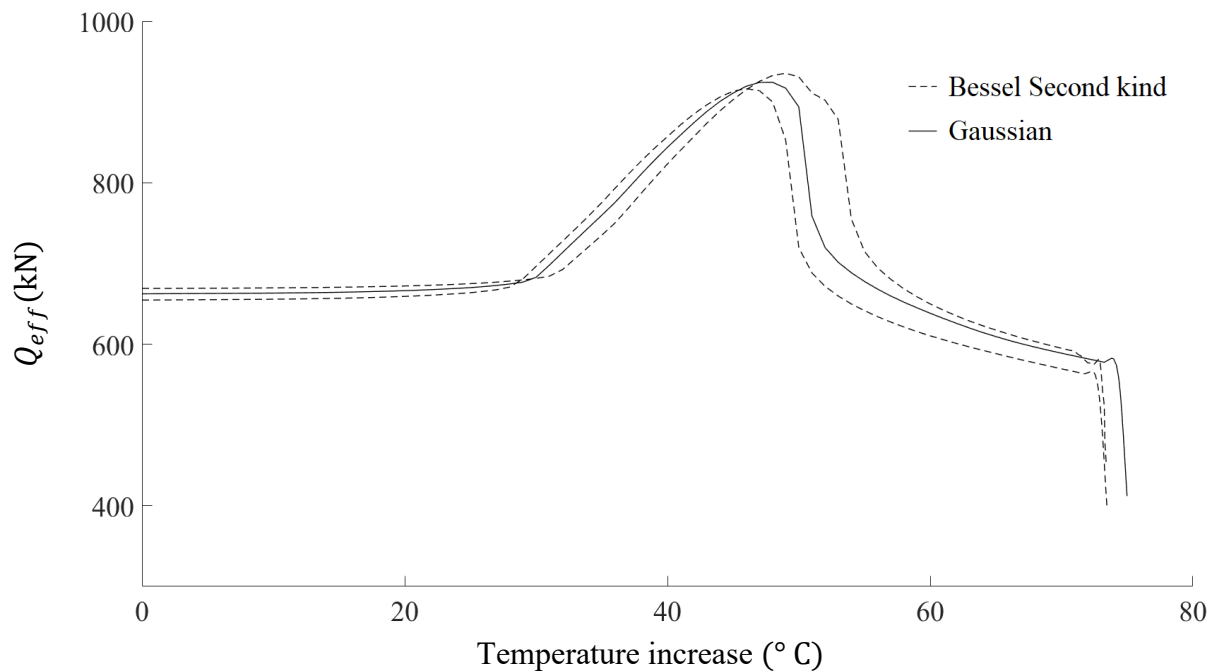


Figure 2.20 Case 18 Maximum and minimum variability while using Bessel Second kind type of correlation.

2.4 Conclusions

The effects of the friction angle spatial variability on the UHB for onshore pipelines, laydown over hill-type imperfections, have been investigated. The soil is characterized from common stochastic characteristics of natural deposits, presented by Phoon ^[38]. The soil properties include, correlation length and exponential correlation structure. The expansion optimal linear estimation (EOLE) method proposed by Li ^[28] is adopted to model the random field. For comparison, the friction angle is also assumed to be represented by a single random variable (i.e., a random field with an infinitely long correlation length), and a random field with independent, identically distributed (iid) random variables at every node (i.e., a random field with a zero-correlation length).

Steel pipes are model following, the Ramberg-Osgood stress-strain relationship as Timoshenko beams in FE analysis. For simplicity, the residual stresses at the cold-formed bends are ignored. Equivalent force-displacement relationships are used to model the pipe-soil interaction according to Oil and Gas Pipeline System (CSA-2019) ^[14]. The acting forces; self-weight, internal pressure, and temperature are model as deterministic.

Selected analysis cases were performed to investigate the effects of the correlation length, influence of the correlation function and the inherent variability of common geotechnical properties ^[38]. The variability of the critical UHB load is measured by means of numerical simulation. Ignoring the effects of the soil spatial of the soil friction angle may lead to overconservative conclusions in the assessment of UHB for onshore pipelines. Up to one order of magnitude, in comparison to single random variable stochastic models.

The effects of the spatial variability of friction angle on the UHB are more relevant for pipe lines laid down over narrow hills, or sharp imperfections. As the available resistance is more distributed along the total arc length of the pipe the effects of the spatial variability of friction are less relevant. This behaviour holds for all the parametric cases, due the fact the UHB location is still dominated by the imperfection size and shape.

Weak soil and strong granular soil conditions are considered. The variability of the friction angle has more relevance for pipelines with strong downward soil load, dominated by the static component. The dynamic component is less sensitive to the variability of the soil friction angle. The spatial variability of the friction angle is significant for pipelines over narrow hill-type imperfections and less significant for smooth imperfection. This applicable for all the imperfection types consider in the parametric analysis. The correlation structure type has marginal impact in the study cases. The type of correlation studied were bounded by the Triangular type and the Bessel Second kind. Given the magnitude of the studied correlation length. The influence of the decrement in correlation as function of distance between random field FE points is relevant for soil correlation length similar or smaller than the imperfection size. The correlation length has some relevance if it less in magnitude in comparison with the total length of the hill type imperfection. It has marginal effects otherwise. The most dominant deterministic parameters in the UHB problem were identified in order of relevance; the imperfection shape, the soil download force, the soil axial force and the pipeline mechanical properties. The dominant stochastic parameters of the friction angle, governing the UHB variability are; variability of the soil, correlation and correlation structure. The inherent soil variability being the dominant source of uncertainty.

2.5 References

1. Liu, R., and S. Yan. 2013. “Brief history of upheaval buckling studies for subsea buried pipeline”. *J. Pipeline Syst. Eng. Pract.* 4 (3): 170–183.
2. Martinet, M. 1936. “Flambement des voies sans joints sur ballast et rails de grande longueur”. *Revue Générale des Chemins de Fer* 55(2),212- 230.
3. Kerr, A. 1978b. “Lateral buckling of railroad tracks due to constrained thermal expansion” A. Kerr, ed., *Railroad Track Mechanics & Technology*, Pergamon Press.
4. Hobbs, R. 1984. “In-service buckling of heated pipelines”. *Journal of Transportation Engineering*. ASCE 110(2), 175- 189.
5. E.N. Dvorkin, R. Toscano. 2001. “Effects of internal/external pressure on the global buckling of pipelines”. *First MIT conference on computational fluid and solid mechanics*, pp 159-164.
6. Washizu K. “Variational Methods in Elasticity and Plasticity” 1982. New York, NY: Pergamon Press.
7. Palmer, A. C., and Baldry, J. A. S. 1974. “Lateral buckling of axially-compressed Pipelines”. *J. of Petroleum Technol.*, 26, 1283–1284

8. Klever, F. J., Van Helvoirt, L. C., & Sluyterman, A. C. 1990. "A dedicated finite-element model for analyzing upheaval buckling response of submarine pipelines". In Offshore Technology Conference. OnePetro.
9. Palmer, A. C., Ellinas, D.M. Richards, and Guijt J. 1990. "Design of submarine pipelines against upheaval buckling". Proc. 22nd OTC, Houston, Texas, pp. 540-550
10. Guijt, J. 1990. "Upheaval buckling of offshore pipeline: Overview and introduction." Proc., 22nd Annual Offshore Technology Conf., Offshore Technology Conference, Richardson, TX, 573–578.
11. R. Liu, S.W. Yan. 2013 "Brief history of upheaval buckling studies for subsea buried pipeline" J Pipeline Syst Eng Pract ASCE, pp. 170-181
12. Villarraga, J. A., Rodríguez, J. F., and Martínez, C. 2004. "Buried pipe modeling with initial imperfections." J. Pressure Vessel Technol., 126(2), 250–257.
13. Cheuk, C. Y., D. J. White, and M. D. Bolton. 2008. "Uplift mechanisms of pipes buried in sand." J. Geotech. Geoenviron. Eng. 134 (2): 154–163.
14. CSA, Oil and Gas Pipeline System, CSA Standard Z662:19, 2019 "Canadian Standard Association", Mississauga, Ontario, Canada.

15. Roy, K., Hawlader, B., Kenny, S., & Moore, I. 2018. "Upward pipe–soil interaction for shallowly buried pipelines in dense sand". *Journal of Geotechnical and Geoenvironmental Engineering*, 144(11), 04018078.
16. Liu, R., Wang, W., & Yan, S 2013. "Finite element analysis on thermal upheaval buckling of submarine burial pipelines with initial imperfection". *Journal of Central South University*, 20(1), 236-245.
17. Burkov, P., Chun, W., Burkov, V., & Burkova, S. 2017. "FEM analysis of soil-pipe interaction. In *AIP Conference Proceedings*" (Vol. 1863, No. 1, p. 560027). AIP Publishing LLC.
18. Ning, J. H., Liu, S. W., Wan, J. H., & Huang, W. 2021. "Line-element formulation for upheaval buckling analysis of buried subsea pipelines due to thermal expansion". *Advanced Steel Construction – Vol. 17 No. 2* 210–220.
19. Roy, K. 2018. "Numerical modeling of pipe-soil and anchor-soil interactions in dense sand." Ph.D. thesis, Dept. of Civil Engineering, Faculty of Engineering and Applied Sciences, Memorial Univ. of Newfoundland.

20. Matheson, I., Zhou, W., Zhou, J., & Gailing, R. 2008. "An upheaval buckling limit state function for onshore natural gas pipelines". In International Pipeline Conference Vol. 48593, pp. 781-791)
21. Rajeev, P., Robert, D. J., Thusyanthan, I., & Kodikara, J. 2013. "Reliability analysis of upheaval bucking of offshore pipelines". Australian Geomechanics Journal, 48, 137-148.
22. Ismail, S., Najjar, S. S., & Sadek, S. 2018. "Reliability Analysis of Buried Offshore Pipelines in Sand Subject to Upheaval Buckling". In *Offshore Technology Conference*. OnePetro.
23. Gallegillo, M., Cerulli, M., & Cooper, C. (2016, June). "Upheaval Buckling Assessments Considering an SRA Methodology and DNV-RP-F110 Guidelines". In The 26th International Ocean and Polar Engineering Conference. OnePetro.
24. Mesmar, S., Robert, D. J., Wang, J., & Haigh, S. K. 2011. "Upheaval Buckling Assessment Based on Pipeline Features". In Proceedings of the Annual Offshore Technology Conference.
25. White, D.J., Westgate, Z.J., and Y. Tian. 2014 "Pipeline Lateral Buckling: Realistic Modelling of Geotechnical Variability and Uncertainty". Paper presented at the Offshore Technology Conference, Houston, Texas.

26. White D. J., Cheuk C. Y. and Bolton M. D. 2008. "The uplift resistance of pipes and plate anchors buried in sand". *Géotechnique* 58, No. 10, 771–779.
27. Dewaikar, D. M., Mohapatro, B. G., Sawant, V. A., & Chore, H. S. 2008. "Computation of bearing capacity factor N_q –Terzaghi and Prandtl mechanism". *ASEAN Journal on Science and Technology for Development*, 25(2), 227-236.
28. Li, C. C., & Der Kiureghian, A. 1993. "Optimal discretization of random fields. *Journal of engineering mechanics*", 119(6), 1136-1154.
29. Nazari, Ali & Rajeev, Pat & Sanjayan, 2015. "Modelling of upheaval buckling of offshore pipeline buried in clay soil using genetic programming". *Engineering Structures*.
30. Westgate, Z. J., Haneberg, W., & White, D. J. 2016. "Modelling spatial variability in as-laid embedment for high pressure and high temperature (HPHT) pipeline design". *Canadian Geotechnical Journal*, 53(11), 1853-1865.
31. Maitra, S., Chatterjee, S., & Choudhury, D. 2016. "Generalized framework to predict undrained uplift capacity of buried offshore pipelines". *Canadian Geotechnical Journal*, 53(11), 1841-1852.
32. Trautmann, C. H. 1983. "Behavior of pipe in dry sand under lateral and uplift loading". *Geotechnical Engineering Report 83-6*, Cornell University, Ithaca, New York.

33. DNV. Recommended failure rates for pipelines 2017 About: Report No.: 2017-0547, Rev2
34. Li, C. C., & Der Kiureghian, A.1993. Optimal discretization of random fields. *Journal of engineering mechanics*, 119(6), 1136-1154.
35. Vanmarcke EH. “Random Fields: Analysis and Synthesis”. Cambridge: Mass. and London Massachusetts Institute of Technology Press; 1983
36. Saadawi, H. 2001. “Upheaval buckling of gas injection pipelines onshore Abu Dhabi—A case study”. Society of Petroleum Engineers.
37. Taylor Neil and Tran Vinh. “Experimental and theoretical studies in subsea pipeline buckling. *Marine Structures*”. s.l., v. 9, n. 2, p.211-257, Jan. 1996. Elsevier BV.
38. Phoon, K.-K., and Kulhawy, F.H. 1999. “Characterization of geotechnical variability”. *Canadian Geotechnical Journal*, 36: 612–624.
39. Ching, J., Wu, T. J., Stuedlein, A. W., & Bong, T. 2018. “Estimating horizontal scale of fluctuation with limited CPT soundings”. *Geoscience Frontiers*, 9(6), 1597-1608.

40. Firouzianbandpey, S., Ibsen, L. B., Griffiths, D. V., Vahdatirad, M. J., Andersen, L. V., & Sørensen, J. D. 2015. "Effect of spatial correlation length on the interpretation of normalized CPT data using a kriging approach". *Journal of Geotechnical and Geoenvironmental Engineering*, 141(12), 04015052.
41. Jaksa, M. B., Goldsworthy, J. S., Fenton, G. A., Kaggwa, W. S., Griffiths, D. V., Kuo, Y. L. & Poulos, H. G. 2005. Towards reliable and effective site investigations. *Géotechnique* 55, No. 2, 109–121.
42. Rasti, A., Adarmanabadi, H., Pineda, M., & Reinikainen, J. 2021. "Evaluating the Effect of Soil Particle Characterization on Internal Friction Angle". *American Journal of Engineering and Applied Sciences*.
43. Vangla, P., & Latha, G. M. 2015. "Influence of particle size on the friction and interfacial shear strength of sands of similar morphology". *International Journal of Geosynthetics and Ground Engineering* 6.
44. Simoni, A., & Houlsby, G. T. 2006. "The direct shear strength and dilatancy of sand–gravel mixtures". *Geotechnical & Geological Engineering*, 24, 523-549.
45. Weerasekara, Lalinda. "Pipe-soil interaction aspects in buried extensible pipes". Diss. University of British Columbia, 2011.

46. Suchomel, R. & Masín, D. 2010. “Comparison of different probabilistic methods for predicting stability of a slope in spatially variable c-soil”. *Computers and Geotechnics* 37, No. 1-2, 132–140
47. Naghibi, F., Fenton, G. A. & Griffiths, D. V. 2016. “Probabilistic considerations for the design of deep foundations against excessive differential settlement”. *Canadian Geotechnical Journal* 53, No. 7, 1167–1175.
48. Sert S., Luo, Z., Xiao, J. H., Gong, W. P. & Juang, C. H. 2016. “Probabilistic analysis of responses of cantilever wall-supported excavations in sands considering vertical spatial variability”. *Computers and Geotechnics* 75, 182–191.
49. American Lifelines Alliance, 2001 “Guidelines for the Design of Buried Steel Pipe”.
50. Zeng X, Duan M, Che X. 2014 “Critical upheaval buckling forces of imperfect pipelines. *Appl Ocean Res*”; 45:33–9.
51. Liu P.-L. and Der Kiureghian A., 1991b, “Optimization algorithms for structural reliability”. *Struct. Safety*, 9, 161-177.
52. Der Kiureghian A. “Multivariate distribution models for structural reliability”. *Transaction of the 9-th conference on structural mechanics in reactor technology*. Vol. M. 17–21 Aug 1987. Lausanne. pp. 373-379.

3 An Empirical Equation for Upheaval buckling Capacity Considering Soil Spatial Variability.

Buried gas pipelines usually transport fluid at elevated temperatures to optimize the productivity of the wells. Upheaval buckling (UHB) is a limit state for buried pipelines that operate at high pressure and temperature ^[1]. Due to these conditions, an overall compressive force is induced along the pipes. This compression, may cause the pipeline to buckle upward or even break out of the ground if the soil cover or restraining measures are not sufficient. Additionally, out-of-straightness (OOS) imperfections or features along the line topography can further reduce the buckling capacity of the pipeline. UHB is analogous to the Euler column buckling susceptibility or the localised global buckling, depending on the pipe and soil characteristics. The UHB of pipelines, is usually not considered as an ultimate limit state condition. However, it can lead to high strains concentrations on the pipe wall. If excessive deformation occurs, expensive remediation measures may be needed to avoid high cycle fatigue, or lost of pressure integrity ^[2].

Experimental and theoretical studies have been conducted to investigate the uplift resistance of buried pipelines. The current state of the art allows for estimations of the critical axial UHB force considering different soil-pipe interaction models and pipe geometric conditions. The most common geometric considerations include lay-down straight, lines over hill type imperfection or prop-type imperfections ^[1] and partially restrained ground supported ^[5], as show in Fig. 3.1

In general, the relationship between the compressive force and upward movement of a buried pipeline is nonlinear. The soil download reaches a maximum value at relatively small vertical

displacement, when the pipeline starts buckling due to the induced axial load. After the peak resistance, the soil download decreases to zero when the pipe reaches a breakthrough condition. The soil-pipe interaction during the upheaval buckling, together with the operating conditions and pipe material and geometric properties has a significant influence on the estimation of the UHB forces. One can observe that the UHB is a complex process and approximations to estimate the UHB critical force may not be always conservative due to the non-linearity and specific site conditions. Further, it has been shown experimentally ^[3] that in some cases the initial part of the force-displacement characteristics of soil in the UHB phenomena is of secondary importance. This may be counterintuitive because the inelastic buckling of columns tends to be governed by the initial departure of the constitutive relationship from the linear-elastic phase. However, when considering an elastic pipe embedded in a nonlinear material, the behaviour is different, ^[6-7] apparently being dominated by fully mobilized soil resistance instead.

Since 1990, considerable efforts were made to predict the UHB behavior of offshore pipelines. Mostly because submarine pipelines can operate at higher pressure and temperature differentials, and the implementation of restraining measures can be more expensive in contrast to onshore pipelines. However, some UHB incidents have occurred in onshore pipelines crossing water bodies, swamps, tundra and desert conditions ^[8]. Onshore pipelines have unique design challenges to prevent UHB arising from natural, construction and operating conditions; for instance, soil displacement in swamps areas, frost heave and thaw settlement for pipelines in extreme latitudes ^[9], high temperature gradients in desert conditions, the long-term stability of anchor devices, the use of cold-formed pipe bends to build pipelines over natural features, obstructions and imperfections along the line. Some operating conditions, could trigger large differential settlements or induce

pipe stresses^[8], that had to be taken into account for the design and during operation of the pipeline to ensure safety.

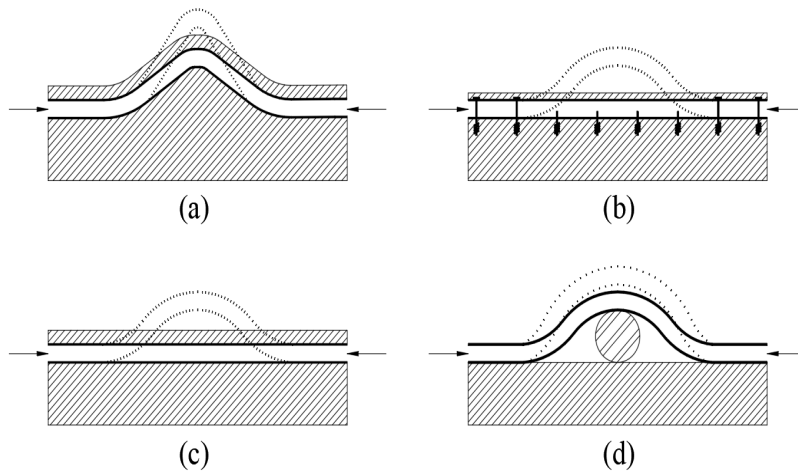


Figure 3.21 Most common imperfection idealization types; (a) hill imperfection, (b) partially restrained, (c) lay-down straight, (d) prop imperfection

Previous studies to predict the UHB can be classified in four main groups by their formulation: 1) closed-form solutions derived from the virtual work principle^[6,7,9,10] and validated/calibrated by experimental results for realistic buckling length; 2) simplified, finite element (FE)-based approach as recommended in various pipeline design guidelines^[13,14]; 3) sophisticated numerical models, which is primarily used to analyze specific UHB mechanisms for academic proposes^[15], and 4) empirical expressions derived from experimental data and parametric FE analysis. This approach may be a practical way analysis the UHB phenomena for a wider set of realistic conditions. The last approach may be a practical way to analyze the UHB for a wider set of realistic conditions.

3.1 Motivation

The reliability-based design and assessment (RBDA) methodology has gained increasing acceptance in the pipeline industry as a viable alternative for the design and assessment of onshore natural gas pipelines. The UHB is a key limit state for buried pipelines that operate at high pressures and temperatures. A common feature of onshore pipelines is the formed bends or elbows, to follow the topology of the pipeline route.



Figure 3.22 Cold formed bends over a hill (Source: Argonne National Laboratory) ^[4].

Empirical formulations for pipelines laid down by welding cold-formed bends over hill-crest type of imperfections have been reported in the literature ^[2]. From simplified numerical analysis, a critical force expression for the onset UHB was developed ^[2]. The influence of the dominant variables involved in critical UHB force was investigated using empirical relationships obtained from parametric analysis. The UHB limit state function was established in ^[2] as the critical UHB force (i.e., UHB capacity) minus the applied compressive force. The limit state function can be employed to efficiently calculate the probability of UHB of pipelines. This limit state function can be used to further explore the effects of the inherent uncertainties in soil properties on UHB.

The model developed in [2] assume a piece-wise geometry for numerical model of the pipeline and force-displacement models for soil cover and axial friction with the pipe [13] to calculate the critical axial UHB load and the length of the buckled pipeline. Although some design guidelines recognize the post-peak reduction of the uplift resistance for medium to dense sand and recommended a multi-linear force-displacement model to characterize the uplift resistance [14], the influence of nonlinear uplift soil resistance and cover depth of the pipeline is likely varying along the length of the pile, having an effect that may be enough to trigger a localised vertical buckling. This buckling mechanism is trigged by a distinct restriction on the lateral displacement of a pipeline, analogous to a mechanism dominated by a Hamiltonian-Hopf bifurcation instead of Euler buckling [17]. Thus, the spatial variability of the soil may have significant impact on the overall stability of pipelines [13].

Prediction of upheaval buckling resistance of buried pipelines has been a challenge as a result of uncertainty in the behaviour of seabed and cover soils, operating conditions and new pipe materials [18]. The effect of the spatial variability in soil properties on the resistance against the UHB has not been reported in the literature. There are few studies that address the effect of soil uncertainty on the UHB for buried straight pipelines, with no geometric imperfections [22]. Recent research [18-21], have presented numerical procedures to assess the UHB of pipelines without considering the inherent spatial variability of the geotechnical parameters, using pipe-soil interaction (PSI) models to account for the variability of the soil as a single independent random variable instead. The findings on previous studies [18-21] clearly show the effects of the soil variability are significant to assess the UHB of pipelines.

The main objective of the research reported in this chapter is aimed at developing an empirical UHB limit state function that can be easily incorporated in RBDA as a viable alternative for onshore pipelines. Extensive parametric finite element (FE) analyses are carried out to improve on an empirical equation developed in a previous study [2] to predict the critical axial UHB force for pipelines laid down by welding cold-formed bends over hill-crest imperfection types. The accuracy of FE analyses conducted in the present study is confirmed by comparing the corresponding results with those reported in [2]. Comprehensive numerical simulations are used to characterize the statistical properties of the model error associated with the improved empirical equation for the critical UHB force.

A variance reduction expression to account for the spatial variability of the soil friction angle is presented as secondary objective in this chapter. The proposed expression yields a single factor to modify the variability of the empirical equation for the critical UHB force. It can be fully characterized from the random properties of the soil friction angle. These improvements can be readily implemented in a RBDA framework to calculate the pipeline failure probability due to upheaval buckling, on the cold formed bends considering the spatial variability of granular soils.

3.2 Methodology

A non-linear FE parametric study was performed to replicate a set of results obtained in a previous study [2]. From these verified results, a matrix of upheaval buckling analysis cases are generated. This includes; common soil properties, pipe sections and imperfection shape found along onshore pressured gas pipelines. The results from the parametric analysis are used to fit a new UHB

empirical equation for pipelines build from cold formed bends and lay down over Hill-type imperfections. The critical force at the onset of UHB Q_{app} , is defined as the maximum axial force, induced by internal pressure and temperature that the pipeline can hold, before becoming unstable. The empirical expression for critical applied axial force Q_{app} , is a function of the acting or effective compressive force near the top or crown of the imperfection (Fig. 3.3) where the pipe section experiences the maximum compressive force Q_{eff} , due to axial force and UHB. Both effective and applied forces are model as total section forces.

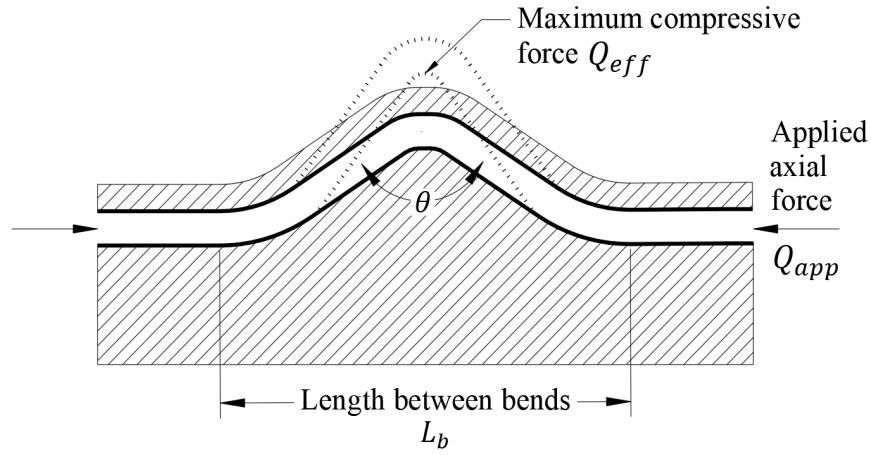


Figure 3.23 critical applied axial force Q_{app} , function of the acting or effective compressive force.

The scope or applicability of the proposed empirical equation for UHB is detailed on Table 3.1. The new critical effective force Q_{eff} is detailed on Eq 2.6. This account for pipe properties, the soil cover, and the imperfection shape. Model error statistics are obtained for the new empirical equation to assess pipelines in a RBDA framework.

From the parametric analysis results the limit state function, g , is defined as follows:

$$g = B \cdot Q_{crit} - Q \quad (3.43)$$

where: Q_{crit}	the Critical Upheaval Buckling Force
B	the model error associated with Q_{crit} . It is normally distributed with unitary mean and CoV of 4%.
Q	the compressive force (due to internal pressure and temperature)

given by:

$$Q = Q_T + Q_P \quad (3.44)$$

$$Q_T = E\alpha_T(T_2 - T_1)\pi(D - t)t \quad (3.45)$$

$$Q_P = \left(1 - \frac{2\nu(D - t)}{(D - 2t)}\right) \frac{\pi(D - 2t)^2}{4} P \quad (3.46)$$

where: Q_T	temperature induced force (positive for compression)
Q_P	pressure induced force (positive for compression)
E	Young's modulus
α_T	thermal expansion coefficient for steel ($11.7 \times 10^{-6} \text{ }^\circ\text{C}$)
T_2	operating temperature
T_1	tie-in temperature
D	pipe outside diameter
t	wall thickness
ν	Poisson's ratio
P	operating pressure

$$Q_{crit} = Q_{eff} \cdot F_{app} \quad (3.47)$$

$$Q_{eff} = Q_{eff_base} \cdot F_{hs} \cdot F_{ys} \cdot F_{Dt} \cdot F_{dia} \quad (3.48)$$

$$Q_{eff} = Q_{eff_base} \cdot F_{app} \quad (3.49)$$

$$Q_{eff} = Q_{eff_base} \cdot F_{hs} \cdot F_{ys} \cdot F_{Dt} \cdot F_{dia} \quad (3.50)$$

Q_{eff}	effective force (kN). Defined as the total section force at the buckle of the crown.
Q_{eff_base}	base case effective force (kN)
F_{app}	ratio between the applied force to effective force.
F_{hs}	hoop stress correction factor, accounting for the hoop stress to internal pressure ratio.
F_{ys}	material grade correction factor.
F_{Dt}	Diameter to wall thickness correction factor.
F_{dia}	Pipe outside diameter correction factor.

After the improved Eq 2.10 was fitted from the FE analysis. The same parametric cases were used to investigate the effects of the spatial variability soil ϕ on the UHB. The soil is characterized as a gaussian random field. Using common statical properties found in natural soil deposits ^[25].

From the perspective of the pipeline safety, two bounds in terms of the soil spatial variability are also considered: the soil domain being treated as homogenous and fully correlated field, i.e., represented by a single random variable, and the soil being treated as an uncorrelated random field, i.e., represented by a series of independent, identically distributed (iid) random variables at different spatial locations.

Thousand sets, a probability density function (PDF) was fitted for each increment of applied axial load. Using the empirical expression instead of the FE model an equivalent set of PDFs was obtained. These two sets, were compared in order to stablish a new empirical relationship that allows for a reduction in the variance of the geotechnical properties. In order to achieve more realistic probability of UHB estimations.

After the numerical simulation, the probability of the effective axial force being greater or equal to the UHB critical load, was calculated at each at each increment of applied axial force from the fitted PDF set. In other to obtain the cumulative distribution CDF of the probability of UHB as function of the applied axial loading. The former, was compared to the probability obtained from the empirical equations to verify that the probability estimations here in proposed, are more realistic but still on the conservative side

3.2.1 Finite Element Modelling

The pipeline examples considered in the parametric analysis are the same as those considered in Chapter 2. For easy reference, the basic attributes of the examples are summarized in Table 3.1. The commercial FEA package ABAQUS is employed to carry out the analysis.

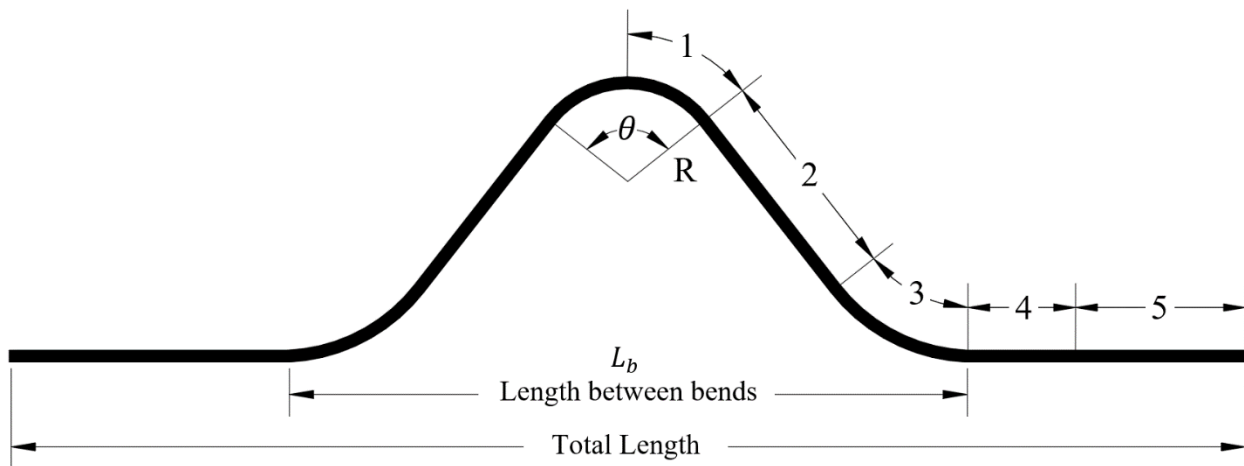


Figure 3.24 Diagram of buried pipeline over a Hill-Crest imperfection ^[2] $L_b = 100\text{m}$, and the Total Length is 300m.

3.2.2 Soil Model

The axial soil resistance was modeled as a bilinear force-displacement relationship. Where the mobilization displacement was assumed as 0.0015m and the fully mobilized friction force is given by: Two soil mobilization displacements were considered 10mm and 40mm.

The soil uplift resistance was modelled by a static download and a dynamic download. The dynamic component is only mobilized by upward movement of the pipe. The peak dynamic component is reached at the vertical mobilization displacement, and a linear uplift force-displacement is assumed for lower values of the uplift displacement. The download – uplift response is illustrated in Fig. 3.3

Typical cover height may range from 0.75 m to 1.0 m and backfill may be mechanically compacted. Regular soil backfill has a bulk density of around 18kN/m³, but could reach 20kN/m³ or higher if the backfill contains high content of gravel or rock. However, in swamp areas the effective density could be close to zero.

To develop a limit state function, a range of typical soil responses need to be considered. In addition, the analysis matrix considers a range of pipes with differing diameters and pipe weights. The soil download should be normalized as much as possible between differing pipe configurations.

The static soil download is linearly proportional to pipe diameter. Hence, it is proposed to define the static soil download as normalized to pipe diameter. This avoids the need to model the soil density, and the bury deep as explicit variables.

The dynamic download for a cohesive soil is linear proportional to the shear strength of the soil. For backfilled soils it is prudent to assume fairly low values of homogeneous shear strength. In the following example two shear strengths of 10 and 50 kPa were assumed.

The mobilization displacement Δq_u is taken as 0.1 H to 0.2 H for soft to stiff clay but with a maximum of 0.2D (e.g., for 0.7 m cover height Δq_u is 70 to 140 mm although for the 24" and 16" pipelines the upper bound displacement would be limited to 122 and 81 mm, respectively) The mobilization displacement Δq_u is taken as 0.01 H to 0.02 H for dense to loose sands (e.g., for 0.7 m cover height Δq_u is 7 to 14 mm)

The base case mobilization displacement, is proposed to be 10 mm with a sensitivity case of 40 mm. The base case mobilization reflects non-cohesive conditions, whilst the sensitivity case aims to reflect some increase in displacement which may occur if the soil is partly cohesive.

3.2.3 Empirical Critical Upheaval Buckling Force Function.

Q_{eff_base} is the base case effective force in kN (i.e., the effective force developed assuming a fixed material grade (448 MPa), D/t ratio (60), diameter (24 inches), and ratio between hoop stress and yield strength (0.6) from the parametric analysis. The formulation obtained in previous studies is denoted by $Q_{eff_base}[2]$.

$$Q_{eff_base}[2] = -99.89 \left(\frac{1}{\sin \theta/2} - 3.297 \right)^{0.6285} w_{tot}^{0.5771} \quad (3.51)$$

The former formulation was improved due the fact it contains the vertical soil contribution in a condensed in a single variable w_{tot} . The proposed expression is

$$Q_{eff_base} = -129 \left(\frac{w_{\text{tot}}}{\sin \theta/2} - 7.69 w_{\text{tot}}^{0.798} \right)^{0.567} \quad (3.52)$$

$$w_{\text{tot}} = w_{\text{pipe}} + q_s + q_d \quad (3.53)$$

Where:

- w_{tot} total download in kN/m
- w_{pipe} pipe weight per unit length
- q_s static soil download (i.e., overburden)
- q_d the dynamic soil download
- θ the angle of the imperfection detailed on Fig. 3.3

The improvement of the new expression is detailed in Table 3.1. These parameters are those used to develop the base line case for the effective force Q_{eff_base} from Eq. 3.10

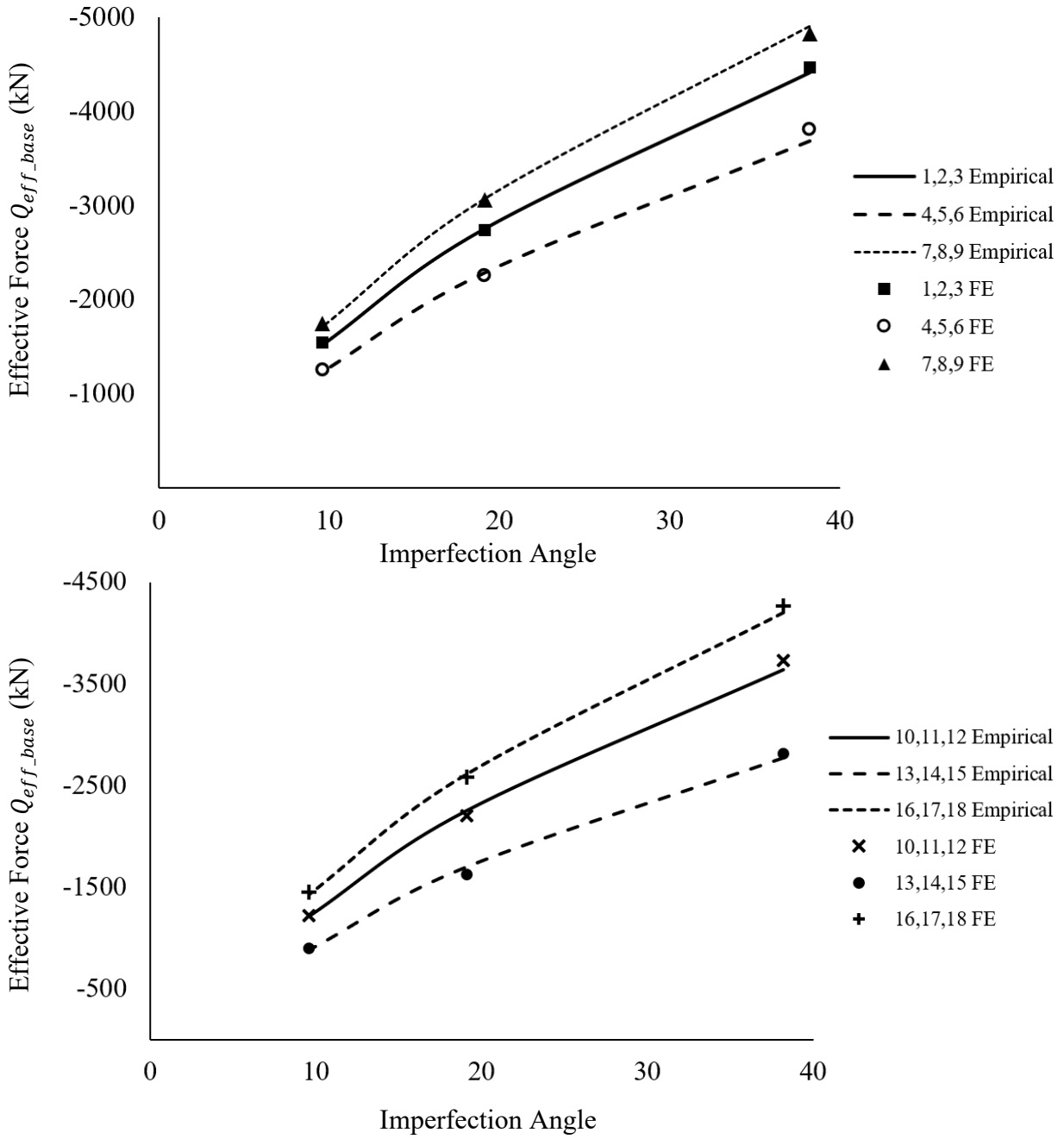


Figure 3.25 Effective Force Q_{eff_base} , Bend Angle. Case number for Q_{eff_base} obtained from the Empirical Eq 2.6, Q_{eff_base} obtained from FE Parametric analysis.

Case number	Imperfction	q_s (kN/m)	q_d (kN/m)	w_{tot} (kN/m)	Q_{eff} (kN/m)				
					FE	$Q_{eff}^{[2]}$	Error [2]%	Q_{eff}	Error%
1	38.2	7.32	6	15.06	-4465	-4455	-0.21	-4415	-1.17
2	19.1	7.32	6	15.06	-2738	-2708	-1.08	-2751	0.45
3	9.6	7.32	6	15.06	-1541	-1514	-1.69	-1515	-1.30
4	38.2	7.32	2	11.06	-3807	-3728	-2.08	-3688	-3.25
5	19.1	7.32	2	11.06	-2252	-2266	0.65	-2284	1.37
6	9.6	7.32	2	11.06	-1249	-1267	1.49	-1231	-1.02
7	38.2	7.32	9	18.06	-4825	-4948	2.55	-4907	1.63
8	19.1	7.32	9	18.06	-3060	-3008	-1.72	-3069	0.24
9	9.6	7.32	9	18.06	-1742	-1682	-3.46	-1709	-1.54
10	38.2	3.05	6	10.79	-3728	-3676	-1.39	-3636	-2.58
11	19.1	3.05	6	10.79	-2202	-2235	1.47	-2250	2.10
12	9.6	3.05	6	10.79	-1224	-1249	2.09	-1211	-0.67
13	38.2	3.05	2	6.79	-2810	-2814	0.14	-2774	-1.33
14	19.1	3.05	2	6.79	-1625	-1710	5.24	-1698	4.29
15	9.6	3.05	2	6.79	-895	-956	6.86	-879	-1.37
16	38.2	3.05	9	13.79	-4261	-4235	-0.60	-4195	-1.63
17	19.1	3.05	9	13.79	-2579	-2574	-0.17	-2610	1.12
18	9.6	3.05	9	13.79	-1448	-1440	-0.56	-1429	-0.95

Table 3.7 Comparison of FE and Calculated Values for Effective Force for a pipeline that weights 1.741 (kN/m), material grade (448 MPa), D/t ratio (60), diameter (24 inches), and ratio between hoop stress and yield strength is (0.6)

For internal pressures other than that which induces a hoop stress of 0.6 yield stress a hoop stress correction a correction factor F_{hs} can be applied:

$$F_{hs} = 1 - \frac{\bar{\sigma}_h - 0.6}{0.6} \left(\frac{Q_{eff_base}}{8633} \right)^2 \quad (3.54)$$

Where: $\bar{\sigma}_h$ ratio of hoop stress to yield stress

For steel grades different than X65 a yield stress correction factor F_{ys} can be applied:

$$F_{ys} = 1 + \left(\frac{\sigma_y - 448}{448} \right) \left(\frac{Q_{eff_base}}{-4094 - 4.681\sigma_y} \right)^{2.631 \frac{\sigma_y}{448}} \quad (3.55)$$

Where: σ_y yield stress (Mpa)

For D/t ratios other than D/t = 60 a correction factor can be applied:

$$F_{Dt} = 1 - 0.371 \ln \left(\frac{D_o/t}{60} \right) \quad (3.56)$$

Where: D_o pipe outside diameter
t Pipe wall thickness

For outside diameters other than 24 inch a correction factor can be applied:

$$F_{dia} = \left(\frac{D_o}{24} \right)^{1.335} \quad (3.57)$$

Where: D_o pipe outside diameter in inches

With the previous factors, the effective UHB force Q_{eff} can be applicable in kN (positive for compression), which is defined as the total section Force at the buckle crown (note that the effective force is different from the applied force, defined as the force remote from the buckle crown, due to axial feed-in to the developing buckle);

$$Q_{eff} = Q_{eff_base} \cdot F_{hs} \cdot F_{ys} \cdot F_{Dt} \cdot F_{dia} \quad (3.58)$$

$$Q_{app} = 0.8593 \cdot \exp\left(\frac{-661.4 - 53.71 \cdot f}{Q_{eff} \left(\frac{D_o}{60}\right)^{0.55} \cdot \left(\frac{24}{D_o}\right)^{1.33}}\right) \cdot Q_{eff} \quad (3.59)$$

Where: f Pipe-soli axial resistance (kN/m) from equation (1.2)

3.2.4 Variance Reduction Empirical Equations

In order to assess the assess inherent soil variability, it is also necessary to account for measurement error, transformation uncertainty ^[2]. However, the transformation uncertainties associated with the soil Force-Displacement models are seldom analyzed with statistical rigor. Because they are, in part empirical and it may be lack sufficient information about them for further analysis that can be applied to general cases. However, it is still possible to obtain practical and conservative expressions to consider some relevant stochastic properties.

A practical expression to account for the effects of the spatial variability with the empirical Eq. 3.10 is obtained as follows:

The FE analysis was performed with the range of parameters described on Table 3.1. This computation was performed for 1000 random field realizations. A set of critical buckling forces for each deterministic combination of factors was obtained from these results. One can notice the effects of the soil spatial variability in Fig. 3.5

Maximum and minimum critical UHB force values, were observed after these realizations. These are significant, depending on the idealization of the soil. If the model is fully homogeneous along its domain, the results obtained are more disperse and different from the mean value. In the opposite extreme, if the soil is considered to be a fully random media (i.e., each discrete point in the soil model has fully independent properties) the maximum and minimum values of critical UHB force are more similar or closer to the mean value. Whereas, if the soil is idealized with some correlation structure, the maximum and minimum of critical UHB force values were always bounded by former two extreme cases.

A best fitting Probability Density Function (PDF) was obtained for each set of critical buckling forces obtained from models with random field properties. Best fitting distribution criteria for Q_{eff} was obtained from the logarithm or maximum likelihood.

$$l(\theta; \xi) = -\frac{n}{2} \ln(2\pi) - \frac{n}{2} \ln(\sigma^2) - \frac{1}{2\sigma^2} \sum_{i=1}^n (x_i - \mu)^2 \quad (3.60)$$

Then, the equivalent analysis was replicated by means of the empirical equations. The empirical equations were characterized with equivalent soil stochastic properties. The former, excluding the effects of the spatial variability of the soil. Given the fact that, all the soil parameters are lumped on the w_{tot} variable in Eq. 3.10 it is not possible to measure the uncertainty directly from basic soil properties through the Force-displacement relationship. A simple reduction was used instead.

The PDFs obtained from the random field FE model are different from the PDFs obtained with the empirical equations. A brief summary of this is presented on Table 3.3. The variances of the critical UHB force obtained from the empirical equations were always larger than those obtained from the

FE analysis. To artificially reduce this discrepancy, a reduction factor $F_{\sigma_\phi^2}$ for the variance of the critical force due to the soil properties (e.g., friction angle, density) was obtained from successive approximations. This factor is a base line to eliminate the smallest difference in variance of critical UHB force for all cases studied in the parametric analysis. A second reduction factor is proposed $F_{\sigma_I^2}$, to further reduce the critical UHB force variance due to the imperfection size. For wider or smooth type of imperfections, according to the idealization shown in Fig. 3.5 The effects of soil spatial variability are expected to be more relevant than those observed if the imperfection is sharp or narrow. Bearing in mind that, the soil mass cover is acting over a longer buckling length. Further, if the imperfection is sharp the total downward force resisting the buckling is less significant in comparison with the total axial friction force developing along the pipeline. The following expressions, $F_{\sigma_\phi^2}$, $F_{\sigma_I^2}$ are an empirical reduction factor in the variance of the PDF obtained from Eq. 3.10. The applicability range is, $q_d[2\text{kN/m}, 9\text{kN/m}] \cup \theta[3^\circ, 12^\circ]$ for $F_{\sigma_\phi^2}$ and $F_{\sigma_I^2}$:

$$F_{\sigma_\phi^2} = \frac{q_d + 5}{7} \quad (3.61)$$

$$F_{\sigma_I^2} = \frac{16\theta}{153} - \frac{13}{51} \quad (3.62)$$

3.3 Results

To ensure the applicability of these reduction factors, it was empirically verified to never reduce the variance below that of that obtained from the FE analysis for the studied cases. Also, that this condition holds up to 10000 trials to verify convergency. PDFs obtained from the FEM analysis is

it compared with the PDFs obtained from the empirical equations. For the parameters controlling the critical buckling force.

3.3.1 Empirical equation

Eq. 3.10 was fitted after the 252 parametric cases. An example set of 18 cases is shown in Table 3.3. A new normally distributed model error was fitted with $\mu = E(X) = 1.008$, $\sigma^2 = Var(X) = 0.001$. Proving the assumption made on previous studies^[2] still holds conservative, if used with the Eq. 3.10. The probability density function (PDF) of the model error and the histogram of the true/predicted ratios are shown in Fig. 3.6. Where Q_{effFE}/Q_{eff} it is the ratio, between the numerical values obtained from the FE analysis for the critical buckling force. And the numerical values over Empirical Eq. 3.10.

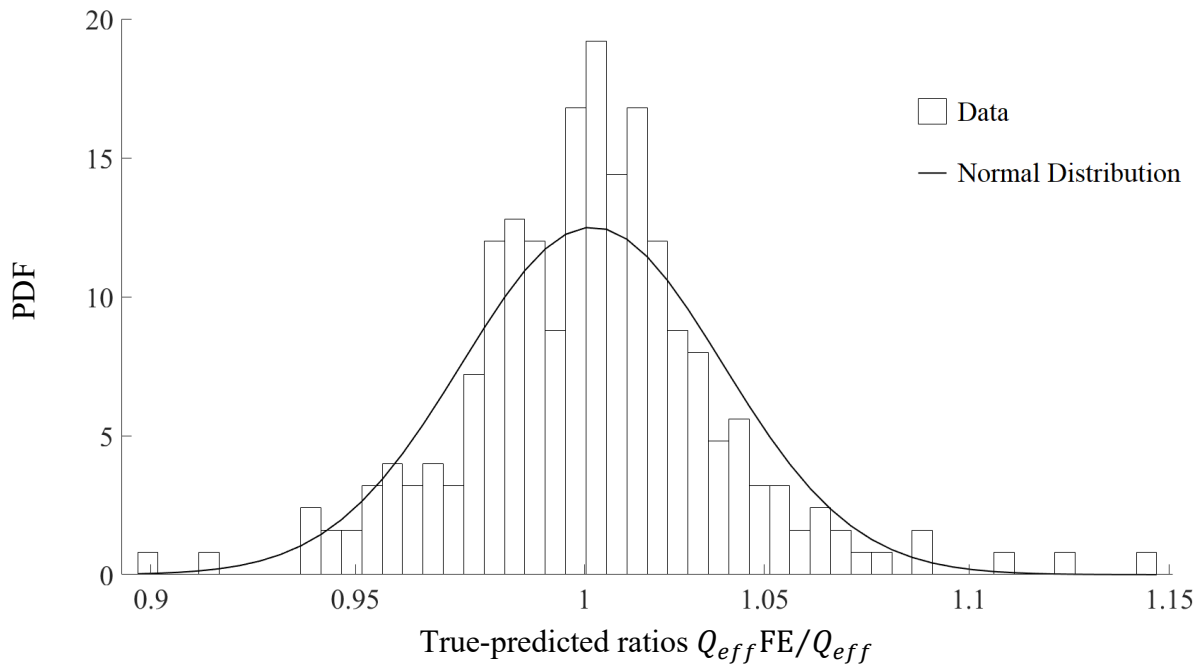


Figure 3.26 The best fitting Model error B

A statistical analysis was performed to assess the variability and best fitting distribution Q_{eff} due to random soil friction angle. The most convenient distribution to characterize the critical buckling force is Lognormal for simplicity. The improvement of Kernel and GEV are not significant, having only marginally better likelihood.

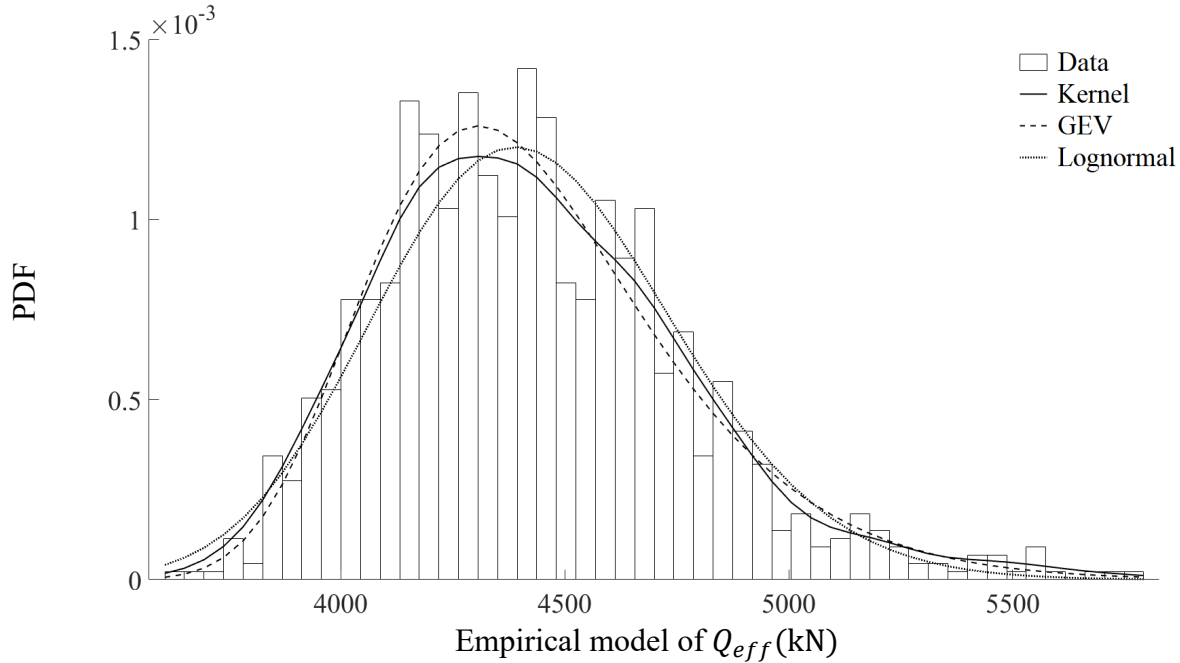


Figure 3.27 Empirical model of Q_{eff} , by maximum likelihood estimator Eq. 3.10. Case 1

For all the cases in the metric analysis a Lognormal distribution of Q_{eff} was fitted for all 252 analyses. The biggest model errors in the empirical equation were about 10% in three cases. Observed in combination of the largest dynamic downforce, and sharpest imperfection type:

Case	Imp $\theta(^{\circ})$	OD ($^{\circ}$)	Grade	q_s (kN/m)	q_d (kN/m)	w_{tot} (kN/m)	$\bar{\sigma}_h$	Q_{eff} (kN/m)		
								FE	Q_{eff}	Error%
166	3	24	X80	12	9	16.32	60	-5270	-4599	-12.73
202	3	24	X65	12	9	16.32	60	-3681	-4104	11.51
220	3	16	X65	12	9	13.88	60	-2309	-2529	9.54

Table 3.8 Largest error cases in empirical Eq. 3.10 vs FE analysis.

Largest errors in the empirical equation occur when dealing with the sharpest imperfection and the biggest soil resistance but only in three particular cases.

The use of the empirical Eq. 3.10 alone does not account for the effects of the soil spatial variability. The implicit assumption being, the soil is perfect homogenous. Hence, one can obtain over conservative results of the Q_{eff} variance while performing reliability analysis while using the lumped empirical variable that accounts for the soil resistance. After the parametric analysis it was shown that the biggest overestimation is about one order of magnitude. As show in Fig. 3.8

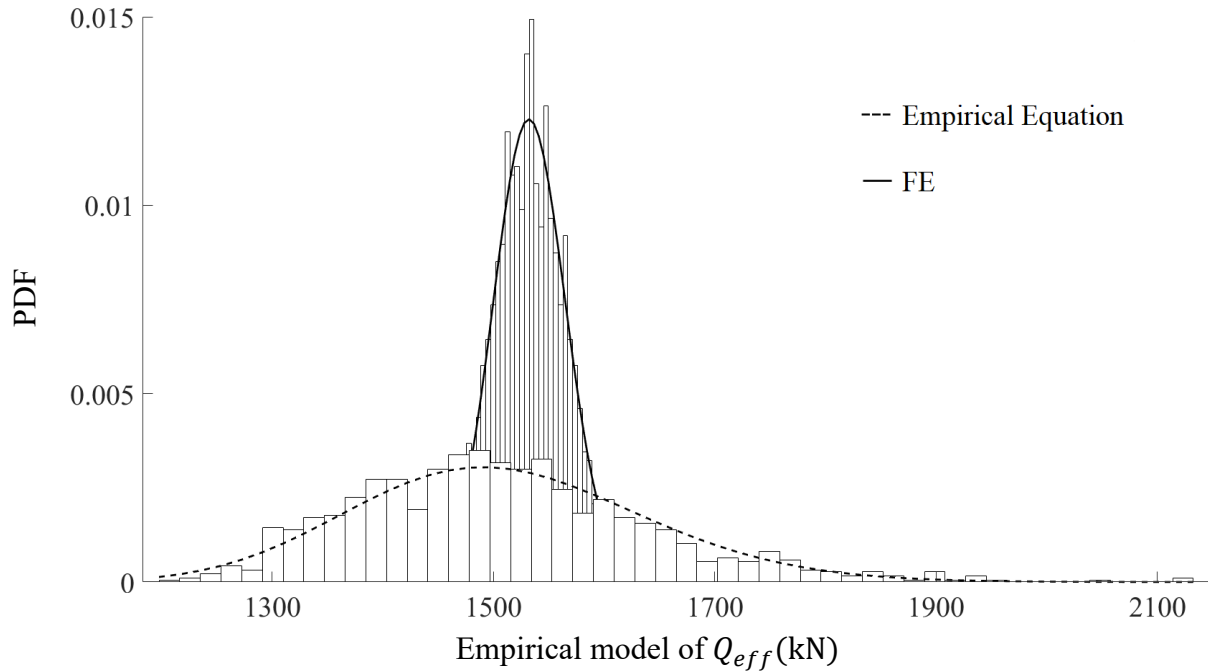


Figure 3.28 Variability comparison between, the empirical Q_{eff} vs FE Q_{eff} Case 3

Results obtained form the empirical equation, are equivalent to those obtained directly from FE model where the soil has perfect correlation. Note that empirical equations yield the most conservative values in most cases and also yield wider variability, when applied on RBDA methods.

Following the method to develop the empirical equation a set of base cases were studied. To obtain the variability of Q_{eff} due to the inherent variability of the soil friction angle. As show in following figures. The linear reduction factors form Eq. 3.19 and Eq. 3.20 were obtained from the parametric analysis. The variability of the empirical Eq. 3.10 was compared with the variability obtained directed from the numerical models over 1000 simulations. These results are summarized on Table 3.3.

case	FE	Eq. 3.10		Random Field FE	
	Q_{eff}	Q_{eff}	E(X) Var(X)	Q_{eff}	E(X) Var(X)
1	-4465	-4413	111999	-4465	1137
2	-2738	-2750	41423	-2738	506
3	-1541	-1521	17258	-1541	1002
4	-3807	-3687	83494	-3807	1344
5	-2252	-2283	32514	-2252	380
6	-1249	-1236	11076	-1249	460
7	-4825	-4905	141555	-4825	82
8	-3060	-3067	55924	-3060	334
9	-1742	-1716	20891	-1742	415
10	-3728	-3634	69952	-3728	2938
11	-2202	-2249	31515	-2202	89
12	-1224	-1216	10942	-1224	468
13	-2810	-2773	42215	-2810	2183
14	-1625	-1698	16946	-1625	286
15	-895	-883	6596	-895	308
16	-4261	-4193	99079	-4261	2085
17	-2579	-2608	41581	-2579	168
18	-1448	-1434	15725	-1448	454

Table 3.9 Comparison of Q_{eff} considering the soil spatial variability from FE models vs the empirical values.

3.4 Conclusions

A parametric analysis was conducted to investigate the effects of the soil spatial variability on the UHB phenomena for onshore pipelines, laydown over hill-type imperfections and constructed with

cold formed joints. The scope of the parametric analysis includes 252 parametric cases. The studied parameters are: pipe diameter, steel grade, imperfection size, operating internal pressure and soil. A result matrix was formed to fit an empirical equation to estimate the critical UHB load.

The resulting empirical expression has a maximum absolute error less than 5% with respect to the deterministic FE parametric analysis. This represents a 50% increase accuracy with respect to similar equations [2]. A model error was calibrated using Maximum Likelihood criteria. of equations can be used to account for the effects of the soil spatial variability in simplified manner. New equation always underestimates the critical buckling force. The proposed empirical equations yield conservative values to asses the variability of the critical buckling for all applicable cases.

A pair of conservative variance reduction factors for the critical UHB empirical equation is proposed to account for the effects of the soil spatial variability in the upheaval buckling problem. The proposed expressions are simple and can be readily implemented in RBDA analysis to assess the safety of cold formed pipeline bends, laid down over hill-top crest type of imperfections. The variability of the critical buckling is adjusted considering the imperfection shape and the soil dynamic download. The most dominant parameters were identified in order of relevance. The imperfection shape, the soil dynamic download force and the pipeline mechanical properties. The soil being the dominant source of uncertainty.

3.5 References

1. Liu, R., and S. Yan. 2013. “Brief history of upheaval buckling studies for subsea buried pipeline”. *J. Pipeline Syst. Eng. Pract.* 4 (3): 170–183.
2. Matheson, I., Zhou, W., Zhou, J., & Gailing, R. 2008. “An upheaval buckling limit state function for onshore natural gas pipelines”. In *International Pipeline Conference Vol. 48593*, pp. 781-791.
3. Taylor, N., and Tran, V. 1996. “Experimental and theoretical studies in subsea pipeline buckling.” *Marine Struct.*, 9(2), 211–257.
4. Argonne National Laboratory, S.M. Folga. 2007. “Natural Gas Pipeline Technology Overview” <https://corridoreis.anl.gov>.
5. Wang, Z., Tang, Y., Feng, H., Zhao, Z., & Liu, H. 2017. “Model Test for Lateral Soil Resistance of Partially Embedded Subsea Pipelines on Sand during Large-Amplitude Lateral Movement”. *Journal of Coastal Research*, 333, 607–618.
6. Maltby, T., Calladine, C. 1995a. “An investigation into upheaval buckling of buried pipelines-I”. *Theory and analysis of experimental observations. Int.J.Mech.Sci.* 37(9), 943–963.

7. Maltby, T., Calladine, C. 1995b. "An investigation into upheaval buckling of buried pipelines-II". Theory and analysis of experimental observations. *Int.J.Mech.Sci.*37(9),965–983.
8. Saadawi, Hisham. 2001. "Upheaval Buckling of Gas Injection Pipelines Onshore Abu Dhabi - A Case Study." Paper presented at the SPE Middle East Oil Show, Bahrain.
9. Palmer, A.C. and Williams, P.J. 2003 "Frost heave and pipeline upheaval buckling". *Canadian Geotechnical Journal*, 40: 1033-1038
10. Nixon, J. (Derick), & Burgess, M. 1999. "Norman Wells pipeline settlement and uplift movements". *Canadian Geotechnical Journal*, 36(1), 119–135.
11. Palmer, A. C., Ellinas, D.M. Richards, and Guijt J. 1990. "Design of submarine pipelines against upheaval buckling". *Proc. 22nd OTC*, Houston, Texas, pp. 540-550
12. Taylor, N., & Tran, V. 1996. "Experimental and theoretical studies in subsea pipeline buckling. *Marine Structures*", 9(2), 211-257.
13. American Lifelines Alliance (ALA) 2005. "Guidelines for the design of Buried Steel Pipe".

14. Det Norske Veritas (DNV) 2007. “Global Buckling of Submarine Pipelines—Structural Design due to High Temperature/High Pressure”, DNV-RP-F110, Det Norske Veritas, Baerum, Norway.
15. Galler, R., Volderauer, C., Marcher, T. et al. 2013 “Numerical Simulation in the Field of Geotechnics and Underground Engineering—Examples of Research and Development Projects”. Berg Huettenmaenn Monatsh 158, 189–197.
16. PASS piping and equipment analysis and sizing suite 2021 “Upheaval Buckling of Buried Pipelines” www.passuite.com.
17. Hunt GW, Bolt H, Thompson J. 1989 “Structural localization phenomena and the dynamical phase-space analogy”. Proceedings of the Royal Society of London A: Mathematical, Physical & Engineering Sciences. 425:245-67.
18. Rajeev, P., Robert, D. J., Thusyanthan, I., & Kodikara, J. 2013. “Reliability analysis of upheaval bucking of offshore pipelines”. Australian Geomechanics Journal, 48, 137-148.
19. Ismail, S., Najjar, S. S., & Sadek, S. 2018. “Reliability Analysis of Buried Offshore Pipelines in Sand Subject to Upheaval Buckling”. In Offshore Technology Conference. OnePetro.

20. Mesmar, S., Robert, D. J., Wang, J., & Haigh, S. K. 2011. "Upheaval Buckling Assessment Based on Pipeline Features". In Proceedings of the Annual Offshore Technology Conference.
21. White, D.J., Westgate, Z.J., and Y. Tian. 2014 "Pipeline Lateral Buckling: Realistic Modelling of Geotechnical Variability and Uncertainty". Paper presented at the Offshore Technology Conference, Houston, Texas.
22. Thusyanthan, N. I., et al 2008. "Upheaval buckling resistance of pipelines buried in clayey backfill". The 18th International Offshore and Polar Engineering Conference. OnePetro.
23. GL, Det Norske Veritas (DNV). 2017. "Recommended failure rates for pipelines". Energy Rep.
24. Ballet, J. P., and Hobbs, R. E. 1992. "Asymmetric effects of prop imperfections on the upheaval buckling of pipelines." *Thin-Walled Struct* 13(5), 355–373.
25. Phoon, K.-K., and Kulhawy, F.H. 1999. "Characterization of geotechnical variability". *Canadian Geotechnical Journal*, 36: 612–624.
26. Liu, R., Xiong, H., Wu, X., & Yan, S. 2014. "Numerical studies on global buckling of subsea pipelines". *Ocean Engineering*, 78, 62-72.

27. Nazari, A., Rajeev, P., & Sanjayan, J. G. 2015. Modelling of upheaval buckling of offshore pipeline buried in clay soil using genetic programming. *Engineering Structures*, 101, 306–317.

4 Upheaval buckling of onshore pipelines considering spatial cross correlation of the soil properties

Lateral and Upheaval buckling are possible global buckling mechanisms for pipelines that operate at high pressure and high temperature. Both, heat and pressure, induce axial compressive stresses on restrained pipes. Analogous to the Euler buckling, a pin-ended column made of commonly used steel pipes, may develop global buckling under modest axial loading, if it is left unsupported for only tens of meters along its length.

Above ground or pipelines laid-down on shallow buried trenches are more susceptible to Lateral Buckling due to inadequate provisions to allow for axial stress relief, during extreme operating conditions. Whereas, the Upward or Upheaval Buckling (UHB) can occur if there is sufficient lateral restraint and pipeline can only buckle by overcoming its self-weight and the vertical restraining measures.

Trenched or buried pipelines are design to protect the pipe from external actions and ensure structural stability. However, the first reported UHB incident took place in 1986, in the Danish sector of the North Sea, on a Maersk Oil's gas pipeline ^[1], generating concern and research efforts to better understand the phenomena ^[2-8].

Global buckling is not an ultimate failure mode. Buckled pipelines, inside the soil or even exposed out of the soil may have structural stability in post buckling configurations, within acceptable limits and could be easy repaired in a new stable state. However, this is not always the case. The

UHB may also lead several failure modes; fracture, fatigue, local buckling or collapse of the pipe cross-section and unacceptable plastic deformations due to excessive bending stress.

Although the global buckling mechanism of pipelines was understood in the open literature since 1974 ^[9], sporadic UHB events have taken place in the years after. Late as 2016, one thermally-driven UHB of a tar-sands pipeline and subsequent cool down from the turnaround was responsible for the rupture at Nexen Long Lake explosion ^[10]. This may be due to unforeseen conditions that sometimes arise in the most particular cases.

The understanding of the uplift capacity of buried pipelines is critical for designing an adequate burial depth that ensures the line stability against upheaval buckling. After the North Sea 1986 incident, robust efforts to predict the upheaval were made. Resulting in design recommendations ^[11-14]. Several geotechnical pipe-soil interaction models are available to estimate the critical UHB force by means of Finite Element (FE) analysis or by closed-form formulations that require experimental calibration. Such approaches consider, simplified force-displacement relationships to characterize drained or undrained soil conditions. Further, the experimental data of the soil characteristics and the project specific conditions, allows for some predictions for the amplitude and length of the UHB geometric, given thermal and pressure critical values, since early studies ^[7]. However, a clear track of the uncertainty involved in such approximations is not readily available.

Reliability-based design and assessment (RBDA) is the current practice for common structural design codes to ensure an acceptable standard of safety. Pipelines are critical infrastructure, that need to be design and operated safely for economic, environmental and public health reasons. A

key limit state of buried pipelines that operate at elevated temperatures is UHB. The assessment of the critical force for the onset of buckling depends on several key parameters that are random in nature.

Backfill soil materials have mechanical properties that could be generalized up to some extent. Extrapolating the soil properties could not be done without increasing the uncertainty in the translation. In contrast, the pipeline geometric and material properties are orders of magnitude more certainty due to quality manufacturing controls and design tolerances during construction. The natural variability of the soil cannot be reduced but can be account for. Usually, geotechnical designs consider the soil inherent variability by increasing the factor of safety and introduce redundancy at the expense of over-design.

A number of the soil property statistics reported in the geotechnical literature have been determined from total variability analyses that implicitly assume a uniform source of uncertainty. Clearly, these lumped statistics are only applicable to the specific set of site conditions, measurement techniques, correlation models for which the design soil properties were derived ^[15].

There are some soil parameters, that require additional consideration, apart from the provisions in the design recommendations ^[11-14]. Onshore, pipelines are installed through diverse environments from desert to swampy soils with poor soil cohesion. Soils with partial drainage conditions, due to low-permeability silty sand, has not been studied in detail. As well as the displacements required to mobilize a dynamic download reaction of the soil or even the static download for partially drained soils. It has been shown that these drainage rate effects can be significant, and the drainage

conditions will depend on the dimensionless velocity, of the soil particles, as suggested by previous researchers studying penetration and foundation problems ^[18]. A change in normalized pipeline velocity will trigger different degrees of drainage and generate different deformation mechanisms in the soil, and these will affect the force-displacement response, especially in silty sands.

The variability of the backfill materials used to restrain entrenched pipelines may be considerable. Depending on three main categories: 1.-The inherent variability of the natural soil due to geological forming processes. 2.- The conditioning from construction techniques. 3 Environmental and long-term effects during the life cycle of the pipeline.

Additional to the soil inherent variability. The uncertainty involved in forced-displacement models, recommended in design codes ^[11-14] is likely to vary from particular soil conditions that are not specified in the guidelines.

The uncertainty involved in the sampling from geotechnical surveys is a well-studied subject ^[15]. And can be adopted to assess the UHP risk of pipelines. The former uncertainty sources can be categorized by the randomness they introduce in soil models. The inherent variability being the greatest contribution and the sampling being the most certain parameter among them. Recent technological improvements have increased the availability of high-quality survey data to assess the pipeline geometric configuration and soil properties ^[16-17]. This opens the new possibility to adopt the RBDA methodologies for buried pipelines, by using more specialized statistical analysis. Leading to more efficient design, assessment of safe pipelines.

4.1 Motivation

From a parametric analysis in Chapter 3. The critical UHB load for onshore pipelines made with cold formed bends and laydown over hill type of imperfections, has proven to be dependent on the imperfection shape θ and the soil parameters; static download, $q_s(\gamma, H, D)$ and dynamic download $q_d(c, \phi, \gamma, H, D)$. One can assume, the pipe outside diameter D , and pipeline total self-weight w_{pipe} , have small variability when compared to the soil, parameters; cohesion coefficient c , the soil friction angle ϕ and density γ . The buried deep H can be measure in a newly precise ways ^[16-17] directly from surveys. Or at least, it is true that variability of D is fully independent from c , ϕ and γ . The small variability of D is due to manufacturing processes, and the buried deep H varies as a result of construction techniques, external or environmental processes and long-term effects, after construction. $Q_{\text{eff_base}}$ is the base-line case to calculate the critical axial loading given by,

$$Q_{\text{eff_base}} = -129 \left(\frac{w_{\text{tot}}}{\sin \theta/2} - 7.69 w_{\text{tot}}^{0.798} \right)^{0.567} \quad (4.1)$$

$$w_{\text{tot}} = w_{\text{pipe}} + q_s + q_d \quad (4.2)$$

Where:

- w_{tot} total download in kN/m
- w_{pipe} pipe weight per unit length
- q_s static soil download (i.e., overburden)
- q_d the dynamic soil download
- θ the angle of the imperfection detailed on Fig. 4.1

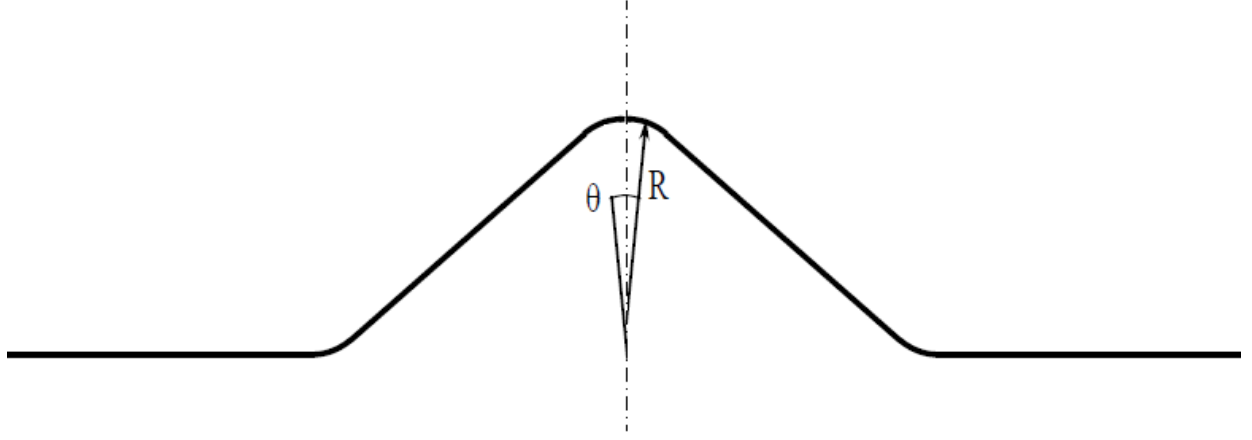


Figure 4.1 Diagram of buried pipeline over a Hill-Crest imperfection

$$q_s = \gamma H D \quad (4.3)$$

Where: γ bulk unit weight of soil
 H cover depth of the trench (0.7m)
 D outer diameter of the pipe

The dynamic component q_d , according to ALA ^[6] is given by:

$$q_d = Q_u = N_{cv} c D + N_{qv} \gamma H D \quad (4.4)$$

Where: N_{cv} vertical uplift factor for clay (0 for $c = 0$)
 c backfill shear strength
 N_{qv} vertical uplift factor for sand (0 for $\phi = 0^\circ$)
 ϕ backfill friction angle
 N_{cv} $2 \frac{H}{D} \leq 10$ applicable for $\frac{H}{D} \leq 10$
 N_{qv} $\frac{\phi H}{44D} \leq 10$ where $N_q = \exp(\pi \tan \phi) \tan^2 \left(45 + \frac{\phi}{2} \right)$

Two soil mobilization sensitive displacements were considered as 10mm and 40mm.

In Chapter 2, the effects of the spatial variability of the friction angle ϕ were investigated while keeping c and γ constant. By ignoring the spatial correlation struct of ϕ , overconservative

estimations for the actual variability of critical axial buckling force were obtained. It was proven that more realistic approximation can be employed to assess the pipeline susceptibility to UHB.

Diverse types of soils have been studied as random fields in other geotechnical, environmental and geological applications. The current state of the art mathematical models, allows for the use of all available statistical information to estimate the pipeline susceptibility to UHB in a more realistic manner. Including, empirical or project specific spatial-correlation structures of (c, ϕ, γ) and their spatial cross-correlation among each geotechnical property.

If the statistical properties are not available, one can always use simplified models at the expense of excessive mitigation measures being adopted, such as sleepers or counteract structures like helical piles or increase of the soil cover. The spatial variability of pipeline embedment can be approached in a more realistic way, by adopting state random fields models that have been successfully used in practice in other scientific disciplines. Although, the understanding of the physical mechanism of UHB is simple and accurate, improvements in RBDA to better account the uncertain involved may lead to more efficient design and assessment of pressurized gas pipelines. This paper illustrates how the influence of these physical mechanisms that drive embedment can be extracted from field survey data and then modelled synthetically in design analyses.

The soil properties can be model as random field, providing a numerical approach compatible with well accepted (EF) models to deal with inherent variability of each geotechnical property that can be resembled as one specific backfill material. In this approach, measurement fluctuations of the soil parameters are interpreted as random occurrences that are somehow related to each other

depending on how far apart the measurement points were taken. If a measurement is taken at the same location is very likely to be of identical value. Two measurements are considered to be statically independent if they are taken far enough from each other. This minimum separation is known as scale of fluctuation. The function that predicts how similar two measurements can be to each other is formally known as spatial variability structure. Such functions can be characterized from empirical data. The slight differences of measurements taken very close to the same location, are technically modelled as nugget or remanent uncertainty.

The random field theory has been used to investigate the random behavior of physical parameters in the context of a variety of classical problems ^[23-27].

There are two main objectives of this Chapter: 1.- Provide a review of selected ad hoc mathematical models that can be used to include the most specific statistical data in the assessment of pipelines against UHB. 2.- Investigate the effects of considering the spatial variability of the soil geotechnical properties c, ϕ, γ by adopting a more general and straightforward random field characterization.

4.2 Methodology

The spatial variability of the natural soil structure can be considered by modelling c, ϕ, γ as a Tri-variate random field. The choice of probability density function (PDF) and correlation structure is not straightforward as the information available in the literature is mostly for idealized soil types.

In a more realistic case, the PDF and correlation structure of a particular soil deposit is very likely to have unique statistics and spatial variability structure.

The observed values of these spatial variables are referred to as multivariate spatial data, which often possess two kinds of spatial correlation: spatial autocorrelation that exists between observations of an individual variable at different locations, and spatial cross-correlation that describes the correlation between two different variables measures at either the same or different locations. It is an important problem to model both kinds of spatial correlation. By appropriately accounting for and modeling the spatial correlation, efficient estimation, and better prediction can be achieved. For example, cokriging is a technique for linear prediction of one variable by making use of observed values of other variables, and can result in more precise prediction than the kriging methods that utilize only the spatial auto-correlation of this particular variable being predicted.

A number of commonly used models for the covariance structure, including the spherical, the exponential and the Gaussian provide no flexibility with regard to this local behavior and essentially assume it is known a priori. An alternative model for general adoption is a more robust model. There are general case of valid correlation functions the named after, Matérn. These models include a parameter that allows for any degree of differentiability for the random field and includes the exponential model as a special case and the Gaussian model as a limiting case.

Matérn class of covariograms has received much attention in recent years because it has a parameter that controls how smooth the process is. The reason is that these parameters determine how smooth the processes are and hence have more to do with the variogram cross-variogram at small lags. In the UHB case this type of correlation structures could allow to model the contribution

of multi scale properties (i.e., the soil lumps that are distributed uniformly along the trenches during construction, the graded granular materials to improve mechanical properties of the soil and smaller scale properties those found on silty soils).

A valid Matérn class of cross-covariance functions for multivariate random fields with any number of components procedure was developed. This method may allow for great flexibility on the characterization of specific soil conditions. However, a main draw back of this method is that there are number of fitting parameters for each Matérn class function, and these parameters can only be accurate optimized by Maximum likelihood procedures, that relay on even more parameters. Estimates can be hard to find for two reasons, one being the potential high dimension of parameter space, and the other being the constraints on the parameters that are necessary for a valid variogram. A method to address the former, Maximum likelihood the optimization was develop and it presented to provide an actionable procedure to model the soil parameter as realistic random fields.

Finally, to investigate the more general effects of the tri-variate $\mathbf{c}, \boldsymbol{\varphi}, \boldsymbol{\gamma}$ spatial variability of the soil. A comparison is present, by using a simple and robust method to simulate cross correlated random fields was first developed in 1990^[19].

In general, the simulation and generation of sample functions of stochastic fields is straight forward and can be performed by means of: (1) Spectral representation (Series expansion methods); (2) Average discretization methods like ARMA (auto-regressive moving average) modeling; and (3) Orthogonal expansion by means of covariance matrix decomposition procedures.

4.2.1 Tri-variate Friction Angle/Cohesion/Density spatial random field.

The Matérn class of positive definite functions has become the standard covariance model for univariate fields ^[20]. The popularity in large part is due to the work of who showed that the behavior of the covariance function near the origin has fundamental implications on predictive distributions, particularly predictive uncertainty ^[Stein (1999)]. The key feature of the Matérn is the inclusion of a smoothness parameter that directly controls correlation at small distances. The Matérn correlation function Given by:

A p -dimensional multivariate random field $\mathbf{Y} = \{Y(x_1)^T, \dots, Y(x_n)^T\}^T$ defined on a space region $\mathcal{D} \subset \mathbb{R}^d$, $d \geq 1$, where $Y_i(s)$ represents the i -th variable, $i = 1, \dots, p$, at locations $s \in \mathcal{D}$. \mathbf{Y} is Gaussian, if only its mean and cross-covariance functions are need to fully define \mathbf{Y} .

\mathbf{Y} is considered to be stationary if its cross-covariance satisfies,

$$\text{cov}\{Y_i(s_1) - Y_j(s_2)\} = C_{ij}(s_1 - s_2), \quad i, j = 1, \dots, p, \quad s_1, s_2 \in \mathcal{D} \quad (4.5)$$

\mathbf{Y} is considered to be isotropic if its cross-covariance satisfies,

$$C_{ij}(\mathbf{h}_1) = C_{ij}(\mathbf{h}_2) \quad \text{if} \quad \|\mathbf{h}_1\| = \|\mathbf{h}_2\| \quad \text{where} \quad \|\cdot\| \text{ is the Euclidian norm} \quad (4.6)$$

For Gaussian, stationary and isotropic fields one can use the spatial covariance function given by \mathbf{M} (Matérn).

$$\mathbf{M}(\mathbf{h}|\nu, \alpha) = \frac{1}{2^{\nu-1}\Gamma(\nu)} (\alpha\|\mathbf{h}\|)^{\nu} K_{\nu}(\alpha\|\mathbf{h}\|), \quad \mathbf{h} \in \mathbb{R}^d, \quad (4.7)$$

K_v is a modified Bessel function of the second kind, $v > 0$ is a smoothness parameter and $\alpha > 0$ is a scale parameter. The ratio $1/\alpha$ is the correlation length and v models a decrement in correlation per unit length, larger values correspond to smoother fields.

The cross-covariance function on this method is characterized by co-allocated covariance coefficients σ_{ij} , smoothness parameters v_{ij} and scale parameters α_{ij} in to a Matérn class function,

$$C_{ij}(h) = \sigma_{ij} M(h|v_{ij}, \alpha_{ij}), \quad i, j = 1, \dots, p, \quad h \in \mathbb{R}^d, \quad (4.8)$$

$$C_{ij}(h) = \frac{\frac{\sqrt{\sigma_{ii}\sigma_{jj}} \cdot R_{v_{ij}} \cdot \Gamma\left\{\frac{(v_{ii}) + (v_{jj})}{2}\right\}}{\sqrt{\Gamma(v_{ii}) \cdot \Gamma(v_{jj})}}}{\frac{\left(\frac{\alpha_{ii}^2 + \alpha_{jj}^2}{2}\right)^{\left(\frac{v_{ii}+v_{jj}}{2}\right)}}{\sqrt{\alpha_{ii}^{2v_{ii}} \cdot \alpha_{jj}^{2v_{jj}}}}} \cdot M\left(h \left| \frac{(v_{ii}) + (v_{jj})}{2}, \sqrt{\frac{\alpha_{ii}^2 + \alpha_{jj}^2}{2}} \right.\right) \quad (4.9)$$

For $i, j = 1, \dots, p$, where $R_{v_{ij}}$ are the cross-correlations and σ_{ii} are the variances for each p in the conventional sense. In the present case;

Friction Angle φ	$C_{11}(h) = \sigma_{11} M(h v_{11}, \alpha_{11})$	(4.10)
Soil Cohesion c	$C_{22}(h) = \sigma_{22} M(h v_{22}, \alpha_{22})$	
Soil Density γ	$C_{33}(h) = \sigma_{33} M(h v_{33}, \alpha_{33})$	

where the correlation is given by

$$\rho_{ij} = \frac{\sigma_{ij}}{\sqrt{\sigma_{ii}\sigma_{jj}}} \quad (4.11)$$

A multivariate spatial linear coregionalization model is considered that incorporates the Matérn class of covariograms. An algorithm is presented for the maximum-likelihood estimation of the parameters show in 4.10.

A version of (EM) algorithm has been developed by Zhu et al. (2005) for multivariate spatiotemporal generalized linear mixed model, in which the random effects or latent variables follow an LCM with exponential covariograms. In that we provide explicit expression in closed form for the estimate of each iteration, while these estimates are given by constrained maximization in [Zhu et al. (2005)]

A multivariate second-order stationary process. Let $\mathbf{Y}(s) = (Y_1(s), \dots, Y_p(s))'$, $s \in \mathbb{R}^d$ be a p -variate stochastic process, where $Y_i(s)$ represents the value of the i -th variable at location s . The process is said to be second-order stationary if for all $s, h \in \mathbb{R}^d$ and $i, j = 1, \dots, p$.

$$E[Y_i(s)] = m_i, \text{cov}[Y_i, Y_j(s + h)] = C_{ij}(h) \quad (4.12)$$

where the functions $C_{ij}(\cdot)$ are direct cov if $i = j$ and cross-cov if $i \neq j$. The matrix function $C(h) = C_{ij}(h)$ is the multivariate covariogram, that must be positive definite in the sense that for any spatial locations s_1, \dots, s_n and any vectors $a_i \in \mathbb{R}^p$, $i = 1, \dots, n$,

$$\text{Var}\left(\sum_i a_i' \cdot \mathbf{Y}(s_i)\right) = \sum_{i,j=1}^n a_i' C(s_i - s_j) a_j \geq 0 \quad (4.13)$$

Because of this constraint, it is a difficult problem to specify a valid multivariate covariogram that is not too complex to be estimated and yet capable of modeling a wide range of spatial correlations.

Only a few multivariate covariogram models have been proposed and used in analyzing real multivariate spatial data. The simplest model is the proportional correlation model ^[22]:

$$C(h) = \mathbf{V}\rho(h), \quad h \in \mathbb{R}^d \quad (4.14)$$

where \mathbf{V} is a $p \times p$ positive definite matrix and $\rho(h)$ is a correlation function. This proportional model can be used to build a nested covariogram in the form of:

$$C(h) = \mathbf{V}_0 + \sum_{k=1}^k \mathbf{V}_k \rho_k(h) \quad (4.15)$$

This covariogram corresponds a linear coregionalization model (LCM) [22] Subsection 5.6.5; [23], Chapter 26):

$$\mathbf{Y}(s) = \mu(s) + \sum_{k=0}^k \mathbf{V}_k \rho_k(h) \quad (4.16)$$

for each k , \mathbf{V}_k there is a positive semi-definite matrix and $\rho_k(h)$ is a correlogram that depends on some additional parameters. Rackwitz ^[24] provides examples for $\rho_k(h)$ as exponential or spherical.

$$C(h) = \mathbf{V}_0 + \sum_{k=1}^k \mathbf{V}_k \rho_k(h) \quad (4.17)$$

where $X_0(s)$ is a stationary but uncorrelated p -variate process with mean 0, that is;

$$E[Y_0(s)] = 0, \text{cov}[X_0(s), Y_0(s+h)] = \mathbf{V}_{0\{h \neq 0\}} \quad (4.18)$$

$X_k(s)$ is a p -variate stationary process with mean 0 and a multivariate covariogram $\mathbf{V}_k \rho_k(h)$. The $(1+k)$ processes are uncorrelated in the sense that for any $k \neq j$,

$$\text{cov}[X_k(s), X_j(\tilde{s})] = 0, \quad \forall s, \tilde{s} \quad (4.19)$$

If $\rho_k(h)$ is a Matérn type correlation function is fully defined by $\psi_k = (v_k, \phi_k)'$ as

$$\rho(h; \psi) = \frac{1}{2^{\nu-1}\Gamma(\nu)} \left(\frac{2\nu^{\frac{1}{2}}\|h\|}{\phi} \right)^{\nu} K_{\nu} \left(\frac{2\nu^{\frac{1}{2}}\|h\|}{\phi} \right) \quad (4.20)$$

and K_{ν} is the modified Bessel function of order ν as discussed by Abramowitz. The parameter ν_k control the smoothens of the process $\mathbf{X}_k(s)$, $k = 1, \dots, k$, which different smoothness parameters, are capable of representing different scales of variation.

Goulard and Voltz (1992) developed an algorithm for estimating \mathbf{V}_k in the linear coregionalization model when the correlograms ρ_k are known. Hence, their method does not estimate the correlogram parameters such as

ν_k and ψ_k , $k = 1 \dots k$. That method is an extension of the least squares fitting of variogram in the univariate case. It first calls for non-parametric estimation of the direct variograms and cross-variograms γ_{ij} at some lags h_1, \dots, h_N and then minimizes through an iterative procedure

$\sum_{j=1}^N \text{tr} \left(\hat{\mathbf{Y}}(h_j) - \mathbf{Y}(h_j) \right)^2$, where $\mathbf{Y}(h)$ is the variogram matrix whose (i, j) -th element is

$$\gamma_{ij}(h) = (1/2) \text{cov}[Y_i(s+h) - Y_i(s), Y_j(s+h) - Y_j(s)] \quad (4.21)$$

and $\hat{\mathbf{Y}}(h_j)$ is the empirical variogram matrix. The minimization is subject to the constraint that the estimates of the matrices \mathbf{V}_k are all positive semi-definite.

There

The EM algorithm is applied when there are missing values or latent variables. In the LCM (3), the processes $\{X_k(s)\}$, $k = 1, \dots, k$ are unobservable, and therefore the EM algorithm can be applied. We first introduce the following notations before introducing the EM algorithm. Recall that $\mathbf{Y}(s) = \left(Y_1(s), \dots, Y_p(s) \right)'$ is a p -variate process. Let s_1, \dots, s_n be the sampling locations

where at least one of the p variables is observed and Y be the vector of all observations. Hence Y consists of all those $Y_i(s_j)$ that are observed. Let $\mathbf{X}_{ki}(s)$ be the i -th element of $\mathbf{X}_k(s)$ as

$$\mu = (\mu_1, \dots, \mu_p)' = E(\mathbf{Y}(s)) \quad (4.22)$$

$$\mathbf{X}_{ki} = (\mathbf{X}_{ki}(s), \dots, \mathbf{X}_{ki}(s))', \quad \mathbf{X}_k(s) = (\mathbf{X}'_{k1}, \dots, \mathbf{X}'_{kp})' \quad (4.23)$$

$$\mathbf{X} = (\mathbf{X}'_2, \dots, \mathbf{X}'_p)' \quad (4.24)$$

$$\mathbf{Y}_i = (Y_i(s_n), \dots, Y_i(s_n)), \quad \mathbf{Y}^* = (\mathbf{X}'_1, \dots, \mathbf{X}'_p)' \quad (4.25)$$

$$R_k(\psi_k) = (\rho(s_i - s_j), \psi_k)_{i,j=1}^n, \quad \Sigma_k(\psi_k) = V_k \otimes R_k(\psi_k) \quad (4.26)$$

where \otimes is the Kronecker product. Note that we do require that at each of the location s_i , all p variables $Y_1(s_i), \dots, Y_p(s_i)$ are observable. Hence the observed vector \mathbf{Y} may be a subset of \mathbf{Y}^* . The complete-data log likelihood is given by

$$\begin{aligned} \text{Log } L(\theta, \mathbf{Y}^*, \mathbf{X}) = & -\frac{1}{2} \log(\Sigma_0) - \frac{1}{2} \left(\mathbf{Y}^* - \sum_{k=1}^k \mathbf{X}_k - \mu \otimes \mathbf{1} \right)' \Sigma_0^{-1} \left(\mathbf{Y}^* - \sum_{k=1}^k \mathbf{X}_k - \mu \otimes \mathbf{1} \right) \\ & - \frac{1}{2} \sum_{k=1}^k \left(\log(|\Sigma_k(\psi_k)| + \mathbf{X}'_1 \Sigma_k^{-1}(\psi_k) \mathbf{X}_k) \right) \end{aligned} \quad (4.27)$$

where $\theta = (\mu, V_0, V_k, \psi_k, k = 1, \dots, k)$ denotes all parameters in the LCM. The EM iterates as follows. At each iteration, there are two steps, the E-step and the M-step. The E-step find the conditional expectation of the complete-data log likelihood. Specifically, given the estimate θ^m in the m -th, compute the conditional expectation of the complete-date log likelihood

$$Q(\theta | \theta^{(m)}, \mathbf{Y}) = E_{\theta^{(m)}}[(\log L(\theta, \mathbf{Y}^*, \mathbf{X}) | \mathbf{Y})] \quad (4.28)$$

where the conditional expectation is evaluated under the parameter $\theta = \theta^{(m)}$. At the M-step, $Q(\theta|\theta^{(m)}, \mathbf{Y})$ is maximized with respect to θ and the new estimate is

$$\theta^{(m+1)} = \text{ArgMax } Q(\theta|\theta^{(m)}, \mathbf{Y}) \quad (4.29)$$

we now show that the maximization can be carried out mostly in closed-form. In view of Eq. 4.27, $Q(\theta|\theta^{(m)}, \mathbf{Y})$ is a sum of $(1 + k)$ terms, each of which depends on a different subset of parameters. Hence maximizing $Q(\theta|\theta^{(m)}, \mathbf{Y})$ can be broken down into several separate maximization problems. Specifically, $V_k^{(m+1)}$ and $\psi_k^{(m+1)}$, $k \geq 1$ maximize

$$-E_{\theta^{(m)}}[\log|\Sigma_k| + \mathbf{X}'_k \Sigma_k^{-1} \mathbf{X}_k] \quad (4.30)$$

which, because of $\log|\Sigma_k| = n\log|V_k| + p\log|R_k(\psi_k)|$ and $\Sigma_k^{-1} = V_k^{-1} \otimes R_k^{-1}(\psi_k)$ can be written as

$$-n \cdot \log|V_k| - p \cdot \log|R_k(\psi_k)| - \sum_{i,j=1}^p v_{ij,k} \cdot E_{\theta^{(m)}}[\mathbf{X}'_{ki} \cdot R_k^{-1}(\psi_k) \cdot \mathbf{X}_{kj} | \mathbf{Y}] \quad (4.31)$$

where $v_{ij,k}$ is the (i, j) th element of V_k^{-1} . From the well-known property of matrix derivative [Schott 1997]

$$-\frac{\partial \log|V_k|}{\partial v_{ij,k}} = \frac{\partial \log|V_k^{-1}|}{\partial v_{ij,k}} = \text{tr} \left(\frac{\partial V_k^{-1}}{\partial v_{ij,k}} \right) = d_{ij} \sigma_{ij,k} \quad (4.32)$$

where d_{ij} is 2 if $i \neq j$ and 1 otherwise. It follows immediately that the derivative of with respect to $v_{ij,k}$ is

$$d_{ij} (n \cdot \sigma_{ij,k} - E_{\theta^{(m)}}[\mathbf{X}'_{ki} \cdot R_k^{-1}(\psi_k) \cdot \mathbf{X}_{kj} | \mathbf{Y}]) \quad (4.33)$$

hence, for any fixed ψ_k , Eq. 4.26 as a function of V_k or V_k^{-1} is maximized at $V_k = V_k^m(\psi_k)$ this trace equals p and 4.31

$$-n \cdot \log|V_k^m(\psi_k)| - p \cdot \log| R_k(\psi_k)| - np \quad (4.34)$$

Therefore, in the EM algorithm, estimates for ψ_k and $V_k(k = 1, \dots, k)$ are updated by

$$\psi_k^{(m+1)} = \text{ArgMin}(n \cdot \log|V_k^m(\psi_k)| + p \cdot \log| R_k(\psi_k)|) \quad (4.35)$$

$$V_k^{(m+1)} = V_k^m(\psi_k^{(m+1)}) \quad (4.36)$$

Next, we give the closed-form solution for $V_0^{(m+1)}$ and $\mu^{(m+1)}$, which minimizes

$$\log(|\Sigma_0|) + E_{\theta(m)} \left[\left(\mathbf{Y}^* - \sum_{k=1}^k \mathbf{X}_k - \mu^m \otimes \mathbf{1} \right)' \cdot \Sigma_0^{-1} \cdot \left(\mathbf{Y}^* - \sum_{k=1}^k \mathbf{X}_k - \mu \otimes \mathbf{1} \right) \middle| \mathbf{Y} \right] \quad (4.37)$$

Thus, the new estimate has to satisfy $\mu^{(m+1)}$

$$E_{\theta(m)} = \left(\frac{\partial h(\mu)}{\partial \mu'} \middle| \mathbf{Y} \right) = 0$$

The EM iterative process can be summarized as follows:

Initial value θ^0 while $m = 0$;

Given θ^m , calculate $\theta^{m+1}(\mu^{m+1}, \mathbf{V}_0^{m+1}, \mathbf{V}_k^{m+1}, \psi_k^{m+1}, k = 1, \dots, k)$ by

$$\mu^{m+1} = \mu^m + \left(\frac{1}{n} \right) \mathbf{V}_0^m \mathbf{Y}_{ma}^m$$

$$\mathbf{V}_0^{m+1} = \mathbf{V}_0^m + \left(\frac{1}{n} \right) \mathbf{V}_0^m \mathbf{Y}_{ma}^m \mathbf{Y}_{ma}^m \mathbf{V}_0^m - \left(\frac{1}{n} \right) \mathbf{V}_0^m \mathbf{B}_0^m \mathbf{V}_0^m - \left(\frac{1}{n} \right)^2 \mathbf{V}_0^m \mathbf{Y}_{ma}^m \mathbf{Y}_{ma}^m \mathbf{V}_0^m$$

$$\psi_k^{m+1} = \text{ArgMin}(n \cdot \log|V_k^m(\psi_k)| + p \cdot \log| \mathbf{R}_k(\psi_k)|)$$

$$\mathbf{V}_k^{m+1} = \mathbf{V}_k^m(\psi_k^{(m+1)})$$

where \mathbf{B}_0^m is a $p \times p$ matrix whose (i, j) -th element is the trace of Γ_{ij}^m

given the estimate θ^m at the m -th iteration, Γ^m is the inverse of the covariance matrix

$$\text{Var}(\mathbf{Y}) = \mathbf{V}_0^m \otimes \mathbf{I}_n + \sum_{k=1}^k \mathbf{V}_k^m \otimes \boldsymbol{\psi}_k^{(m)}$$

$$\Gamma^m = (\Gamma_{ij}^m)_{ij=1}^p$$

were each Γ_{ij}^m is $n \times n$ defines

$$\mathbf{Y}^m = \Gamma^m (\mathbf{Y} - \mu^m \otimes \mathbf{I}_n)$$

$$\mathbf{Y}_i^m = \sum_{j=1}^k \Gamma_{ij}^m (\mathbf{Y}_j - \mu_j^m \mathbf{I}_n), \quad i = 1, \dots, p \quad (4.38)$$

The iteration of θ^{m+1} stops until $\|\theta^{m+1} - \theta^m\|^2 < \delta$

4.2.2 Simplified cross correlation model

A simple and straight forward method to study the tri-variate $\mathbf{c}, \boldsymbol{\varphi}, \boldsymbol{\gamma}$ spatial variability of the soil for the UHB problem is by statistical preconditioning. This method was developed by Shinozuka et al.1988. And is very straight forward. It uses a similar orthogonal decomposition of the cross-correlation matrix to “condition” a set of pseudo independent random variables that are to be used with for each single random field estimation.

The method requires all cross correlated fields over the domain to share an identical autocorrelation function and the cross-correlation structure between each pair of simulated fields to be simply defined by a cross correlation coefficient. Such relations result in specific properties of eigenvectors of covariance matrices of discretized field over the domain.

the covariance matrix Σ of the random vector $\{Z(x_1)^T, \dots, Z(x_n)^T\}^T \in \mathbb{R}$ must be positive definite for any positive integer n at any points x_1, \dots, x_n in \mathbb{R} . The covariance is often defined as a parametric family of functions whose members are proven to be positive definite.

$$C_{XX}(X_1, X_i) = \prod_{i=1}^{dim} \exp\left(\frac{\|X_1, X_i\|}{d_i}\right)^{pow_i} \quad (4.39)$$

The covariance matrix of \mathbf{X} is, corresponds to the 3 soil variables studied in this chapter, defined by

$$C_{XX} = \begin{bmatrix} \text{var}(X_1) & \text{cov}(X_1, X_2) & \text{cov}(X_1, X_3) \\ \text{cov}(X_2, X_1) & \text{var}(X_2) & \text{cov}(X_2, X_3) \\ \text{cov}(X_3, X_1) & \text{cov}(X_3, X_2) & \text{var}(X_3) \end{bmatrix} \quad (4.40)$$

Assuming homogeneity and zero mean of the stochastic field, ij -component of C_{XX} is obtained from the auto-correlation function $R_{XX}(\cdot)$ of the stochastic field as

$$C_{XXij} = \text{cov}(X_i, X_j) = R_{XX}(\xi_{ij}) \quad (4.41)$$

in which ξ_{ij} is a separation vector between two points i and j . The eigenvalues and eigenvectors of C_{XX} can be obtained by solving the following eigenequation:

$$C_{XX}\Phi_X = \Phi_X\Lambda_X \quad (4.42)$$

where Λ_X is the (diagonal) eigenvalue matrix and Φ_X is the modal matrix as follows:

$$\lambda_X = \begin{bmatrix} \lambda_1 & 0 & 0 \\ 0 & \lambda_2 & 0 \\ 0 & 0 & \lambda_3 \end{bmatrix}; \quad \Phi_X = [\Phi_1, \Phi_2, \Phi_3] \quad (4.43)$$

where λ_i , is the i th eigenvalue of C_{XX} such that

$$\lambda_1 \geq \lambda_2 \geq \lambda_3 \quad (4.44)$$

Also Φ_i , is the i th eigenvector of C_{XX} normalized to have a Euclidean length of 1, and orthogonal with Φ_j ($i \neq j$). Therefore

$$\Phi_X^T \Phi_X = I \quad (4.45)$$

in which I is identity matrix. Since the covariance matrix C_{XX} is symmetric, all the eigenvalues and eigenvectors are obtained as real values. If a vector $Z = (Z_1 Z_2 Z_3)^T$ is introduced as

$$Z = \Phi_X^T X \quad (4.46)$$

Expected value of Z is

$$E(Z) = \Phi_X^T X \quad (4.47)$$

Eq. 4.46 implies that if X has zero mean, Z is also zero mean. Utilizing Eq. 4.42 and 4.47, the covariance matrix of Z can be shown to be:

$$C_{ZZ} = E\{[Z - E(Z)][Z - E(Z)]\} = \Lambda_X \quad (4.48)$$

Since C_{ZZ} is found to be a diagonal matrix, Z_i ($i = 1, 2, \dots, n$) are uncorrected, if not independent, and their variances are λ_i ($i = 1, 2, \dots, n$), respectively. Thus, by generating a set of independent random variables Z , a corresponding set of correlated random variables X can be easily obtained

$$X = (\Phi_X^T)^{-1} Z = \Phi_X Z \quad (4.49)$$

The modal decomposition method can also be applied to a multivariate stochastic fields problem.

Consider an \mathbf{m} -variate random vector \mathbf{X} with dimension $n \times m$ as

$$\mathbf{X} = \{[X^1]^T [X^2]^T \dots [X^m]^T\} \quad (4.50)$$

$$\mathbf{X}^i = [X_1^i X_2^i \dots X_n^i]^T \quad (i = 1, 2, \dots, m) \quad (4.51)$$

The covariance matrix of the random vector \mathbf{X} is represented by

$$C_{XX} = \begin{bmatrix} C_{XX}^{11} & C_{XX}^{12} & \dots & C_{XX}^{1m} \\ C_{XX}^{12} & C_{XX}^{11} & \dots & C_{XX}^{2m} \\ \vdots & \vdots & \ddots & \vdots \\ C_{XX}^{m1} & C_{XX}^{m2} & \dots & C_{XX}^{mm} \end{bmatrix} \quad (4.52)$$

and each submatrix represents

$$C_{XX}^{ij} = \begin{bmatrix} \text{cov}[X_1^i, X_1^j] & \text{cov}[X_1^i, X_2^j] & \dots & \text{cov}[X_1^i, X_n^j] \\ \text{cov}[X_2^i, X_1^j] & \text{cov}[X_2^i, X_2^j] & \dots & \text{cov}[X_2^i, X_n^j] \\ \vdots & \vdots & \ddots & \vdots \\ \text{cov}[X_n^i, X_1^j] & \text{cov}[X_n^i, X_2^j] & \dots & \text{cov}[X_n^i, X_n^j] \end{bmatrix} \quad (4.53)$$

From a cross-correlation function $R_{XX}^{ij}(\cdot)$ between the zero-mean random vectors \mathbf{X}^i and \mathbf{X}^j the kl -component of the above submatrix is obtained as

$$\text{cov}[X_k^i, X_l^j] = R_{XX}^{ij}(\tau_{ij}) \quad (4.54)$$

where τ_{kl} is a separation vector between two points k and l with the following characteristics;

$$\tau_{kl} = -\tau_{lk} \quad (4.55)$$

The submatrices $C_{XX}^{ij} = (i, j = 1, 2, \dots, m)$ are generally not symmetric except when $R_{XX}^{ij}(\tau_{ij})$ is an even function of τ_{kl} . There is a general relationship between a pair of cross-correlation functions such as

$$R_{XX}^{ij}(\tau_{kl}) = R_{XX}^{ji}(-\tau_{kl}) \quad (4.56)$$

$$R_{XX}^{ij}(\tau_{kl}) = R_{XX}^{ji}(\tau_{lk}) \quad (4.57)$$

C_{XX} is always symmetric, regardless of the form assumed for the auto and cross-correlations. From Eq. 4.48. A truncated approximation or a complete simulated covariance matrix C_{ZZ}^* of \mathbf{Z} to approach C_{ZZ} can be obtained by

$$C_{ZZ}^* = \frac{1}{N_s} \sum_{j=1}^{N_s} \{Z(j)[Z_i(j)]^T - (\bar{Z}^*)(\bar{Z}^*)^T\} \quad (4.58)$$

$$\bar{Z}^* = \frac{1}{N_s} \sum_{j=1}^{N_s} Z(j) \quad (4.59)$$

where N_s is the sample size and $Z(j)$ is the j th sample vector of Z and \bar{Z}^* is the sample mean vector of Z . If sample vector $Z(j)$ is independent of each other, the estimators evaluated by Eq. 4.58 and 4.59 approach the covariance matrix and mean vector when $N_s \rightarrow \infty$ by the law of large numbers. To generate samples of a random vector Z of small size, a trigonometric expansion of the vector Z can be used.

$$Z_i(j) = \sqrt{2}C_i \sum_{m=1}^{N_j} \cos(\omega_k j \Delta t + \psi_k) \quad (i = 1, 2, \dots, n) \quad (j = 1, 2, \dots, N_s) \quad (4.60)$$

with $k = (m - 1)n + i$, $C_i = \sqrt{\lambda_i/N_f}$, N_f is the number of harmonics, ψ_k a random phase angle uniformly distributed from 0 to 2π , and ω_k the frequency.

$$\bar{Z}^* = \frac{1}{N_s} \sum_{j=1}^{N_s} Z(j) \quad (4.61)$$

then, the mean value of the sample is

$$\bar{Z}^* = \frac{\sqrt{2}}{N_s} C_i \sum_{m=1}^N \sum_{j=1}^N \cos(\omega_k j \Delta t + \psi_k) \quad (4.62)$$

$$\begin{aligned} \bar{Z}^* = \frac{\sqrt{2}}{N_s} C_i \sum_{m=1}^N \sum_{j=1}^{N/4} & \left[\cos(\omega_k j \Delta t + \psi_k) + \cos\left(\omega_k j \Delta t + \psi_k + \frac{k}{2} \pi\right) \right. \\ & \left. + \cos(\omega_k j \Delta t + \psi_k + k\pi) + \cos\left(\omega_k j \Delta t + \psi_k + \frac{3k}{2} \pi\right) \right] = 0 \end{aligned} \quad (4.63)$$

for $k = 1, 2, \dots, nN_f$

$$C_{ZZii}^* = \frac{1}{N_s} \sum_{j=1}^{N_s} [Z_i(j)]^2 = \frac{2}{N_s} C_i^2 \sum_{j=1}^{N_s} \left[\sum_{m=1}^{N_f} \cos(\omega_k j \Delta t + \psi_k) \right]^2 \quad (4.64)$$

The sample variance C_{ZZii}^* of Z_i , is actually λ_i

$$C_{ZZii}^* = \frac{2}{N_s} \frac{\lambda_i}{N_f} \sum_{j=1}^{N_f} \sum_{m=1}^{N_s} \cos^2(\omega_k j \Delta t + \psi_k) = \lambda_i \quad (4.65)$$

The orthogonal expansion of the harmonic functions is given by

$$\sum_{j=1}^{N_s} \cos(\omega_\alpha j \Delta t + \psi_\alpha) \cos(\omega_\beta j \Delta t + \psi_\beta) \quad (4.66)$$

$$\sum_{j=1}^{N_s} = \sum_{j=1}^{N_s} \frac{1}{2} (\cos[(\omega_\alpha - \omega_\beta)j \Delta t + \psi_\alpha - \psi_\beta] + \cos[(\omega_\alpha + \omega_\beta)j \Delta t + \psi_\alpha + \psi_\beta]) \quad (4.67)$$

$$\sum_{j=1}^{N_s} = 0 \quad \text{if } \omega_\alpha \neq \omega_\beta, \quad \sum_{j=1}^{N_s} = \frac{N_s \cdot \cos(\psi_\alpha - \psi_\beta)}{2} \quad \text{if } \omega_\alpha = \omega_\beta \quad (4.68)$$

using different set of N_f frequencies for different Z 's, the sample covariance of Z_i and Z_l can be shown to be

$$C_{ZZil}^* = \frac{1}{N_s} \sum_{j=1}^{N_s} Z_i(j) Z_l(j) = 0 \quad \text{if } i \neq l \quad (4.69)$$

the orthogonality of cosine functions is also utilized. Eq. 4.63, 4.66 and 4.69 show that the target value and covariance matrix of Z are exactly reproduced by the sample of size N_s by using Eq. 4.60 where the sample size is N_s

$$N_s = \frac{T}{\Delta t} = \frac{4T_1}{T_{nN_f}} = 4nN_f \quad (4.70)$$

The N_s represented by Eq. 4.70 may be a large number if the dimension of the random vector n is large. It can be approximated in a truncated form by using only the first M modes:

$$X \approx [\Phi_1 \Phi_2 \cdots \Phi_M][Z_1 Z_2 \cdots Z_M]^T \quad (4.71)$$

$$N_s = \frac{T}{\Delta t} = \frac{4T_1}{T_{N_f M/2}} = 2MN_f \quad (4.72)$$

where N_f must be large if the simulated random vector Z is to be approximately Gaussian.

Substituting Eq.4.60 into 4.71.

$$X_s(j) = \sqrt{2} \sum_{i=1}^M \sum_{m=1}^{N_f} \Phi_{si} \sqrt{\frac{\lambda_i}{N_f}} \cos(\omega_k j \Delta t + \psi_k) \quad (s = 1, 2, \dots, n) \quad (4.73)$$

Φ_{si} is the s -th component of vector Φ_i . If $M \times N_f$ is large, $X_s(j)$ is asymptotically Gaussian if M is sufficiently large. It is noted that the sample mean value is still exactly equal to zero while the sample covariances are approximately equal to the target values, even after mode truncation. If the stochastic field is homogeneous, the trace of C_{XX} represents the sum of the variances of $X_s(j)$.

The Karhunen–Loève expansion of a stochastic field $H(x, h)$ is based on the spectral expansion

Let C be a square symmetric positive definite, cross correlation matrix of order N_F with elements $C^{ij} \in (-1; 1)$ for $i \neq j$ and $C^{ij} = 1$ for $i = j$. C defines the correlation structure among N_F random fields. Here, each field is called H , instead of X to identify the simplified method, apart from the original formulation [1]. An approximate spectral representation of matrix C can be obtained from its characteristic representation:

$$\Phi^C = \begin{pmatrix} \Phi_1^C & \Phi_2^C & \dots & \Phi_{N_F,r}^C & \dots & \Phi_{N_F}^C \\ \phi_{1,1}^C & \phi_{1,2}^C & \dots & \phi_{1,N_F,r}^C & \dots & \phi_{1,N_F}^C \\ \phi_{2,1}^C & \phi_{2,2}^C & \dots & \phi_{2,N_F,r}^C & \dots & \phi_{2,N_F}^C \\ \vdots & \vdots & \vdots & \vdots & \dots & \vdots \\ \phi_{N_F,1}^C & \phi_{N_F,2}^C & \dots & \phi_{N_F,N_F,r}^C & \dots & \phi_{N_F,N_F}^C \end{pmatrix} \quad (4.74)$$

$$\Lambda^C = \begin{pmatrix} \Phi_1^C & \Phi_2^C & \dots & \Phi_{N_F,r}^C & \dots & \Phi_{N_F}^C \\ \text{diag}(\lambda_1^C & \lambda_2^C & \dots & \lambda_{N_F,r}^C & \dots & \lambda_{N_F}^C) \end{pmatrix} \quad (4.75)$$

$$\hat{C} = \Phi_I^C \Lambda_I^C [\Phi_I^C]^T \quad (4.76)$$

Block cross correlation matrix D of random variables). Let D be a squared symmetric matrix of order

$$D = \begin{pmatrix} H_1 & H_2 & \dots & H_{N_F,r} & \dots & H_{N_F} \\ H_1 & \begin{pmatrix} I & C^{1,2}I & \dots & C^{1,N_F,r}I & \dots & C^{1,N_F}I \\ \vdots & I & \dots & C^{2,N_F,r}I & \dots & C^{2,N_F}I \\ \vdots & \vdots & \vdots & \vdots & \dots & \vdots \\ \vdots & \vdots & \vdots & \vdots & \dots & \vdots \\ \vdots & \vdots & \vdots & \vdots & \dots & \vdots \\ H_{N_F} & \dots & \dots & \dots & \dots & I \end{pmatrix} \end{pmatrix} \quad (4.77)$$

$$\chi^D = \Phi^D (\Lambda^D)^{1/2} \xi \quad (4.78)$$

$$\chi^D = \{ [\chi_1^D]^T \quad [\chi_1^D]^T \quad \dots \quad [\chi_1^D]^T \}^T \quad (4.79)$$

$$H_i(x) = \sum_{j=1}^{N_{\text{var}}} \sqrt{\lambda_i} \cdot \chi_{i,j}^D \cdot \psi_k(x) \quad (4.80)$$

$$H_i(x) = \sum_{j=1}^{N_{\text{var}}} \frac{\chi_{i,j}^D}{\sqrt{\lambda_j^u}} [\Phi_j^u]^T \Sigma_{H(x)u} \quad (4.81)$$

N_{var} assembled in this way: matrix D consists of $(N_F \times N_F)$ blocks $C_{ij} \times I$, where I is the unit matrix of order N_{var} , and C_{ij} are elements of the cross correlation matrix C defined previously

C_{HH} is symmetric with real λ_H and Φ_H

$$H(x, \theta) = \sum_{j=1}^n \frac{\xi_j(\theta)}{\sqrt{\lambda_j^u}} [\Phi_j^u]^T \Sigma_{H(x)u} \quad (4.82)$$

$$\hat{H}_i(x) = \sum_{j=1}^{N_{\text{var}}} \frac{\chi_{i,j}^D}{\sqrt{\lambda_j^u}} [\Phi_j^u]^T \Sigma_{H(x)u} \quad (4.83)$$

Where the error if truncation is applied is given by

$$\varepsilon_D = \frac{\sum_{j=1}^{N_r} \lambda_j^D}{\sum_{j=1}^{N_{\text{var}} \cdot N_F} \lambda_j^D} = \frac{\sum_{j=1}^{N_{F,r}} N_{\text{var}} \cdot \lambda_j^C}{\sum_{j=1}^{N_F} N_{\text{var}} \cdot \lambda_j^C} = \frac{\sum_{j=1}^{N_{F,r}} \lambda_j^C}{\sum_{j=1}^{N_F} \lambda_j^C} = \varepsilon_C \quad (4.84)$$

4.2.3 Random Field Model Characterization

The optimal linear estimation method OLE was implemented to perform 1000 random field simulations to investigate the effects of tri-variate $\mathbf{c}, \boldsymbol{\varphi}, \boldsymbol{\gamma}$ spatial variability of the soil. The correlation structure was Type I exponential squared. And the soil proprieties described in Table 4.1.

For a few parametric cases, additional simulations were performed to identify the maximum variability between different soil stochastic conditions (i.e., perfect random, perfect homogenous). In Figure 7 and 8, 1000 simulations were performed for each soil idealization. One can observe the mean response in single solid line in middle. Follow by dash lines that were obtained from realizations considering the soil as a perfect random media with zero correlation in all points. Each dash line, represent the maximum observed response and for the minimum.

Case number	Imperfection	q_s (kN/m)	q_d (kN/m)	w_{tot} (kN/m)	Q_{eff} (kN/m)				
					FE	$Q_{eff}^{[2]}$	Error	Q_{eff}	Error
1	38.2	7.32	6	15.06	-	-4455	-0.21	-4415	-1.17
2	19.1	7.32	6	15.06	4465	-2708	-1.08	-2751	0.45
3	9.6	7.32	6	15.06	2738	-1514	-1.69	-1515	-1.30
4	38.2	7.32	2	11.06	1541	-3728	-2.08	-3688	-3.25
5	19.1	7.32	2	11.06	-	-2266	0.65	-2284	1.37
6	9.6	7.32	2	11.06	2252	-1267	1.49	-1231	-1.02
7	38.2	7.32	9	18.06	1249	-4948	2.55	-4907	1.63
8	19.1	7.32	9	18.06	4825	-3008	-1.72	-3069	0.24
9	9.6	7.32	9	18.06	3060	-1682	-3.46	-1709	-1.54
10	38.2	3.05	6	10.79	1742	-3676	-1.39	-3636	-2.58
11	19.1	3.05	6	10.79	3728	-2235	1.47	-2250	2.10
12	9.6	3.05	6	10.79	2202	-1249	2.09	-1211	-0.67
13	38.2	3.05	2	6.79	1224	-2814	0.14	-2774	-1.33
14	19.1	3.05	2	6.79	2810	-1710	5.24	-1698	4.29
15	9.6	3.05	2	6.79	1625	-895	6.86	-879	-1.37
16	38.2	3.05	9	13.79	-	-4235	-0.60	-4195	-1.63
17	19.1	3.05	9	13.79	4261	-2574	-0.17	-2610	1.12
18	9.6	3.05	9	13.79	2579	-1440	-0.56	-1429	-0.95

Table 4.1 Comparison of FE and Calculated Values for Effective Force for a pipeline that weights 1.741 (kN/m), material grade (448 MPa), D/t ratio (60), diameter (24 inches), and ratio between hoop stress and yield strength is (0.6)

4.3 Results

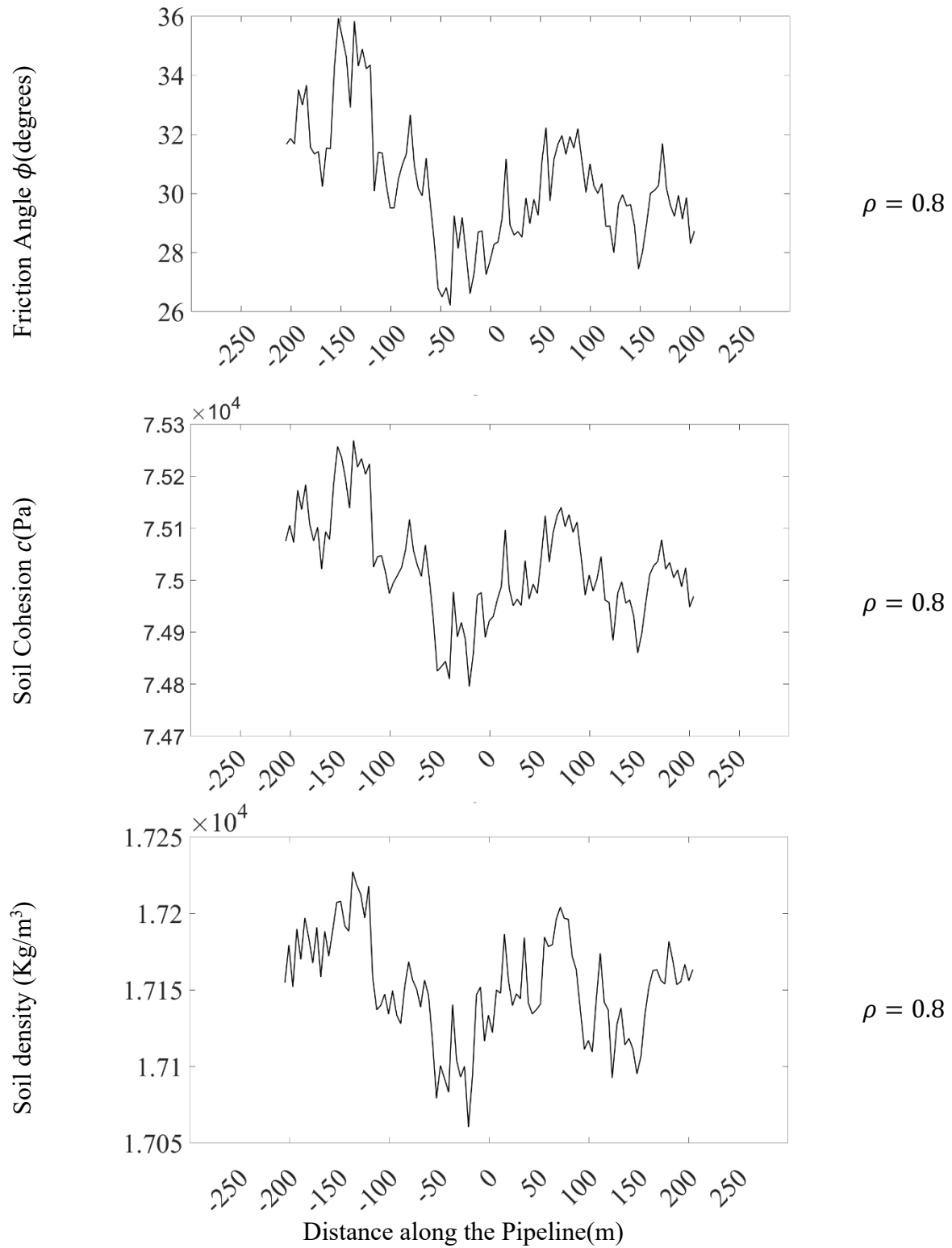


Figure 4.2 Cross correlation field, strong correlation between γ , ϕ and c

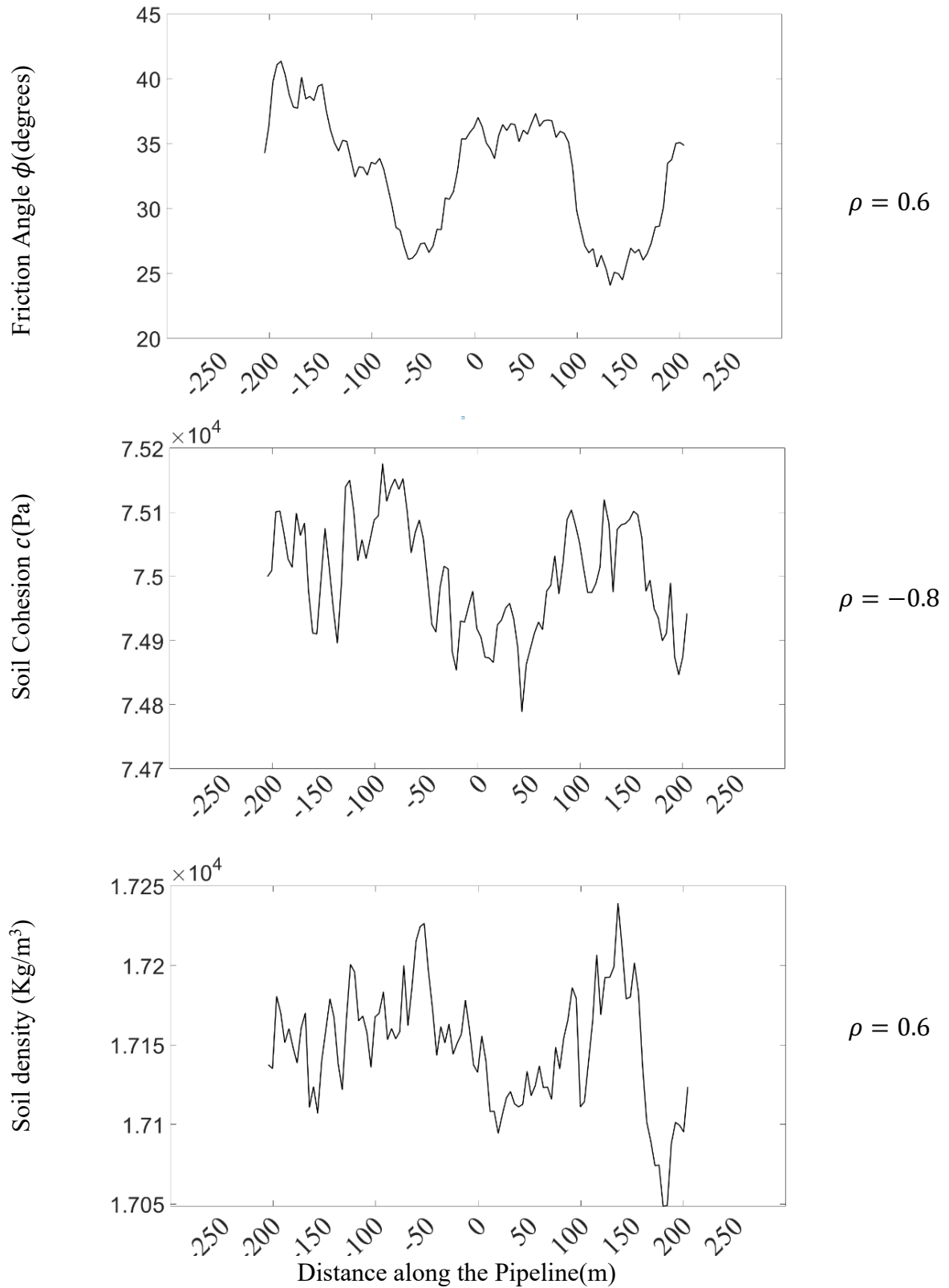


Figure 4.3 Cross correlation field, inverse correlation between γ and ϕ

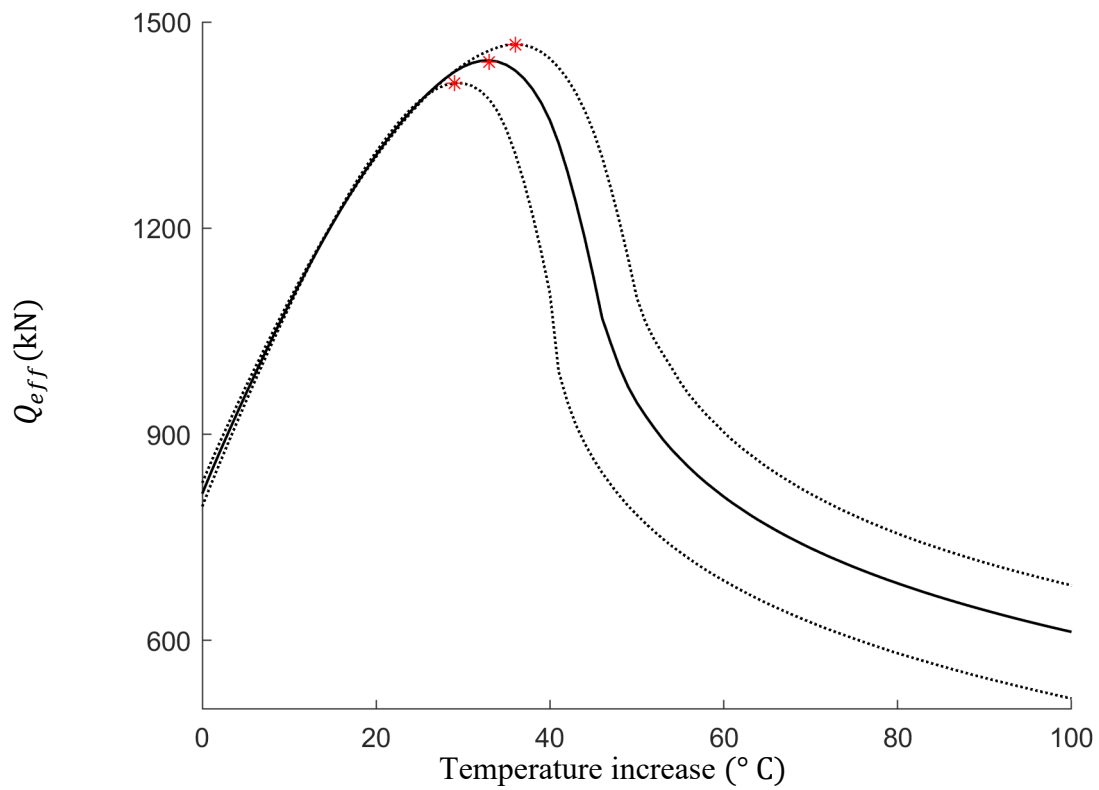


Figure 4.4 Mean Q_{eff} vs Max. and min. values of Q_{eff} . Case 1. From Table 4.1

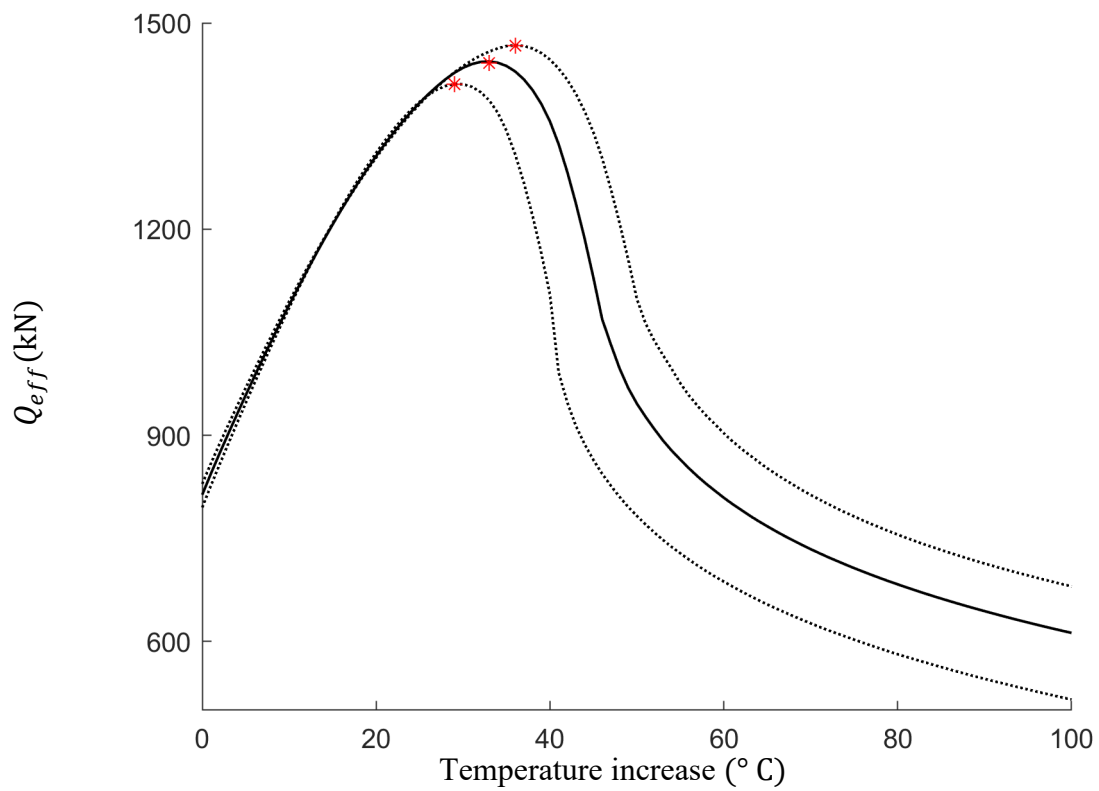


Figure 4.5 Mean Q_{eff} vs Max. and min. values of Q_{eff} . Case 2. From Table 4.1

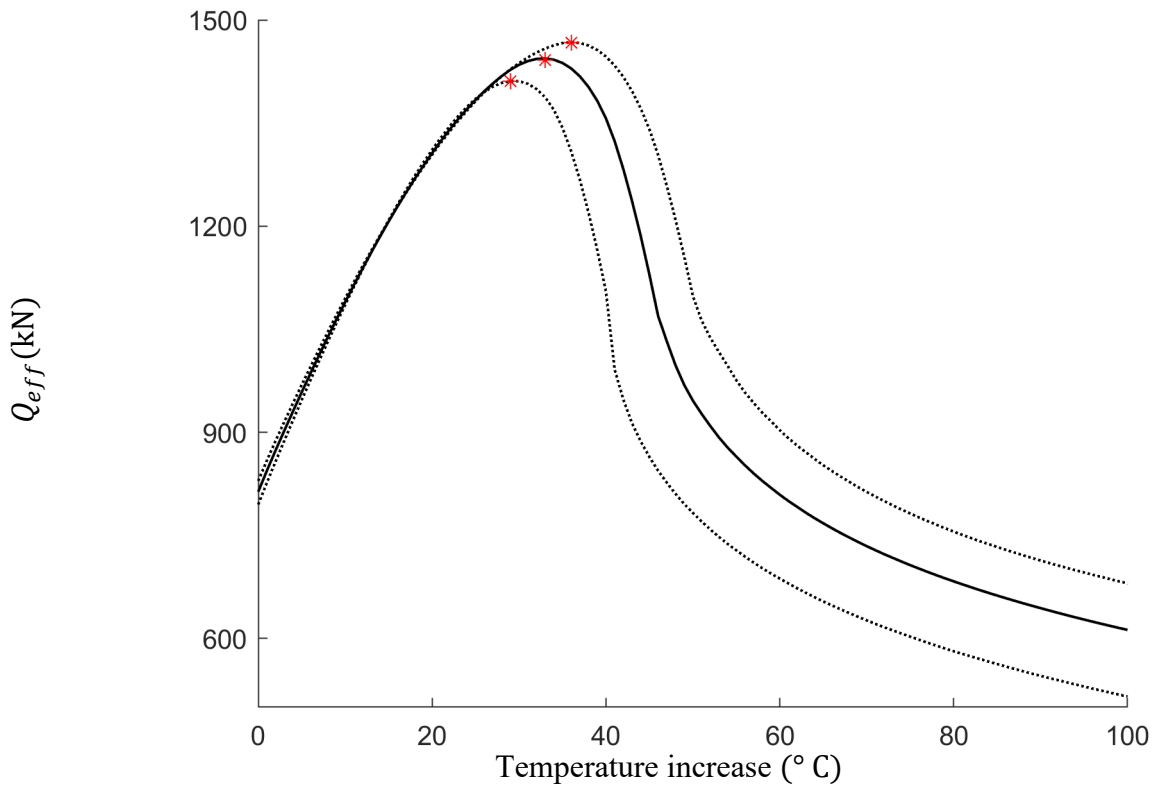


Figure 4.6 Mean Q_{eff} vs Max. and min. values of Q_{eff} . Case 3. From Table 4.1

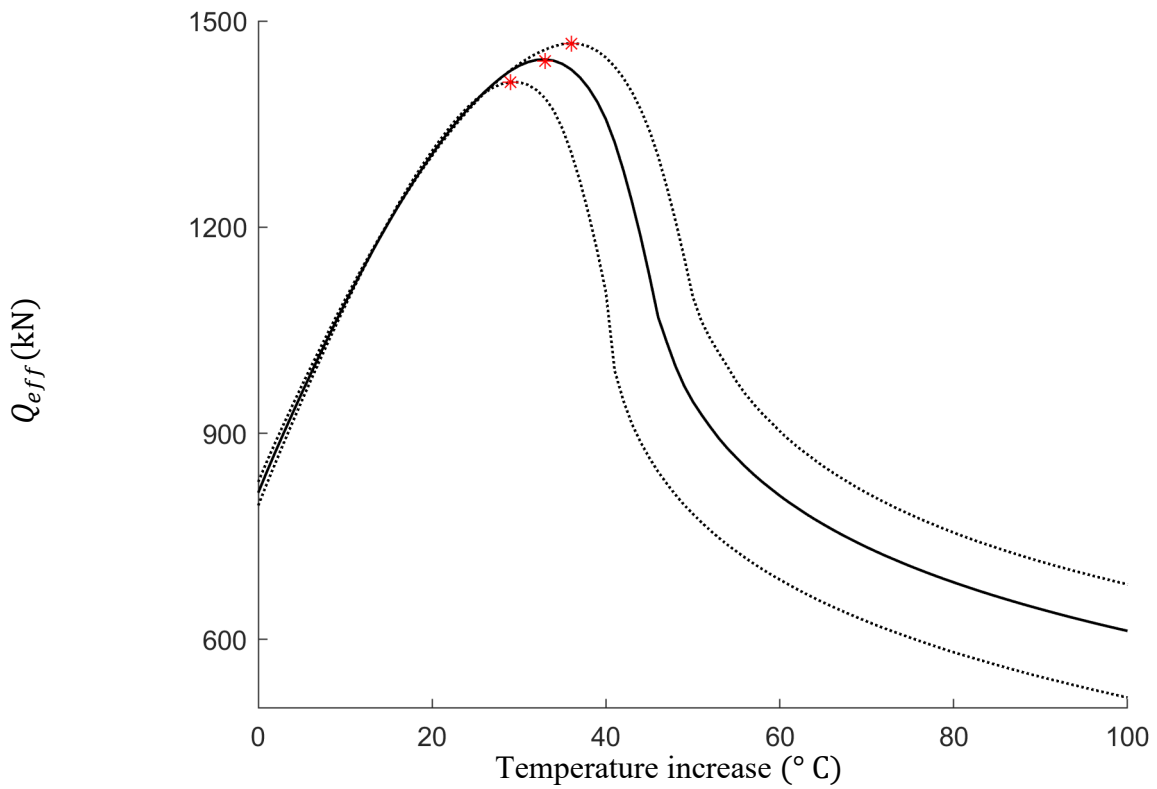


Figure 4.7 Mean Q_{eff} vs Max. and min. values of Q_{eff} . Case 4. From Table 4.1

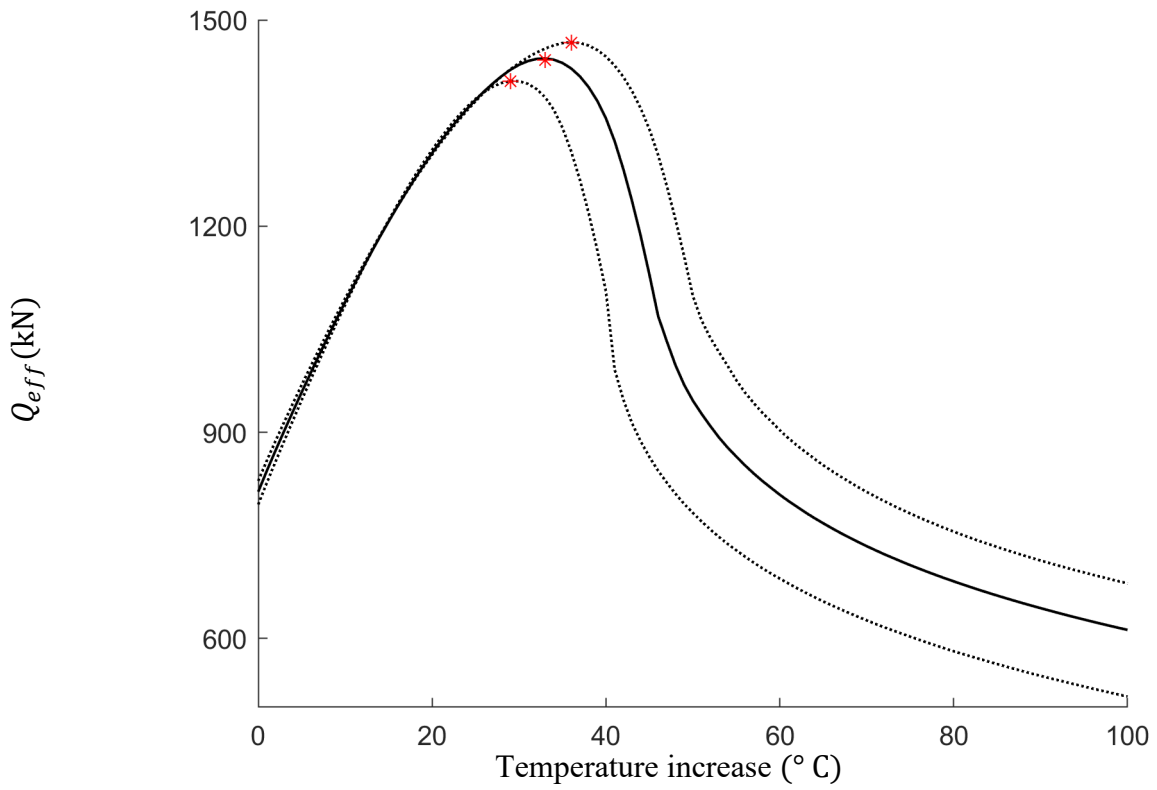


Figure 4.8 Mean Q_{eff} vs Max. and min. values of Q_{eff} . Case 5. From Table 4.1

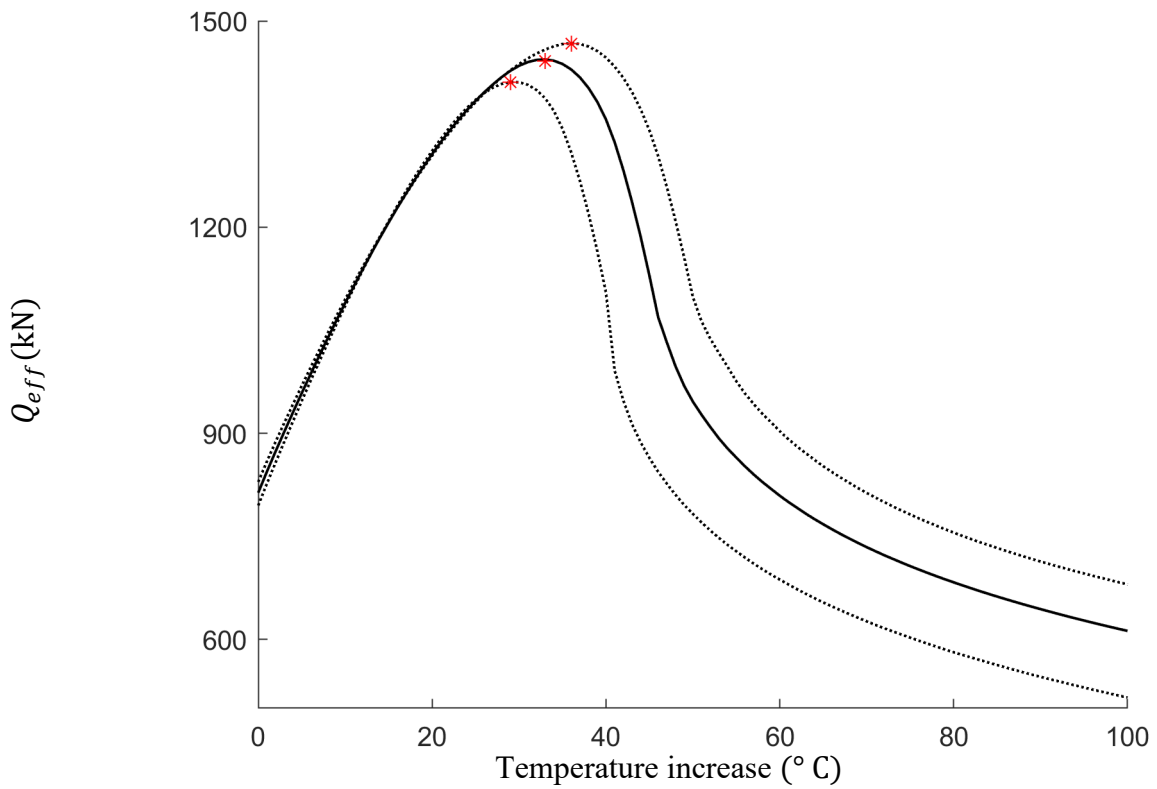


Figure 4.9 Mean Q_{eff} vs Max. and min. values of Q_{eff} . Case 6. From Table 4.1

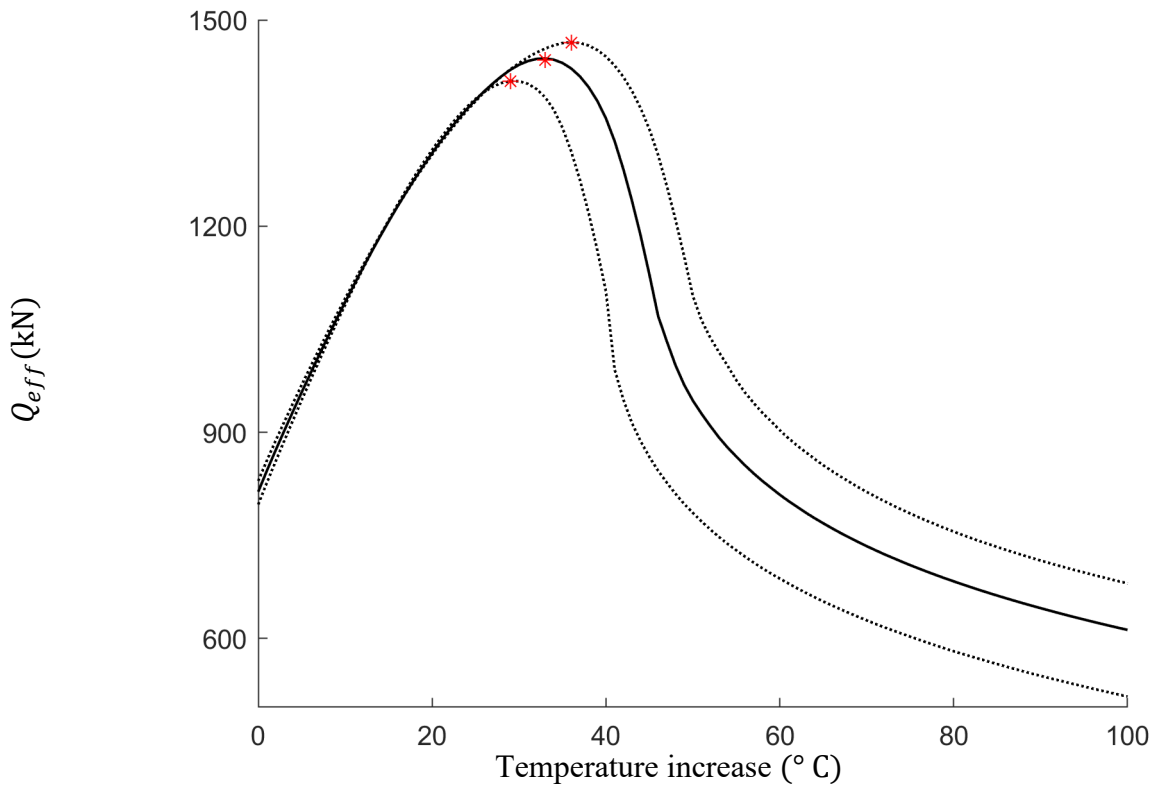


Figure 4.10 Mean Q_{eff} vs Max. and min. values of Q_{eff} . Case 7. Table 4.1

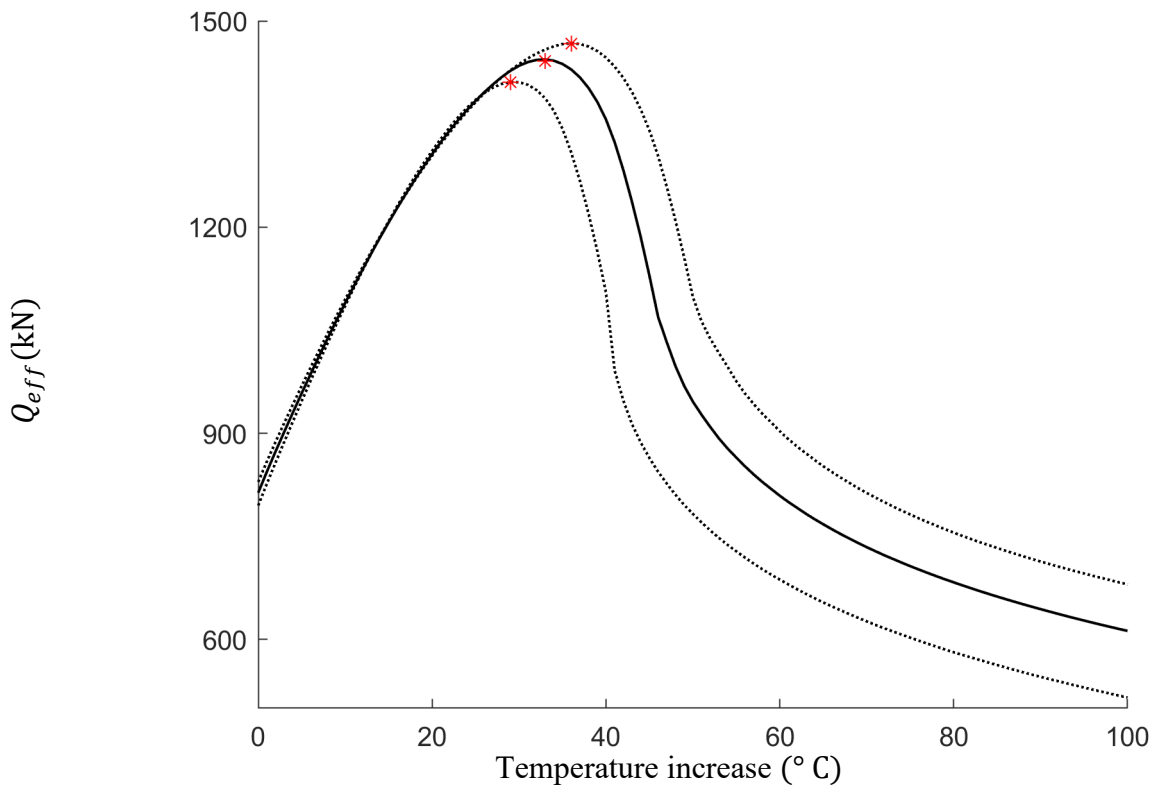


Figure 4.11 Mean Q_{eff} vs Max. and min. values of Q_{eff} . Case 8. From Table 4.1

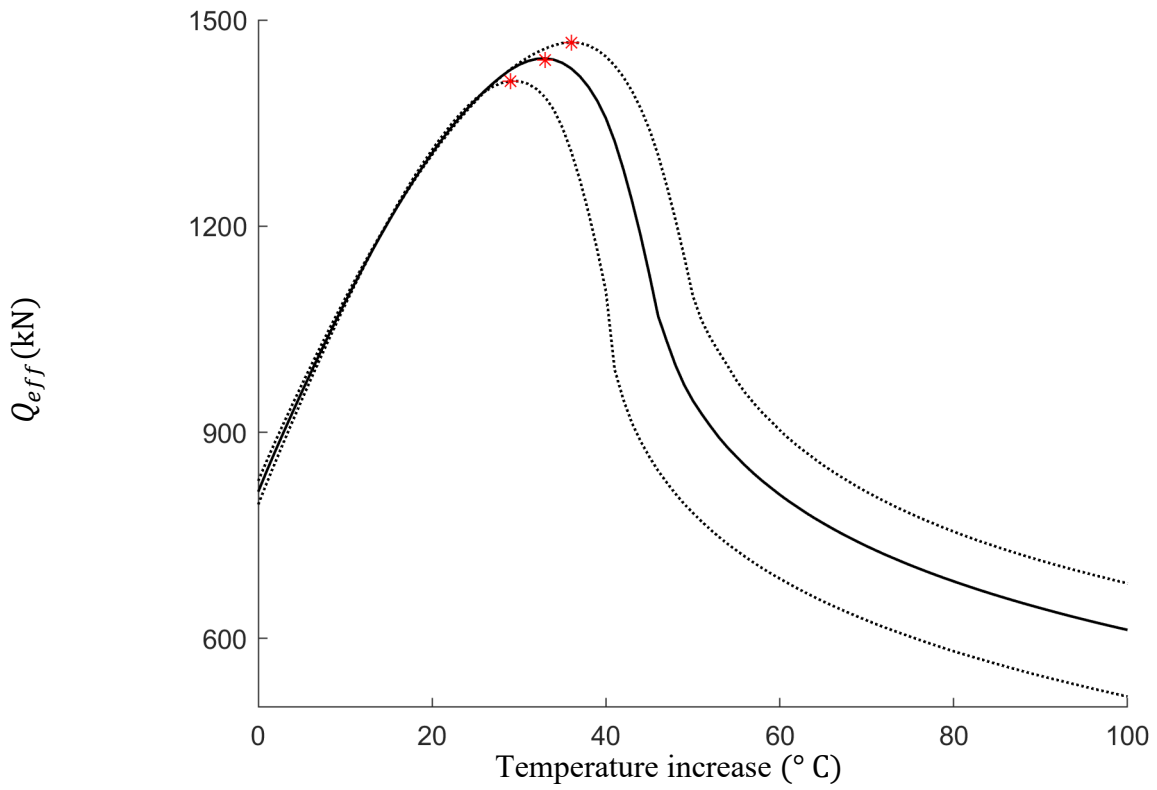


Figure 4.12 Mean Q_{eff} vs Max. and min. values of Q_{eff} . Case 9. From Table 4.1

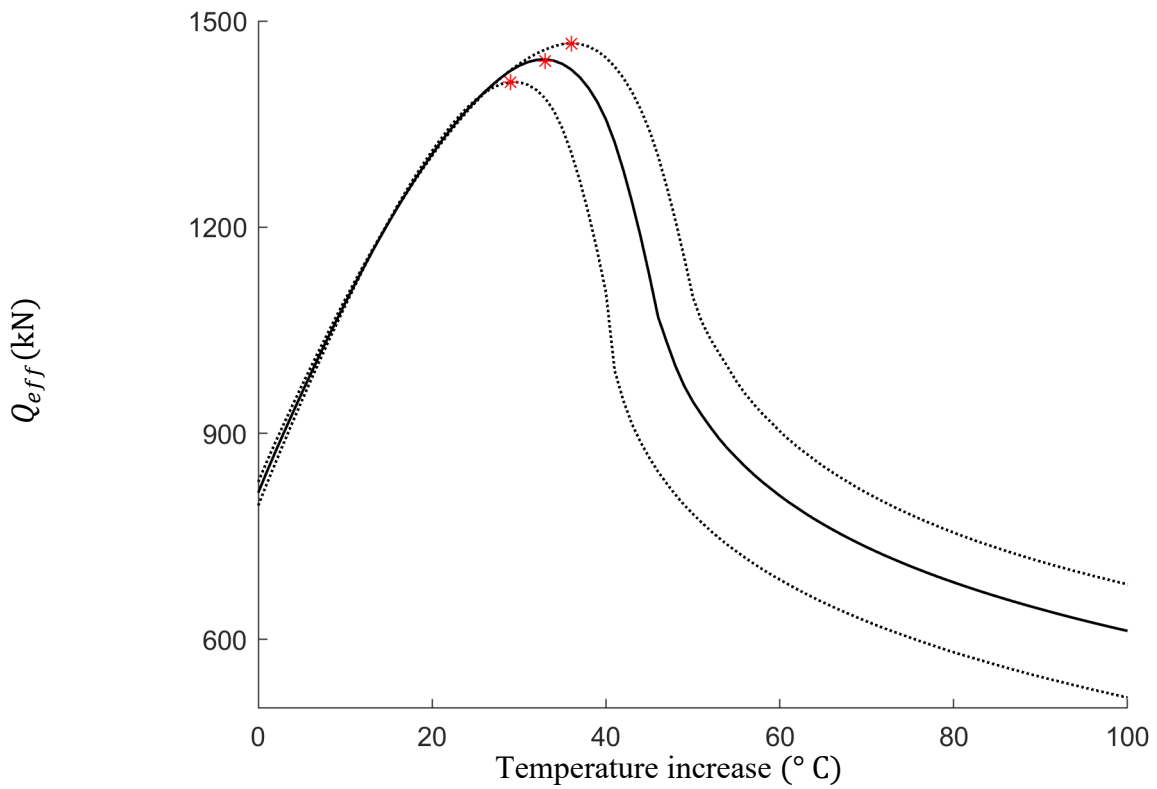


Figure 4.13 Mean Q_{eff} vs Max. and min. values of Q_{eff} . Case 10. From Table 4.1

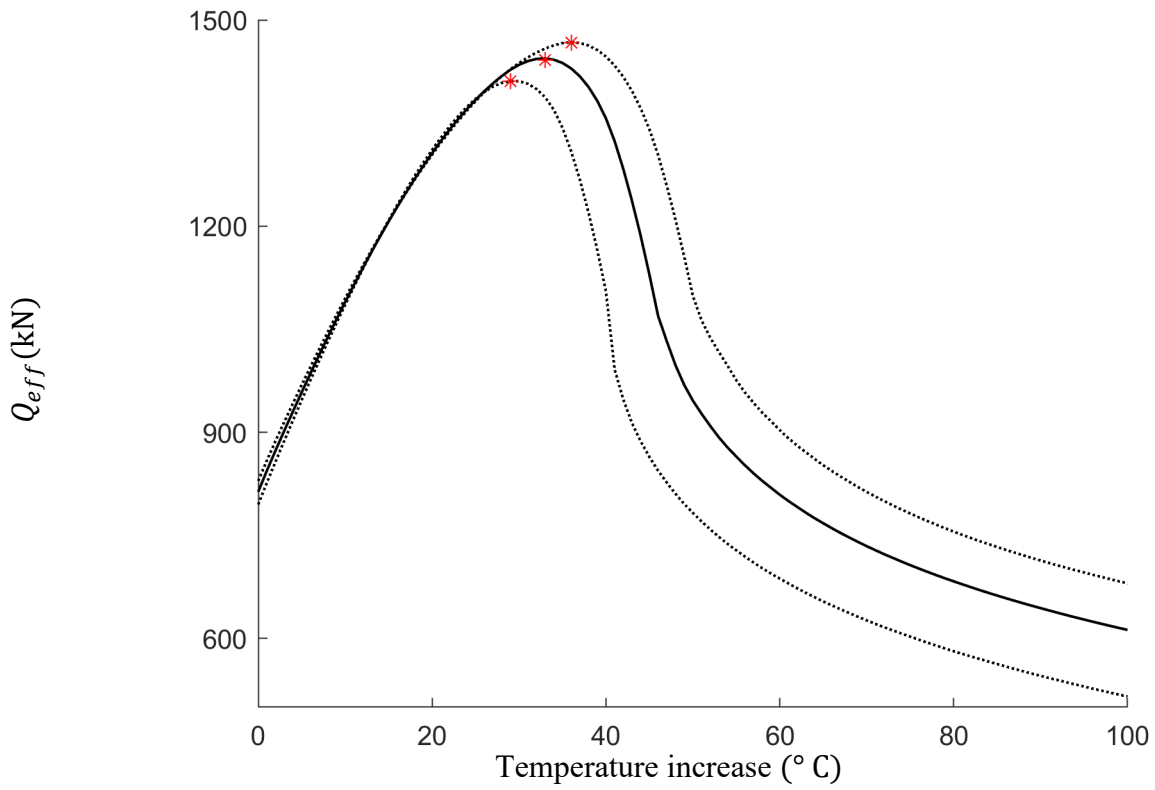


Figure 4.14 Mean Q_{eff} vs Max. and min. values of Q_{eff} . Case 11. From Table 4.1

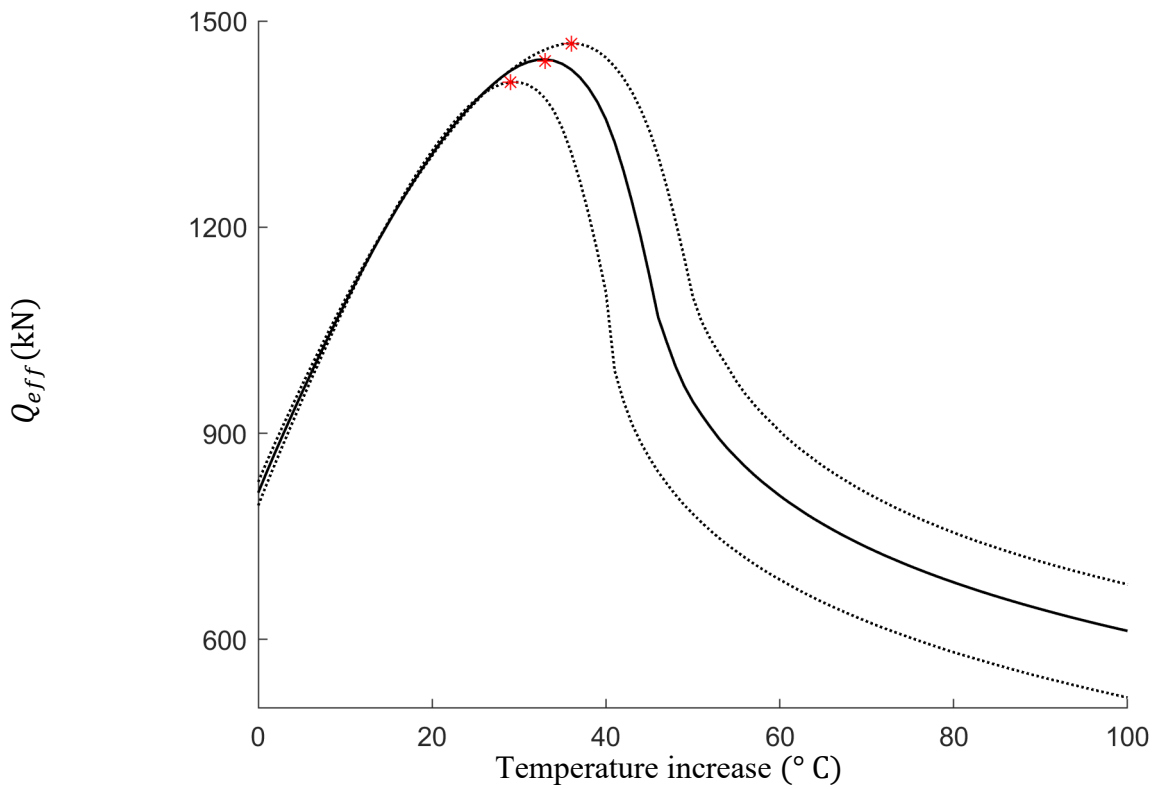


Figure 4.15 Mean Q_{eff} vs Max. and min. values of Q_{eff} . Case 12. From Table 4.1

4.4 Conclusion

A robust approach to discretize multivariable random fields with valid cross-correlated structures is presented. This method is useful to characterize soil variables with PDF, different than normal or lognormal. With correlation structures based on modified Bessel second kind decrement.

This approach is based on the Matérn class of variogram to deal with empirical or measured correlation structures. The discretization of the random field is achieved by linear coregionalization following loglikelihood approximations of the Bessel function parameters.

A simply correlated random field model was used to investigate the effects of the spatial cross-correlation properties of the soil, as a tri-variate $\mathbf{c}, \boldsymbol{\varphi}, \boldsymbol{\gamma}$ random field, on the UHB phenomena for onshore pipelines. The effects were established by variance comparison, between the response of single random field soil-pipe FE models. And the corresponding FE model, considering the cross-correlation a tri-variate soil.

The effect of simply cross-correlation structure, between soil properties, seems to have marginal effects for studied cases. The method used was developed by Shinozuka in 1990, and improved by Vořechovský in 2008. The Gaussian simple cross-correlation structure of the field, seems to be of marginal relevance, for the cases studied. Assuming the soil properties have lognormal PDF, and normal correlation, and correlation structure. The studied cases are representative of a wide range of granular soil parameters close to dry condition. Although it is clear that other types of soil may have different cross-correlated structure.

4.5 References

1. N.Nielsen, B.Lyngberg, and P.Pedersen, 1990. "Upheaval buckling failures of insulated buried pipelines: a case story". Offshore Technology Conference.
2. S.Boer, Hulsbergen, Richards, Klok, and Biaggi, 1986. "Buckling considerations in the design of gravel cover for high temperature oil line". OTC 5294, Houston.
3. D.M.Richards, 1990. "The effect of imperfection shape on upheaval buckling behaviour". Advances in Subsea Pipeline Engineering and Technology, 24, pp 51-66.
4. N.Taylor and A.Gan, 1986. "Submarine pipeline buckling-imperfection studies". Thin-Walled Structures, 4, 4, pp 295-323.
5. G.T.Ju and S.Kyriakides, 1988. "Thermal buckling of offshore pipelines". J. of Offshore Mechanics and Arctic Engineering, 110, pp 335-364.
6. P.Pedersen and J.Jensen, 1988. "Upheaval creep imperfections of buried heated pipelines". Marine Structures, 1, pp 11-22.
7. A.Palmer, C.Ellinas, D.Richards, and G.Guijt, 1990. "Design of submarine pipelines against upheaval buckling". Offshore Technology Conference.

8. F.Klever, L.van Helvoirt, and A.Sluyterman, 1990. “A dedicated finite-element model for analyzing upheaval buckling response of submarine pipelines”. Offshore Technology Conference.
9. A. C. Palmer and J. A. S. Baldry 1974, “Lateral buckling of axially-compressed pipelines”. J. Petroleum Technol. 26, 1283.
10. McMurray, A. B., et al. "Annex J1: Recent pipeline accidents involving crude oil in Canada and the United States." Guidance for the Environmental Public Health Management of Crude Oil Incidents (2018): 131.
11. American Lifelines Alliance, 2001 “Guidelines for the Design of Buried Steel Pipe”.
12. DNV. 2017 “Recommended failure rates for pipelines” About: Report No.: 2017-0547
13. Det Norske Veritas, 2013. “Submarine Pipeline Systems”, DNV-OS-F101
14. DNV. DNV-RP-F110 2007. “Global buckling of submarine pipelines”. Det Norske Veritas.
15. Phoon, K.-K., and Kulhawy, F.H. 1999. “Characterization of geotechnical variability”. Canadian Geotechnical Journal, 36: 612–624.

16. Carneiro, D., Gouveia, J. and Parrilha, R. (2010). “Feedback Analyses of Pipeline Embedment over As-laid Survey Results”, Proc. Int. Conf. Ocean, Offshore and Arctic Engineering, June 6-11, Shanghai, OMAE2010- 20410.
17. Oliphant, J. & Yun, G.J. 2011. “Pipeline Embedment Prediction using As-laid Data”, Proc. Int. Conf. Ocean, Offshore and Arctic Engineering, Rotterdam, June 19-24, OMAE2011-50095
18. Bransby, M. F., & Ireland, J. (2009). Rate effects during pipeline upheaval buckling in sand. Proceedings of the Institution of Civil Engineers-Geotechnical Engineering, 162(5), 247-256.
19. Yamazaki F, Shinozuka M. 1990 “Simulation of stochastic fields by statistical preconditioning”. J Eng Mech;116(2):268–87.
20. Guttorp, P., & Gneiting, T. 2006. “Studies in the history of probability and statistics XLIX On the Matérn correlation family”. Biometrika, 93(4), 989–995.
21. Gneiting, T. 2002. “Nonseparable, Stationary Covariance Functions for Space–Time Data”. Journal of the American Statistical Association, 97(458), 590–600
22. Jean-Paul Chilès and Pierre Delfiner 2012 “Geostatistics: Modeling Spatial Uncertainty”. Second Edition, John Wiley & Sons, Inc.
23. Wackernagel, Hans 2003 "Multivariate Geostatistics, An introduction with applications" Springer Nature Switzerland AG

24. Rackwitz, R. 2000. Reviewing probabilistic soils modelling. *Computers and Geotechnics*, 26(3-4), 199-223.
25. Mateu, J., Porcu, E., and Gregori, P. 2008, “Recent advances to model anisotropic space-time data”, *Statistical Methods and Applications*, 17, 209-223.
26. Zhang, H. 2004, “Inconsistent estimation and asymptotically equal interpolations in model based geostatistics”, *Journal of the American Statistical Association*, 99, 250-261.
27. Zhang, H. 2007, “Maximum-likelihood estimation for multivariate spatial linear coregionalization models”, *Environmetrics*, 18, 125-139.
28. Zhang, H., and Wang, Y. 2010, “Kriging and cross-validation for massive spatial data”, *Environmetrics*, 21, 290-304.
29. Schott JR. 1997. *Matrix Analysis for Statistics*. John Wiley & Sons, Inc.: New York.
30. Goulard, M., Voltz, M. 1992 “Linear coregionalization model: Tools for estimation and choice of cross-variogram matrix”. *Math Geol* 24, 269–286

5 Reliability of Pressurized Pipelines along Unstable Slopes

Due to constraints in routing options, oil and gas pipelines may be buried on unstable slopes. The natural soil may suddenly become unstable and fail (e.g., rock formation and granular soils) or move slowly over time (e.g., tens of millimeters per year). The slow soil movements are generally difficult to mitigate with preventative measures. Further, instability conditions may arise only arise after construction. Due to pore-pressure fluctuations, erosion, and stress relief driving the slow movements in natural slopes ^[1]. This susceptibility to slope instability needs to be assessed and continually monitored in order to ensure the safety of pipelines.

5.1 Motivation

Pipelines on unstable slopes will be subjected to deformation that may lead to failure; tensile rupture at the top of the slope, compressive local buckling or wrinkling at the bottom of the slope. Probabilistic analysis of slope stability problems involving limit equilibrium methods have been implemented with various statistical approaches ^[2]. These included, Monte Carlo method, estimation methods, First Order or Second Moment (FOSM), also Point Estimation methods such as maximum likelihood estimator (MLE) and generalized method of moments.

It has been demonstrated that the soil variability, modeled as point statistics of a material property, implies an infinite spatial correlation ^[3]. Previous studies ^[3,4] accounted for spatial variation of material properties along prescribed failure planes as a function of the correlation distance and failure or slip surface length.

However, the assessment of pipelines failure due to land slide, considering the soil spatial variability is not straightforward. Once the most likely slip surface has been identified in a particular slope, one can find that it has little impact on the overall safety of the pipeline in comparison with other less likely failure surfaces along the slope that may induce significant forces on the pipeline as the soil displacement occurs. Therefore, it is desirable to account for potential slip surfaces dependent on the spatial variability of the soil in order to assess the overall pipeline safety. A simple procedure to assess the safety of pipelines due to land slide, considering the soil spatial variability is presented. The proposed approach relies on Finite Element (FE) Method to model the mechanical behavior of a pipeline buried over a natural unstable slope. The characteristics of the FE model are obtained from random field simulations to provide more realistic modelling of the spatial variation of soil properties and its dependent slip surfaces. The FE is characterized for each trial, with a correlation structure for soil properties along the domain. For each random field realization, a critical surface is calculated.

It is well known that solid element, three-dimensional finite element analyses (FEA) of pipe-soil interaction are time consuming even when used only to calculate deterministically the stress state in the pipe for a given soil movement. Simplified models for evaluating the strain demand in a pressurized pipelines that are buried in unstable soil, have been reported extensively in the literature ^[3-6]. Earlier solutions rely on a simplified analytical model, to calculate the maximum tensile and compressive strains due to a uniform movement of a block of soil in a direction relative to the pipeline. Previous analytical solutions consider; normal plastic flow rule, von Mises yield criterion, and isotropic strain hardening to characterize the pipe steel. The pipe-soil friction in most analytical models is assumed to have an elastic perfectly plastic force-deformation ^[5]. More recent

studies, propose a procedure to calculate the probabilities of tensile rupture and the compressive local buckling for pressurized pipelines. By means of close-form strain demand expressions, to consider the variability of the soil and pipe properties in a simplified manner ^[6]. A more detailed approach is needed to account for the spatial variability of the soil properties on the overall pipeline failure probability due to landslide type of soil instability.

The shape of the moving soil mass and its direction with respect to the pipeline are likely to vary accordingly to soil random properties. These spatial characteristics are not included in previous studies ^[3-6]. Most close form expressions to assess pipelines are applicable only for shallow soil movements with constant shape and direction. To overcome these limitations, a simplified FE models can be used to assess the pipe-soil mechanical behavior ^[7,8] in which the pipe-soil interaction is characterized by the force-displacement elements (FDE) attached to beam pipe elements. Then, the stable soil conditions and the spatial characteristics of the soil displacement can be model directly on the FE. This is efficient enough to account for realistic cases and also to conduct reliability analysis to assess the failure probability of the pipeline.

5.2 Methodology

A simple procedure, presented in this study can be incorporated in a reliability- or reliability-based design and assessment (RBDA) for pipelines. It accounts for tensile and compressive failure modes in the failure probability evaluation. This distinction is important because of the consequences associated with a tensile rupture, which leads to immediate loss of pressure containment, are in general markedly more severe than those associated with a compressive local

buckling, which usually, does not result in immediate loss of pressure containment [2]. Different allowable failure probability levels can be applied to these two failure modes to develop maintenance strategies that result in optimal use of resources. The tensile and the compressive strain capacities are characterized based on the available information in the literature. The spatial viability of the soil and the pipe properties is considered by employing techniques of homogenous random fields. The proposed procedure can be used to calculate the pipeline failure probabilities conditional on a given ground movement magnitude. The failure probabilities can also be evaluated as a function of time, if the probabilistic characteristics of the average ground movement rate is known. Based on numerical simulation to identify the probability of fail between two competing modes (by excessive tension or compression anyway along the pipeline) as function of the average displuming of the soil unstable mass. A simple approach can be summarized as follows:

Step	Characterization
1.-Soil domain	Geotechnical parameters statistical properties. Correlation structure. Cross-field correlation.
2.-Random field Realization	For each realization a critical failure surface is identified.
3.- FE model	Creation of interpolated nodal points in the soil domain to accommodate a critical failure surface. Soil properties from Step 2. Pipeline properties. Induced forces; pressure, temperature, self-weight. Applied soil displacements
4.- Assessment of probability of failure	Probability of failure as function of soil displacement.

Table 5.10 A simple approach to assess the probability of failure of pipeline due to land slide

5.2.1 Soil domain

The procedure in Table 5.1 is easy to implement by adopting ASCE-ALA (2001) equivalent soil force-displacement relationships for the FE model approach to overcome the limitations of the analytical solutions. Soil properties themselves may be regarded as random variables owing to the uncertainties associated with inherent spatial variability and the epistemic uncertainties arising from limited number of soil test data. Additionally, uncertainties inherent to the quality and quantity of soil samples, characteristics of the testing device, and the operator's experience may have a significant effect on the measured geotechnical properties. Therefore, it is useful to relate the force-displacement relationships to the actual experimental data from the actual site^[8], namely; the vertical bearing resistance q_u , the vertical uplift soil resistance q_d , Figure 5.1 and the ultimate axial resistance f Figure 5.2. To account for the soil spatial variability in a simplified manner, one can use the Generalized Slice Method and Critical Slip Surface^[12,13].

5.2.1.1 Axial soil resistance

The use of an elastic-perfectly plastic model to predict the axial f soil–pipe behavior under large axial load has some limitations. The results obtained using the ASCE-ALA (2001) are in good agreement with pipe pullout tests for low to medium density sand soils. In dense sand there is an underestimation of the soil peak resistance up to 20%^[14]. This increase in normal stress is believed to be associated with constrained dilation (interlocked soil particles around the pipe, need to move around each other or brake before mobilization, generating an apparent dilation in the soil around the pile and thus, a peak resistance) during shear deformations. In some soil conditions, such as

over consolidated soils, the proposed simplified soil spring relationships, may not reflect the presence of a post-peak reduction in shear resistance which is observed in the behavior of soil-pipe interfaces ^[14]. Also, the available methods for modeling soil restraint with soil springs assumes that the spring forces always act in the axial, horizontal, and vertical directions relative to the pipeline. In most analyses, the direction of the soil spring forces do not maintain an axial, horizontal, and vertical orientation relative to the pipeline if the pipeline undergoes large rotations. The error introduced by this misalignment is acceptable considering other assumptions and uncertainties inherent in the analysis such as those related to the relationships used to compute soil spring properties. Therefore, the use of the force-displacement is considered acceptable for the present study.

In general, to estimate force displacement relationships in pipe-soil interaction analyses some parameters can be assumed as deterministic ^[15, 16]. CSA 2019 considers that the actual pipe diameter (D) has negligible variability and can be considered equal to the nominal diameter. The mean and coefficient of variation (COV) of the actual-over-nominal pipe wall thickness ratio equals 1.01 and 1.0%, respectively ^[16]. It follows that the pipe wall thickness can be considered a deterministic quantity equal to the corresponding nominal value. Another important parameter to consider is the pipe-soil friction coefficient, which depends mostly on the nature of the pipe surface (roughness, coating type) and the average particle size of the soil. However, it also could have small variability once the friction coefficient is obtained from test between the coating and the particular soil characteristics ^[17]. One can find that the pipe burial depth H may varies significantly (i.e., settlements, frost upheave, eroded or undermined trenches) along the entire route of the pipeline; however, the burial depth of a particular segment along the pipeline may variations of H

that are smaller than the construction tolerance. In this study, H is also assumed to be a deterministic variable.

Some solutions have been developed to estimate the frictional force per unit length of pipe as an elastic perfect-plastic linear spring ^[17]. In the present study, some assumptions haven been made to take advantage of the simplicity of the well accepted ASCE-ALA (2001) ^[11] expressions to perform reliability analysis:

$$f(c, \bar{\gamma}, \varphi, \varepsilon_{K_0}) = \pi D \alpha c + \pi D H \gamma \frac{1 + \varepsilon_{K_0} \cdot K_0}{2} \tan(f_c \varphi) \quad (5.63)$$

where; c is soil cohesion representative of the soil back field, $\bar{\gamma}$ is the unit weight of soil; ε_{K_0} is a model error of K_0 , which is coefficient of pressure at rest, φ is soil friction angle and f_c is a pipe coating dependent factor relating the internal friction angle of the soil to the pipe-soil interface.

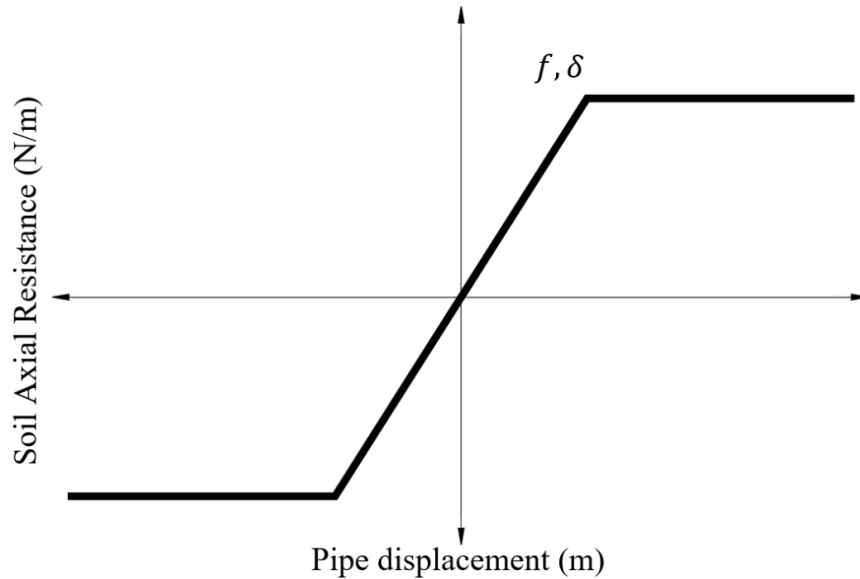


Figure 5.29 Axial Force-Displacement Relationship f soil axial friction per unit length, δ soil displacement

The model error ε_{K_0} has been included to account for uncertainties introduced by the assumptions made in estimating K_0 empirically for different conditions. The characterization of ε_{K_0} is possible due to previous experimental work. The measured axial soil loads from full-scale tests performed on buried pipes are comparable to those predicted using the equation recommended in commonly used guidelines (ASCE 1984, ASCE-ALA 2001) only for loose dry sand conditions ^[19]. On the other hand, the peak axial resistance measured from pullout tests in dense soils was two times higher than the predicted values with the ASCE (1984) expression, due to constrained dilation in dense sand during interface shear deformations.

The coefficient of earth pressure at rest K_0 is defined as the horizontal-to-vertical stress ratio in Eq. 5.1 and it is applicable for the Mohr–Coulomb yield conditions in cohesion-less soils, loose and normally consolidated clays, thus the error ε_{K_0} increases in consolidated soils.

$$K_0 = (1 - \sin\varphi) \frac{1 + \frac{2}{3}\sin\varphi}{1 + \sin\varphi} \approx 1 - \sin\varphi \quad (5.64)$$

The error introduced by the approximation in Eq. 5.65, is negligible ^[20] but it shows that K_0 is a function of the friction angle φ in the model. Other expressions to estimate K_0 ^[14,18] also account for the effective weight of the pipe and the normal pressure distribution along the pipe cross section. In this study, the effective pipe weight considered in the pipe elements, and K_0 is employed as an approximation to consider the average normal stress (K_0 is an average ratio of the overburden stress and lateral pressures at rest at the pipe depth). The K_0 values, back-calculated from (ASCE 1984) expressions almost predict the experimental average stress ratio for loose sand with friction angle of $\varphi = 31^\circ$. In the present study, due to the site geotechnical characteristics (cohesion, granular, consolidated soil) ε_{K_0} is model as a uniform distributed random variable with

a linear variable mean, as function of the friction angle φ , being 1 at 31° up to 2.5 at 45° , based on previous experimental work ^[19,21]. Other sources of uncertainty, different than the former are ignored (i.e., reductions of the normal stress in the pipe wall due to pipe wall deformation under axial and bending loading combinations).

5.2.1.2 Soil bearing capacity

The ASCE (1984) Q_u Fig. 4.1 depends on the bearing capacity factors q_c and q_b . This factors and the formulation of Q_u it self may introduce error in the approximation and the relationship with the basic soil parameters is likely to change for different types of soil. Therefore, practical solutions to account the variability of Q_u may include; recommendation in design codes (DNV-RP-F110) which provides distribution and moments to characterize Q_u as random variable directly in marine environment; or the use of empirical factors that have been used to estimate the bearing capacity factor from in-situ tests. The former approach was used.

$$Q_u = \varepsilon_{N_q} \cdot N_q \bar{\gamma} H D + \varepsilon_{N_\gamma} \cdot N_\gamma \gamma \frac{D^2}{2} \quad (5.66)$$

where; D is the deterministic pipe diameter, H is the deterministic depth to pipe centerline, γ is bulk unit weight of soil, $\bar{\gamma}$ specific weight of the soil. The bearing capacity factor N_q, N_γ are given by

$$N_q = \exp(\pi \tan(\varphi)) \tan^2 \left(45 + \frac{\varphi}{2} \right) \quad (5.67)$$

$$N_\gamma = \exp(0.18\phi - 2.5) \quad (5.68)$$

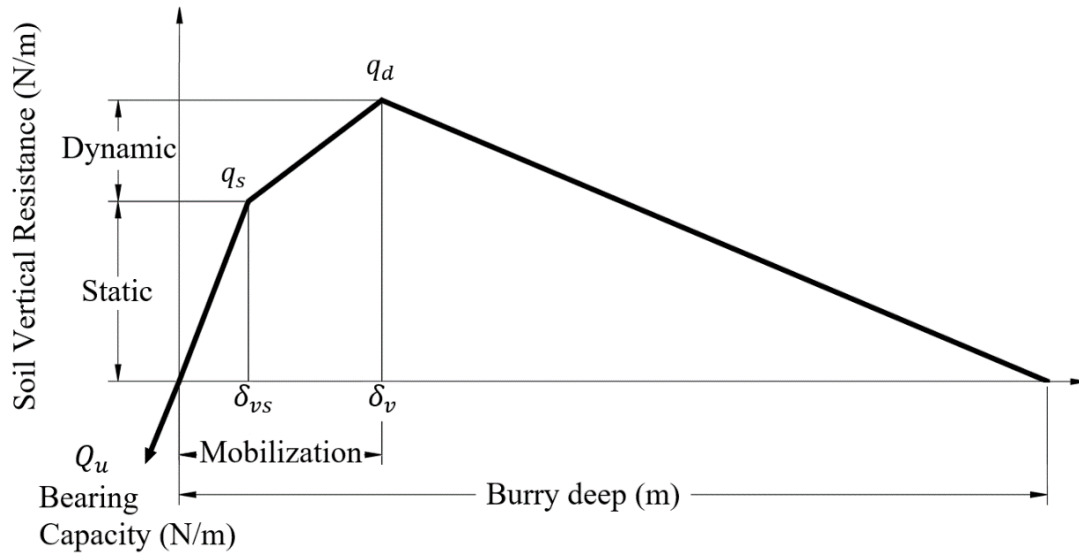


Figure 5.30 Force-displacement diagram for the soil model in the vertical direction; Q_u soil bearing capacity at the bottom of trench, q_s static soil download, q_d dynamic soil download, δ_{vs} static limit displacement and δ_v fully mobilized displacement ^[11]

According to the literature, in some footing analysis with missing reported soil parameters, SPT values have been used for estimation to estimate the bearing capacity of the soil ^[22] to estimate the soil friction angles, with SPT or CPT blow counts corrected using the overburden correction ^[23]. It is known that the sensitivity of the bearing capacity factors increases with the change in soil friction angle for higher friction angles. These conclusions were obtained from a comprehensive database of load tests on closed-ended piles in sand has been reassembled from the original sources to examine the relationship between CPT resistance, q_c , and base capacity, q_b . In contrast to continuum analyses that predict $q_b = q_c$ during steady penetration indicating that the influence of density and stress level on soil resistance is broadly captured by the use of Bolton's correlations in the limit equilibrium solution. The error involved in this factor is likely to change between different soil conditions ^[24]. Therefore, in the present, the statistics of the CPT reported by Phoon

and Kulhawy ^[25] are used to approximate characterize the ASCE (1984) bearing capacity factor Q_u with the assumption that the variability of Q_u is very similar to the variability of the CPT test. However, the Q_u may also include the error terms for each bearing factor ε_{N_q} and ε_{N_γ} if enough data is available.

5.2.1.3 Uplift soil resistance

Various models have been proposed for the calculation of peak uplift resistance based on the mechanisms observed in previous experimental data. All methods assume that tension cannot be sustained between the pipe invert and the soil, allowing a gap to open without resistance ^[26]

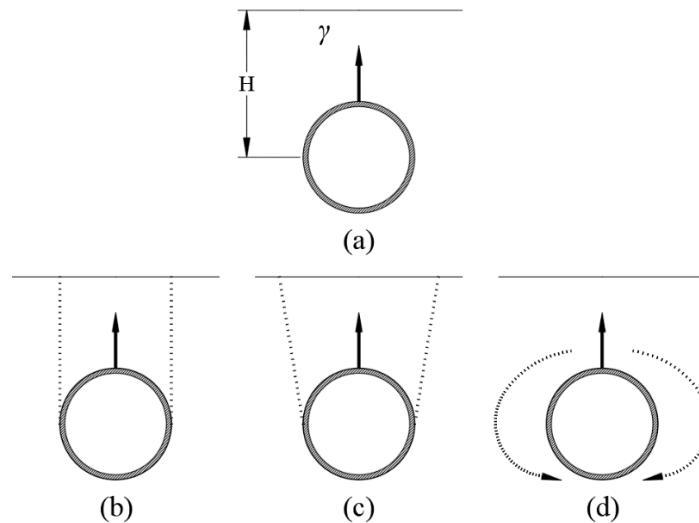


Figure 5.31 Uplift mechanisms of buried pipes in sand: (a) Problem geometry; (b) sliding block with vertical slip surfaces; (c) sliding block with inclined slip surfaces; and (d) flow around the pipe ^[26]

There are three possible failure mechanisms due to a pipe upward moment in the soil that depend on the soil properties and the H/D ratio. The reduction in the resistance after the peak phenomenon

is not observed in loose sands ^[24]. In this study case, it is assumed that the dominant mechanism is of type (b) as shown in Fig. 4.3. due the fact the soil in the landslide will keep piling on the lower part of the slide and the upper part of the affected pipeline is likely to be dominated by axial tension instead, as the sliding soil mass moves down. The force-displacement relationship of the soil is upward direction, idealized in Fig.4.2 has a linear dynamic (fully mobilized soil) component q_d according to the pipe-soil response ASCE-ALA 2001^[11] and a linear decrement to account for the breakthrough condition that happens once the displacement is equal to the depth of the trench. The initial soil resistance or static download reaction q_s , is the weight of the soil above the pipe given as:

$$q_s = \gamma H D \quad (5.69)$$

$$q_d = N_{cv} c D + N_{qv} \gamma H D \quad (5.70)$$

where: N_{cv} vertical uplift factor for clay (0 for $c = 0$), c backfield soil cohesion (Pa), N_{qv} vertical uplift factor for sand (0 for $\varphi = 0^\circ$).

$$N_{cv} = 2 \frac{H}{D} \leq 10 \text{ applicable for } \frac{H}{D} \leq 10 \quad (5.71)$$

$$N_{qv} = \frac{\varphi H}{44D} \leq N_q \text{ where } N_q = \exp(\pi \tan \varphi) \tan^2 \left(45 + \frac{\varphi}{2} \right) \quad (5.72)$$

A comprehensive finite element study of the breakout resistance of buried anchor plates ^[27] set the formulation for eq 4.7. The soil was assumed to have a Mohr–Coulomb failure criterion, and both associated and non-associated flow rules were adopted. Their results, expressed as N_q in the form of simple charts, suggest that soil dilatancy can significantly increase the ultimate anchor capacity at moderate depth in medium to dense sand. In this study, the deformation mechanism has been

observed at a buried depth ratio of $\frac{H}{D} = 13$. Then the only possibility is that the failure given by the soil flow around the pipe. Also, at this buried depth ratio the volume of the soil corresponding to the half of the pipe is not significant. However, if conditions of applicability for the q_d expression exceeded the value of $\frac{H}{D}$. Such a case, will require case-specific geotechnical guidance on the magnitude of soil spring force and the relative displacement necessary to develop this force.

At high embedment depths, the failure mechanism has been studied ^[28] concluding that the depth of this transition depends on the dilatancy of the soil. Also, it was found that the uplift resistance of smooth pipes compared with rough was consistently lower by 10 – 30%, increasing with decreasing embedment ^[21]. Therefore, the mayor source of uncertainty is introduced by using the factor N_{qv} . One can rearranged the q_d expression to include a normally distributed error $\varepsilon_{N_{qv}}$ as follows:

$$q_d = \varepsilon_{N_{cv}} \cdot N_{cv} c D + \varepsilon_{N_{qv}} \cdot N_{qv} \gamma H D \quad (4.8a)$$

where the N_{qv} expression for the deep embedment ratios can be estimated by the following expression ^[29] For $\frac{H}{D} < 8$

$$N_{qv} = \left(\frac{2H}{D} - \frac{H_e}{D} \right) \left(\frac{H_e}{D} \right) (0.95 \tan \varphi) + 1 \quad (5.73)$$

where H_e is the vertical extend of failure surface, given empirically as $\frac{H_e}{D}(\varphi)$. The soil $\varepsilon_{N_{qv}}$ mean value of 1.1 with a standard deviation of 0.17. is taken from experimental studies developed by White et al. ^[30]. $\varepsilon_{N_{cv}}$ is an error correction factor to account for two uncertainties: The correction for differences between the undrain shear strength of the natural soil and the actual shear strength of the backfill material due to remoulding of the soil (DNV 2007) ^[32]. And, the suction force

opposite to the pipe movement relative to the soil. $\varepsilon_{N_{cv}}$ appears to introduce the largest amount of uncertainty of all correction factors studied (Eq.5.4 and 5.8a), it can easily reduce up-to 40% of the cohesive contribution of q_d . Yet, it seems to be highly dependent on variables not included in the formulation of force-displacement relationships (e.g., clay lumps average size in the backfield material and the pressure-dependent drainage properties of the soil) [31]. Due to the lack of statistical data to estimate $\varepsilon_{N_{cv}}$ a conservative normal distribution with mean of 0.9 and CoV 0.1 is assumed in this study. A summary of the soil statistical properties is presented:

Soil Property		PDF	Mean	CoV
φ	friction angle	Lognormal	30°	0.3
c	cohesion	Lognormal	75kPa	0.3
γ	bulk density	Lognormal	18kN/m ³	0.2
Q_u	bearing capacity	ε_{N_q} Normal	1	0.05
		ε_{N_γ} Normal	1	0.1
q_d	dynamic download	$\varepsilon_{N_{qv}}$ Normal	1.1	0.03
		$\varepsilon_{N_{cv}}$ Normal	0.9	0.1
L_h	horizontal scale of fluctuation	deterministic	50m	
L_v	vertical scale of fluctuation	deterministic	5m	
Cross-Correlation	$R_{\varphi c} = R_{c\varphi}$	deterministic	-0.7	
	$R_{c\gamma} = R_{\gamma c}$	deterministic	0.7	
	$R_{\varphi\gamma} = R_{\gamma\varphi}$	deterministic	0.2	

Table 5.11 Soil Statistical properties

The soil Lognormal properties were treated as Gaussian random field by converting into normal space;

$$\mu(X) = \ln(\mu) \frac{\ln(1 + \text{cov}^2)}{2} \quad (5.74)$$

$$\sigma^2(X) = \frac{\sqrt{\ln(1 + \text{cov})}}{\mu(X)} \quad (5.75)$$

$$\Sigma_{XX} = \sigma^2(X) \frac{\ln(1 + \rho_{XX} \cdot \text{cov}^2)}{\ln(1 + \text{cov}^2)} \quad (5.76)$$

where Σ_{XX} correlation structure in gaussian space and ρ_{XX} the correlation of the soil variables.

As a general approximation, the geotechnical soil stochastic properties presented in Table 5.2 were suggested by Phoon and Kulhawy ^[25] as only applicable for most common natural soil deposits. These soil properties are adopted to investigate the effects of inherent soil spatial variability in the assessment of pipelines susceptible to landslides, in a general sense. Also, as a practical example of how to consider its effects using a simple procedure. It is proposed to characterize the well accepted ASCE-ALA (2001) force-displacement relationships with error correction variables to account for the uncertainty involved in the fitting factors, in good agreement with experimental data.

The probability distribution of F_y/SMYS is provided in CSA 2007, however this uncertainty is not comparable with the magnitude of the uncertainty involved in the geotechnical spatial variability. Therefore, the variability of the pipe wall thickness, the ovality imperfections and F_y/SMYS can be ignored in to a good approximation (e.g., less than 5% where the COV of the soil properties is about 30%).

5.2.1.4 Correlation structure

In this approach it is assumed, the in-situ data are statistically homogeneous. Thus, constant mean and constant standard deviation throughout the soil domain. All domain values are fully

characterized from an autocorrelation function independent of location and dependent only on the separation, or lag distance, ξ , (i.e., the correlation between property values at two locations is only a function Euclidian norm).

$$R_{XX}(\xi_1, \xi_2) = \exp \left(- \sqrt{\left(\frac{2\xi_1}{L_h} \right)^2 + \left(\frac{2\xi_2}{L_v} \right)^2} \right) \quad (5.77)$$

where L_h is scale of fluctuation in the horizontal direction. And L_v is scale of fluctuation in the vertical direction. In order to define an admissible cross-correlation matrix between the force-displacement random fields, all the soil properties are assumed to have the same spatial correlation structure along the soil domain. Observation of geological data indicate that this is true in good approximation^[36] Then, the scale of fluctuation in the horizontal direction for this particular case was 50 m and 5 m in the vertical direction for the three basic random variables (φ, c, γ) is consider to be constant. The scales of fluctuation of each soil type in the horizontal direction are larger than those in the vertical direction. This means that the soil has more uncertainty in the vertical direction.

5.2.1.5 Cross-field correlation

The covariance matrix Σ of the random vector $\{Z(x_1)^T, \dots, Z(x_n)^T\}^T \in \mathbb{R}$ must be positive definite for any positive integer n at any points x_1, \dots, x_n in \mathbb{R} . The covariance is often defined as a parametric family of functions whose members are proven to be positive definite.

$$C_{XX}(X_1, X_i) = \prod_{i=1}^{dim} \exp \left(\frac{\|X_1, X_i\|}{d_i} \right)^{pow_i} \quad (5.78)$$

The covariance matrix of \mathbf{X} is, corresponds to the 3 soil variables studied in this chapter, defined by $X_1 = \varphi$, $X_2 = c$, $X_3 = \gamma$

$$C_{XX} = \begin{bmatrix} \text{var}(X_1) & \text{cov}(X_1, X_2) & \text{cov}(X_1, X_3) \\ \text{cov}(X_2, X_1) & \text{var}(X_2) & \text{cov}(X_2, X_3) \\ \text{cov}(X_3, X_1) & \text{cov}(X_3, X_2) & \text{var}(X_3) \end{bmatrix} \quad (5.79)$$

Assuming homogeneity and zero mean of the stochastic field, ij -component of C_{XX} is obtained from the auto-correlation function $R_{XX}(\cdot)$ of the stochastic field as

$$C_{XXij} = \text{cov}(X_i, X_j) = R_{XX}(\xi_{ij}) \quad (5.80)$$

5.2.2 Random Field Realizations

The Morgenstern–Price method ^[37], is commonly used because it can consider noncircular shapes of slip surface, satisfying the force and moment equilibrium, uses the Mohr–Columb failure criterion and involves the least numerical difficulty in comparison with similar methods (Janbu^[38], Lowe^[39], Spencer^[40]). The basic assumption to consider involved in the Morgenstern–Price method is that the ratio of normal to shear interslice forces across the sliding mass is represented by an interslice force function that is the product of a specified function and an unknown scaling factor. The interslice force and the normal force are defined as total forces acting on each slide section of the moving soil mass. They are characterized from the mean value of soil properties at each slide. The dominant parameter that can account for the spatial variability of the soil, while using Morgenstern–Price method is the mobilized shear resistance S_i as show in Figure 5.3 since it depends on the soil properties right at slip surface and the normal force N_i . Thus, one can

consider the soil parameters along the slipping surfaces with a correlation structure along the soil domain to account for the inherent spatial variability of the natural slopes.

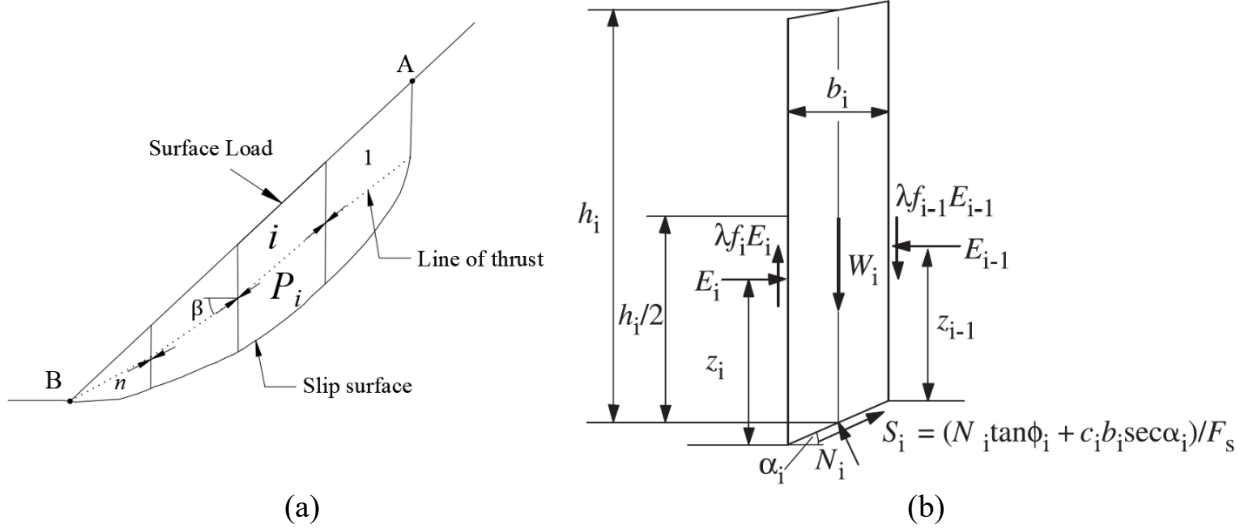


Figure 5.32 limit equilibrium methods of slices. (a) Sliding soil mass, where; A and B, are sliding soil mass boundary points, P_i is interslice force at the i th slide, n is the total number slides. (b) Typical slice forces, where; α_i is inclination angle, h_i is height, b_i is width.

The forces in Figure 5.3 are; W_i the self-weight, E_i and E_{i-1} are normal interslice forces acting at z_i and z_{i-1} vertical distances, $\lambda f_i E_i$ and $\lambda f_{i-1} E_{i-1}$ are interslice shear forces ($\lambda f(x)$ is assumed to be an scaled function for the ratio between the normal and shear interslice forces), N_i is the vertical normal force. S_i is mobilized shear resistance:

$$S_i = \frac{N_i \tan \phi_i + c_i b_i \sec \alpha_i}{F_s} \quad (5.81)$$

Where: ϕ_i friction angle
 c_i soil cohesion
 F_s safety factor

In the Morgenstern–Price method, the factor of safety F_s , is defined as the ratio of the available shear strength to the mobilized shear strength. Both, F_s and λ are unknown and can be solved through optimization ^[12](The minimization objective is $F_s = 1$. Constrained to $P_i = 0$ at A and B, the failure surface is bounded by A and B. Subjected to static equilibrium and Mohr-Coulumb failure criterion). The slope of interslice force is given by β_i as:

$$\tan \beta(x) = f_0 + \lambda \cdot f(x) \quad (5.82)$$

Where: $\beta(x)$ inclination angle of P_i along the Line of thrust

f_0 assumed function $h(A) = f_0$, $h(B) = f_0$

$f(x)$ assumed function

λ coefficient

Equilibrium conditions are defined with a coordinate (x, y) positive from the crown of the slope to its toe. Force $P(F_s, \lambda) = 0$ and moment $M(F_s, \lambda) = 0$:

$$P(F_s, \lambda) = \int_A^B p(x, F_s, \lambda) s(x, F_s, \lambda) dx = 0 \quad (5.83)$$

$$M(F_s, \lambda) = \int_A^B p(x, F_s, \lambda) s(x, F_s, \lambda) t(x, F_s, \lambda) dx = 0 \quad (5.84)$$

$$s(x, F_s, \lambda) = \sec \left(\frac{\tan \varphi_i}{F_s} - \alpha + \beta(x) \right) \times \exp \left(- \int_A^x \tan \left(\frac{\tan \varphi_i}{F_s} - \alpha + \beta(\zeta) \right) \cdot \frac{d\beta(\zeta)}{d\zeta} d\zeta \right) \quad (5.85)$$

$$t(x, F_s, \lambda) = \int_A^x (\sin \beta(\xi) - \cos \beta(\xi) \cdot \tan \alpha) \times \exp \left(- \int_A^\xi \tan \left(\frac{\tan \varphi_i}{F_s} - \alpha + \beta(\zeta) \right) \cdot \frac{d\beta(\zeta)}{d\zeta} d\zeta \right) d\xi \quad (5.86)$$

There are different numerical algorithms deal with nonlinearity in constrained optimization problems ^[41-43]. In this study, a concise algorithm for computing the factor of safety using the Morgenstern–Price method developed by Chen et al. ^[18] is adopted. Due to large number of computations involved in RBDA framework. A brief description of the method is presented, considering only the self-weight of the soil and its resistance with constant water content for simplicity. Considering the force equilibrium of the i -th slice, and resolving perpendicular to the slip surface,

$$N_i = (W_i + \lambda f_{i-1} E_{i-1} - \lambda f_i E_i) \cos \alpha + (E_i - E_{i-1}) \sin \alpha \quad (5.87a)$$

resolving parallel to the slip surface,

$$\frac{N_i \tan \varphi_i + c_i b_i \sec \alpha_i}{F_s} = (W_i + \lambda f_{i-1} E_{i-1} - \lambda f_i E_i) \sin \alpha - (E_i - E_{i-1}) \cos \alpha \quad (4.7b)$$

Substituting Eq. 5.8a into Eq. 5.7b

$$\begin{aligned} & E_i [(\sin \alpha - \lambda f_i \cos \alpha) \tan \varphi_i + (\cos \alpha + \lambda f_i \sin \alpha) F_s] \\ & = E_{i-1} [(\sin \alpha - \lambda f_{i-1} \cos \alpha) \tan \varphi_i + (\cos \alpha + \lambda f_{i-1} \sin \alpha) F_s] + F_s \cdot T_i - R_i \end{aligned} \quad (5.88)$$

in which R_i is the sum of all shear resistance forces acting on the slices except the normal interslice forces and T_i is force causing instability.

$$R_i = W_i \cos \alpha \tan \varphi_i + c_i b_i \sec \alpha_i \quad (5.89a)$$

$$T_i = W_i \sin \alpha \quad (5.9b)$$

Using Eq. 5.9a and 5.9b, and for F_s can be obtained by applying boundary conditions at the points A and B, $E_0 = 0$, $E_n = 0$ and rearranging Eq. 5.8 using variable substitution for simplicity, as follows:

$$F_s = \frac{\sum_{i=1}^{n-1} \left(R_i \prod_{j=i}^{n-1} \Psi_j \right) + R_n}{\sum_{i=1}^{n-1} \left(T_i \prod_{j=i}^{n-1} \Psi_j \right) + T_n} \quad (5.90)$$

recasting Eq. 5.8 on can get;

$$E_i \Phi_i = \Psi_{i-1} E_{i-1} \Phi_{i-1} + F_s \cdot T_i - R_i \quad (5.8a)$$

where;

$$\Psi_{i-1} = \frac{(\sin \alpha_i - \lambda f_{i-1} \cos \alpha_i) \tan \varphi_i + (\cos \alpha_i + \lambda f_{i-1} \cdot \sin \alpha_i) F_s}{\Phi_{i-1}} \quad (4.8b)$$

$$\Phi_{i-1} = (\sin \alpha_{i-1} - \lambda f_{i-1} \cos \alpha_{i-1}) \tan \varphi_{i-1} + (\cos \alpha_{i-1} + \lambda f_{i-1} \sin \alpha_{i-1}) F_s \quad (4.8c)$$

$$\Phi_i = (\sin \alpha_i - \lambda f_i \cos \alpha_i) \tan \varphi_i + (\cos \alpha_i + \lambda f_{i-1} \cdot \sin \alpha_i) F_s \quad (4.8d)$$

F_s is defined in an implicit form in Eq.5.10. An expression for λ factor is derived from the moment equilibrium of the i -th slice. Taking moments of all the forces acting on the slice about the centre of the base:

$$E_i \left(z_i - \frac{b_i \tan \alpha_i}{2} \right) = E_{i-1} \left(z_{i-1} - \frac{b_i \tan \alpha_i}{2} \right) - \frac{\lambda \cdot b_i (f_i \cdot E_i + f_{i-1} \cdot E_{i-1})}{2} \quad (5.91)$$

where;

$$M_i = E_i \cdot z_i, \quad M_{i-1} = E_{i-1} \cdot z_{i-1} \quad (5.92)$$

$$M_i = M_{i-1} - \frac{\lambda \cdot b_i (f_i \cdot E_i + f_{i-1} \cdot E_{i-1}) + b_i (E_i + E_{i-1}) \tan \alpha_i}{2} \quad (5.93)$$

Applying boundary conditions at A and B; $M_0 = E_0 \cdot z_0 = 0$ and $M_n = E_n \cdot z_n = 0$, the moment equilibrium equation is used to form an expression for the scaling factor λ :

$$\lambda = \frac{\sum_{i=1}^n b_i(E_i + E_{i-1}) \tan \alpha_i}{\sum_{i=1}^n b_i(f_i \cdot E_i + f_{i-1} \cdot E_{i-1})} \quad (5.94)$$

μ and ν are smoothness modification exponents for the interslice function $f(x)$. The implication of choosing μ and ν as well as the initial values for F_{s0} and λ_0 is only number of iterations need to reach the convergence tolerance values ε_{F_s} and ε_λ . It must be $0 \leq \mu \leq 0.5$ and $0.5 \leq \nu \leq 2$.

From Eq. 5.8 the effective transfer of the thrust force from one slice to another requires that:

$$\Phi_i = (\sin \alpha_i - \lambda f_i \cos \alpha_i) \tan \varphi_i + (\cos \alpha_i + \lambda f_i \cdot \sin \alpha_i) F_s > 0 \quad (5.95)$$

$$F_s > -\frac{\sin \alpha_i - \lambda f_i \cos \alpha_i}{\cos \alpha_i + \lambda f_i \cdot \sin \alpha_i} \tan \varphi_i \quad (5.96)$$

The expression for is λ explicit, but F_s is implicit because the variable F_s appears on both sides. To resolve this, a concise iterative method was developed by Chen et al. ^[18], adopted as follows:

Step	Action
1	Soil mass discretization
2	Calculate R_i and T_i from Eq. 5.9a and 5.9b
3	Characterize interslice function $f(x)$ from eq. 5.15
4	Set initial values of F_s and λ that satisfies eq. 5.17, common initial values are: $F_s = 1, \lambda = 0$
5	Calculate Φ_i and Ψ_{i-1} from Eq. 5.8d and 5.8b for all slices
6	Calculate of F_s from Eq. 5.10

- 7 with the calculated value of F_s and initial value of λ , repeat step 5 and 6 once more for improved values of Φ_i , Ψ_{i-1} and F_s
- 8 Calculate E_i from Eq. 5.8a for all slices
- 9 Calculate λ from Eq. 5.14
- 10 with the updated values of F_s and λ return to step 3 and proceed to step until the difference in values of F_s and λ between two consecutive iterations are within specified limits of tolerance, ε_{F_s} and ε_λ

Table 5.12 Iterative algorithm for calculating F_s and λ

Values for the geotechnical parameters. φ_i , c_i and W_i are calculated random field realizations. Having, Log-normally distributed statistical properties and simulated by orthogonal decomposition of the correlation structure, using the Expansion, Optimal Linear Estimation EOLE method ^[45] for all FE domain points and Cokriging or Gaussian regression ^[46] to interpolate intermedial points needed for the continuum form of F_s and λ required during the iteration described in Table 5.1.

$$\hat{H}(x) = \mu(x) + \sum_{i=1}^q \xi_i \sqrt{\theta_i} \phi_i \quad (5.97)$$

$\hat{H}(x)$ represents a matrix containing an EOLE approximation, of all nodal values in the FE domain corresponding to soil properties that have a Σ_{xx} spatial correlation structure. $\mu(x)$ is the mean value of the random field. ξ_i is a vector of independent normal standard random variables. θ_i , ϕ_i are Eigenvalues and Eigenvectors of Σ_{xx} $\phi_i = \theta_i \phi_i$.

$$\hat{X}_1(s_0) = \sum_{i=1}^n \lambda_i X_1(s_i) + \sum_{i=1}^n \sum_{j=1}^k \alpha_{ij} a_{ij} \quad (5.98)$$

$\hat{X}_1(s_0)$ is a cokriging approximation of the principal soil property at an unsampled point s_0 . λ_i is scalar variable for $X_1(s_i)$ that minimize the mean square predicting error, obtained by using the method of Lagrange multipliers, with unbiased constraints for the principal soil property. α_{ij} and a_{ij} are the coefficients of basis functions obtained from the secondary soil properties.

$$\hat{H}_i(x) = \sum_{j=1}^{N_{\text{var}}} \frac{\chi_{i,j}^D}{\sqrt{\lambda_j^u}} [\Phi_j^u]^T \Sigma_{H(x)u} \quad (5.99)$$

The cross-correlation structure for the geotechnical parameters ϕ_i , c_i and W_i is given by statistical preconditioning with the method proposed by Shinosuka ^[47] for simulation of multivariate random fields. Eq 4.19 uses the notation proposed by Vořechovský ^[48] for consistency with the use EOLE method. $\hat{H}_i(x)$ is a matrix containing an EOLE approximation, of all nodal values in the FE domain corresponding to the soil i -th property that have a $\Sigma_{H(x)u}$ cross-correlation structure. $\chi_{i,j}^D$ is matrix containing preconditioned random variables. λ_j^u and Φ_j^u are characteristic values of $\Sigma_{H(x)u}$

5.2.3 Finite Element Modelling

The commercial software ABAQUS is employed to carry out the FE model ^[49]. Force-displacement relationships are modeled as PSI elements in ABAQUS to represent spring like behavior of the axial and vertical soil resistance forces on the pipeline elements. The soil-pipe relationship are elastic-perfectly plastic for the axial component of the soil f . The vertical soil reaction, is model as multilinear elastic to account for the bearing capacity of the soil Q_u beneath the pipe for downward soil displacements.

In the upward direction, the force displacement is multilinear to account for the static download force q_s , the fully mobilized soil resistance q_d and the breakthrough condition, once the displacement is equal to the buried depth of the pipeline. A simple nonlinear spring force–relative displacement relationship is defined in ABAQUS to model the soil force-displacement relations as shown in Fig. 4.1 and Fig. 4.2. The FE model represents a 30° natural slope 180m long. It transitions to a flat terrain with two symmetrical bends. The bends have a radius of 80m, transitioning tangent to the slope and the flat terrain. The length of the pipeline at the crown and toe sections is 60m Fig. 4.5. The model incorporates one spring at each far end of pipeline to allow for the feed-in to the buckling. This was done to model the axial stiffness of the pipeline restrained by the soil at the far end condition. Consider P as the total axial force due to internal pressure and temperature. At some point, far away from the hill imperfection, there is an axial force P_0 that is fully constrained by the soil friction per unit length f given a displacement x :

$$P = P_0 - f \cdot x \quad (5.100)$$

the axial stain in the pipe is

$$\varepsilon_x = \frac{P_0 - P}{EA} = \frac{f \cdot x}{EA} \quad (5.101)$$

A force-displacement is given by Eq. 1.17, at the end of the feed-in, as function of P as the total axial force due to internal pressure and temperature, E steel young modulus, A cross-section area of the pipe and the soil friction per unit length f ;

$$\Delta_0 = \int_{L_s}^0 \varepsilon_x dx = \int_{L_s}^0 \frac{f \cdot x}{EA} dx$$

where Δ_0 is the axial displacement at the end of the feed-in, and L_s is between the end of the model and where the virtual anchor occurs and P_M is the axial force at the FE model.

$$\Delta_0 = \frac{f \cdot L_s^2}{2EA}$$

$$L_s = \frac{P_0 - P_M}{f}$$

$$\Delta_0 = \frac{(P_0 - P_M)^2}{2EA \cdot f} = \frac{\Delta P^2}{2EA \cdot f} \quad (5.102)$$

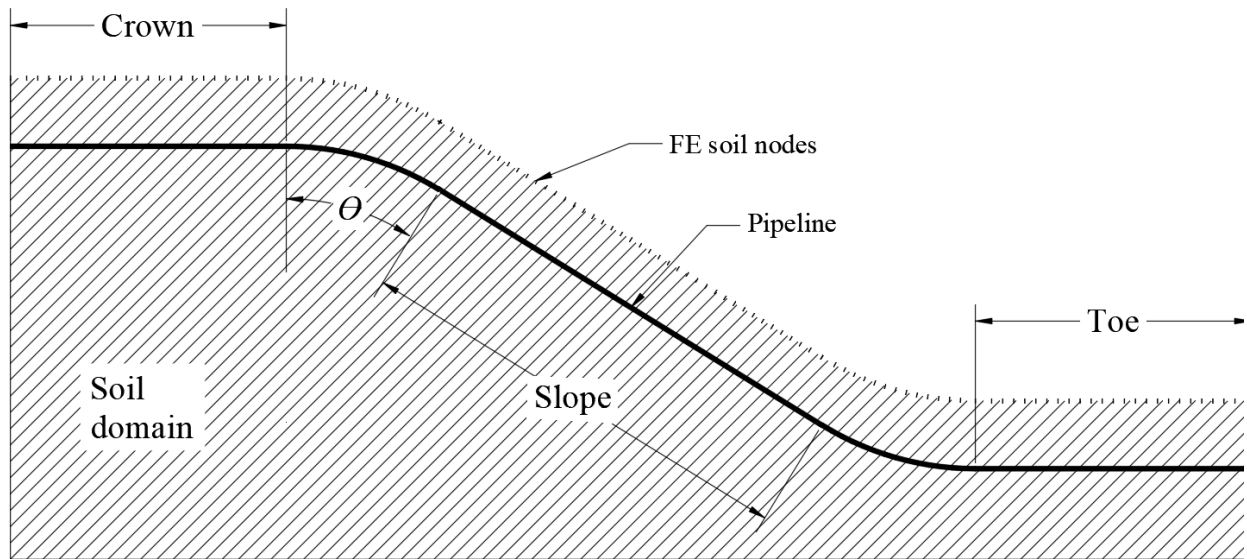


Figure 5.33 FE model; $\theta = 30^\circ$, bending radius is 80m, Slope is 180m long, Toe and Crown are 60m long.

5.2.3.1 Creation of interpolated nodal points

A uniform domain discretization of 0.25m square is perform to identify the critical slip surface by means of The Morgenstern–Price method ^[33]. The iterative processes required to resolve the

optimization problem yields successive approximations to the coordinates of the critical slip surface. These coordinates can have values outside the discrete points, previously characterized in the random field realization. Therefore, new values are obtained from gaussian interpolation. Once the iteration has converged, only the field values along the pipeline are needed to characterize the FE model. Additionally, a master node coordinates are taken from as the center of mass of each soil slice from the last step in the Morgenstern–Price method. Then, the geometry of the FE model is fully defined. The FE model is defined by the points along the pipeline. The points of the soil profile and the coordinates of the master nodes. PSI elements are connected from the pipe nodes to the soil profile, representing the force-displacement reaction of the soil on the pipes. Based on the scale of fluctuation, a cost-effective multi-resolution discretization of the random field could be made; first, from the deterministic FE results the less relevant regions in the domain can be also treated as determinist (i.e., the strains deformations in the pipeline 40m away from the sliding soil are less than 10 micro strains for the maximum imposed displacement in this analysis). Yet the constant resolution was adopted to ensure the statistical properties of field are homogenous to estimate the critical slip surface with the Morgenstern–Price method.

The soil profile nodes are fixed, except for the nodes inside the region corresponding to soil moving mass. The soil prolife nodes inside the moving soil mass are bound to the corresponding master node in each slice defined as last step in the Morgenstern–Price method.

Incremental, linear displacements s and rotations r are imposed to the master nodes. The linear increment is constant among all the soil slices. The rotation, is corresponding to linear displacement $r = \tan^{-1} \left(\frac{s}{0.5 h} \right)$, h being the height of each soil slice. A cumulative density function

(CDF) is latter constructed from the result of a series of FE analysis increasing the magnitude of the imposed displacements.

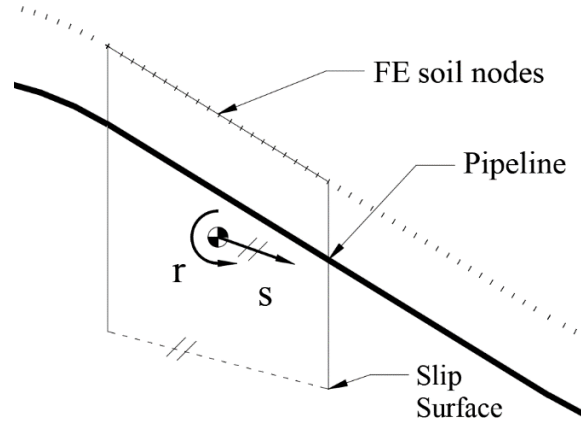


Figure 5.34 Master node, pipeline and soil profile. Direction of imposed displacements.

5.2.3.2 Pipeline properties

Pipe elements are model as Timoshenko beams. The pipeline was discretized by displacement-based beam elements in ABAQUS with a pipe cross-section. The selection of conventional displacement elements was made because of the large number of beam elements needed to model the soil reaction as distributed loads along the pipeline. A common steel grade is studied, X65, to model the effects of the yield strength. The Ramberg-Osgood stress-strain relationship, Eq. 4.41, is assumed to model the elastic and plastic responses. The yield strength is assumed to equal the specified minimum yield strength (SMYS) of the steel grade, 359 MPa. The hardening was characterized by modifying the plastic curve of the X65 steel. As show on Table 5.2.

$$\varepsilon = \frac{\sigma}{E} + \frac{\alpha \sigma_y}{E} \left(\frac{\sigma}{\sigma_y} \right)^n \quad (5.103)$$

Ramberg-Osgood stress-strain relationship; ε is strain, σ is stress, E is the steel elastic modulus, σ_y is the yield strength, α and n are Ramberg-Osgood parameters to characterize hardening behavior.

Grade	Hardening	σ_y	σ_{el}	E	Ramberg-Osgood parameters	
		(MPa)	(MPa)	(MPa)	α	n
X65	Good	448	380.8	205,000	1.29	22.5

Table 5.13 Material Data and Ramberg-Osgood Parameters. σ_{el} is the elastic limit.

5.2.3.3 Induced forces

The impact of the internal pressure is model as an equivalent section force using PIPE21 providing uniform radial expansion of the cross-section caused by internal pressure in ABAQUS. The temperature differential is introduced as a body force in the beam elements. The steel plasticity model is model from the Ramberg-Osgood relationship, detailed on Table 5.6. The external loads on the pipeline are applied in three step load cases: In Step 1, the self-weight of pipe; In Step 2, the internal pressure is applied as a distributed load along the pipeline. The corresponding equilibrium load at the far end, is applied as the same rate, as a fully constrain condition (axial loading applied at both ends of the pipeline); In Step 3, the thermal expansion is applied incrementally as a body force on the pipe elements. A constraining thermal axial load is applied at the far ends, at the same rate as the thermal expansion. The increments are 0.5°C up to the final load, corresponding to a differential of 80 °C. The induced axial forces are given by:

$$Q = Q_T + Q_P \quad (5.104)$$

$$Q_T = E \alpha_T (T_2 - T_1) \pi (D - t) t \quad (5.105)$$

$$Q_P = \left(1 - \frac{2\nu(D - t)}{(D - 2t)} \right) \frac{\pi(D - 2t)^2}{4} P \quad (5.106)$$

where; Q_T temperature force, Q_P pressure induced force, E Young's modulus, α_T thermal expansion coefficient for steel ($11.7 \times 10^{-6} \text{ }^\circ\text{C}$), T_2 operating temperature, T_1 tie-in temperature, D pipe outside diameter, t wall thickness, ν Poisson's ratio and P operating pressure.

After the loading cases are applied the induced displacement are applied at increment of s 50mm, with an initial displacement of 150mm. Each displacement increment is performed in 1000 random realizations (i.e., 1000 FE models with particular soil properties that account, for the spatial variability and cross-correlation of the soil parameters ϕ , c and γ . Considering its characteristic slip surface) To develop a CDF based on the tensile rupture, or compressive wrinkling anywhere along the pipeline as function of the expected displacement increment. This procedure can be extended easily is there is information about the expected soil displaces as function of time.

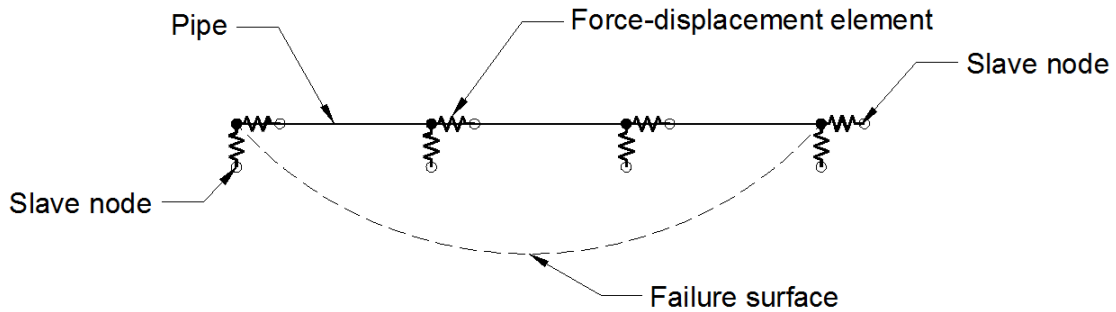


Figure 5.35 Idealization of FE model with soil-pipe, force displacement relationships

5.2.4 Assessment of probability of failure

Two limit state functions were established involving the tensile/compressive strain capacities of the pipeline with the tensile/compressive strain demand imposed by the unstable slope. The tensile and compressive strain capacities of the pipeline are evaluated based on the information in the literature (references), and the maximum tensile and compressive strains in the pipeline induced by the unstable slope are employed to formulate the limit state functions:

$$g_1 = \varepsilon_t - \varepsilon_{t \max} \quad (5.107)$$

$$g_2 = \varepsilon_w - |\varepsilon_{c \max}| \quad (5.108)$$

where ε_w is the compressive strain capacity (as defined in DNV-OS-F101 ^[33]); ε_t is the tensile strain capacity, which is assumed to be the tensile strain capacity for simplicity; $\varepsilon_{t \max}$ and $\varepsilon_{c \max}$ are the maximum tensile and compressive strains induced by the moving soil.

$$\varepsilon_w = 0.78 \left(\frac{t_2}{D} - 0.01 \right) \left(1 + 5 \frac{\sigma_h}{f_y} \right) \alpha_h^{-1.5} \alpha_{gw} \quad (5.109)$$

where; t_2 corroded wall thickness (taken as the nominal wall thickness), D nominal outside diameter, σ_h hoop stress, f_y yield strength (reduced by a factor of 0.96), α_h maximum allowed yield to tensile ratio (assumed to be 0.90), α_{gw} girth weld factor (taken as 0.60 for $D/t = 60$)

Girth welds are considered as a weak part of the pipeline since girth weld cracking is one of the main causes of gas pipeline of accidents. Considerable research efforts have been focused on crack assessment using strain-based crack-tip opening displacement (CTOD), J-integral and simplified or reference engineering solutions ^[34,35] to estimate the total axial strain which could lead to girth

weld fracture. The tensile strain capacity ε_t depends on the residual stresses from, laying and construction, crack or imperfection geometry, girth weld and pipe material properties. For simplicity and applicability to older pipelines, which may have been constructed with less rigorous quality control procedures, a tensile strain limit of 0.5% is considered as a broad limit in this study.

5.3 Numerical example

An idealized steel pipeline of 19 in. diameter for transport natural gas of is buried 2 m in a natural slope 180 m long Fig. 4.5. The slope inclination is $\theta = 30^\circ$. The transition from the slope to the flat terrain is made with two identical cold formed bends of 80m radius. Toe and Crown are 60m long in the horizontal direction. The material grade is X65 with Good hardening properties as show in Table 5.4. The soil mobilization displacement is 20mm, the soil statistical properties are detailed in Table 5.2.

In this case, the possibility that the soil mass is moving along the pipeline in a deep-seated slip is studied. The length along the pipe axis of this mass is between 30 and 120 meters, measured along the inclined slope. Whereas the critical slip failure surface varies for each random field realization. The case study shows that the soil movements in a slope can be quite complex. To derive analytical solutions from soil–pipeline interaction, however, one can assume some idealized ground movement patterns in the slopes. In this case, a linear displacement parallel to the slip surface and the corresponding angular rotations are applied to each soil slide. The width of the slices used in the generalized method of slices is 3m.

In the FE analysis, the pipeline is model with PIPE21, each being 0.25m in length. The force-displacement interaction is model with PSI elements, from the pipe to the soil profile. R2D2 rigid link elements were used to impose the soil displacements from at the master nodes.

The soil force-displacement presented in Table 5.2. where evaluated for each random field realization. A total of 1000 realizations were performed of each displacement increment. To construct a CDF dependent on the expected average displacement.

Tensile strain capacity of the pipe is assumed to have a Lognormal distribution with a mean value of 5% and CoV of 0.12. Th compressive strain capacity is Lognormal with a mean value given by eq 4.47 with a CoV of 0.3.

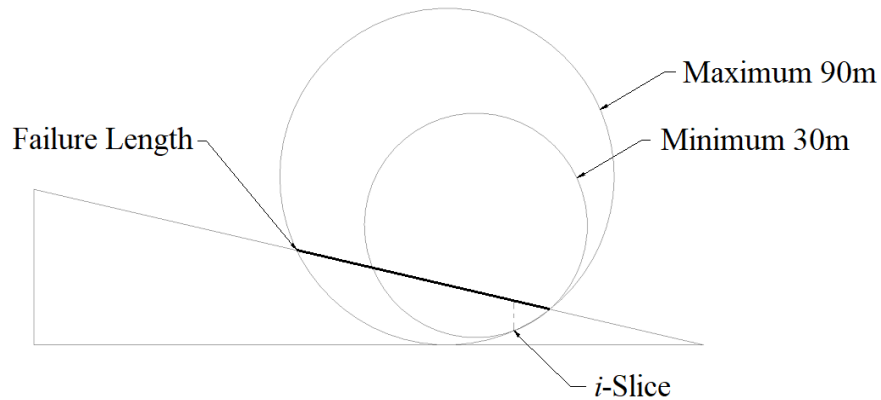


Figure 5.36 Failure surface bounds from geotechnical survey $30 \leq \text{Failure length} \leq 90$

For an imposed deformation of 400 mm the maximum strain in compression in the pipe line the FE deterministic value was 485 microstrains and in tension was 578 microstrains.

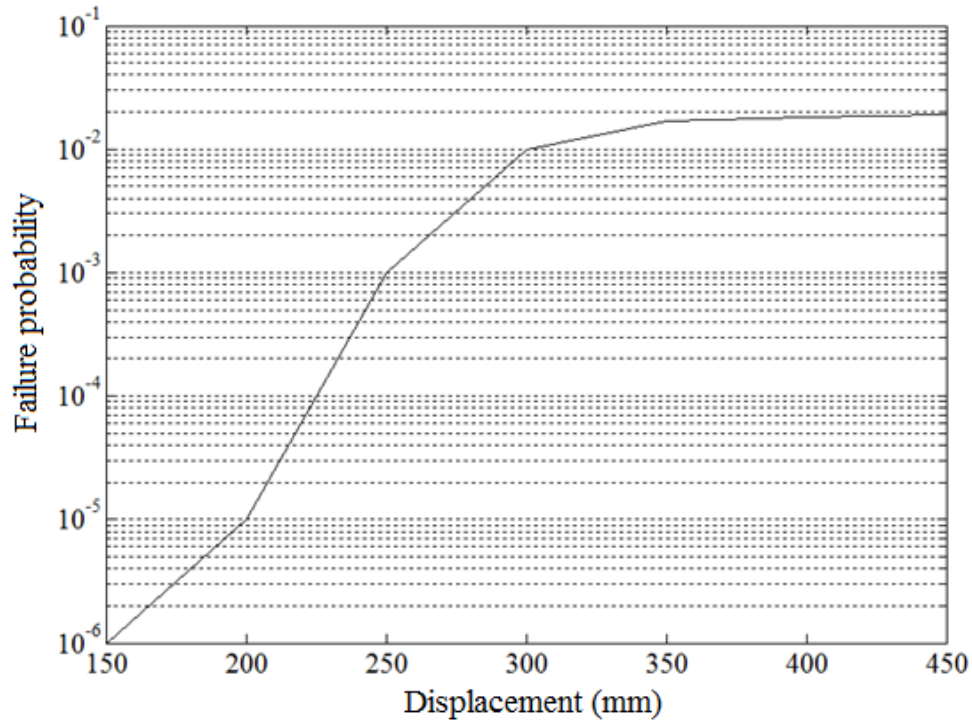


Figure 5.37 Failure probability for an increasing soil displacement

5.4 Conclusion

A strain-based procedure for evaluating the failure probability of pressurised pipelines subjected to longitudinal ground movement imposed by unstable slopes is presented. Two failure modes are considered, namely tensile rupture and compressive local buckling. The strain demand is calculated using analytical and FE models, which accounts for the elastic–plastic behaviour of the pipe under internal pressure and temperature as well as the behaviour of the pipe–soil force-displacement in the vertical and axial directions. The compressive strain capacity is evaluated using a model DNV-OS-F101 2007, whereas a representative deterministic tensile a conservative strain limit capacity is assumed.

The spatial variability of the soil is taken into account in a simplified manner. The soil pipe properties are assumed to have a Gaussian correlation structure and a simple cross-correlation by an exponential function. A difference between competing probabilities of tensile and compressive failures is given for a particular pipeline as a practical numeric example.

A procedure to consider the soil variability impact on the failure probability of pressurized pipelines subjected to a 2D soil movement was presented. From the deterministic FE model, a considerable difference between theoretical formulation and the numerical solution was found. That could be due the fact that in the theoretical formulations the geometry of the pipe at the toe of the slope is not considered. Furthermore, it seems that some uplift soil resistance was assumed equal to the bearing capacity of the soil in the theoretical study case without any consideration about the embedment ratio. Yet the FE based reliability analysis remain conservative because the pipe wall may withstand significant deformation after the yielding point in tension or compression before rupture.

Strain concentration induced by the deformation of the pipe due to the initial geometry and extend of the failure surface are taken into consideration in the FE analysis. For a given pipeline, the failure probabilities conditional on a given ground movement magnitude (i.e. sliding magnitude) can be evaluated. The failure probabilities can be alternatively expressed as a function of time, if the probabilistic characterization of the average ground movement per unit time is known. The methodology can be incorporated in a reliability- or risk-based pipeline integrity management program to facilitate the maintenance decision-making regarding pipelines buried in unstable slopes. The analysis results suggest that the FE based approach have some practical advantages

over the theoretical based solutions (the possibility to account for more realistic geometry). It seems that in similar cases the spatial variability of the soil ultimate resistance tends to decrease the failure probability, because the tensile and the compressive strains at the stable-moving soil interface is governed by the relatively weaker soil on either side of the interface.

The proposed procedure to estimate the pipe failure probability for a given imposed displacement can be easily extended to a variety of problems involving additional external forces to the slope stability problem (e.g., seismic and water pressure) by adding to the lateral force equilibrium equations to identify the critical surface for the pipe-soil interaction reliability analysis due to landslides.

5.5 References

1. Picarelli, L., and Russo, C., 2004. "Remarks on the mechanics of slow active landslides and the interaction with man-made works, Landslides—Evaluation and stabilization, Proceedings of the 9th International Symposium on Landslides: London, A.A. Balkema Publishers, v. 2, p. 1,141–1,176.
2. El-Ramly, Morgenstern, & Cruden. 2002. "Probabilistic slope stability analysis for practice". Canadian Geotechnical Journal, 39(3), 665-683.
3. Vanmarcke. "Random Fields: Analysis and Synthesis". Cambridge: Mass. and London Massachusetts Institute of Technology Press; 1983

4. Mostyn, G. R., & Soo, S. 1992. "The effect of autocorrelation on the probability of failure of slopes". In 6th Australia, New Zealand conference on geomechanics: geotechnical risk (pp. 542-546).
5. CSA, Oil and Gas Pipeline System CSA Standard Z662:19, 2019. "Canadian Standard Association", Mississauga, Ontario, Canada.
6. Wijewickreme, D., et al., 2005. "Seismic vulnerability assessment and retrofit of a major natural gas pipeline system: a case history". *Earthquake Spectra*, 21 (2), 539–567.
7. Nobahar, A., et al., 2007. "Analysis and design of buried pipelines for ice gouging hazard: a probabilistic approach. *Journal of Offshore Mechanics and Arctic Engineering*", 129, 219–228.
8. Yoosef-Ghods, N., Murray, D., and Zhou, J., 2008. "A simplified model for evaluating strain demand in a pipeline subjected to longitudinal ground movement". In: *Proceedings of the 7th international pipeline conference IPC2008*, Calgary.
9. Zhou W. 2010. "Reliability of pressurised pipelines subjected to longitudinal ground movement". *Structure and Infrastructure Engineering* Vol. 8, No. 12, December 2012, 1123–1135.

10. Cocchetti, G., di Prisco, C., and Galli, A. 2009. "Soil–pipeline interaction along unstable slopes: a coupled three-dimensional approach". Part 1: Theoretical formulation. *Canadian Geotechnical Journal*, 46(11): 1289–1304.
11. American Lifelines Alliance, 2001. "Guidelines for the Design of Buried Steel Pipe".
12. Chen, Z. Y., and Morgenstern, N. R. 1983. "Extension to the generalized method of slices for stability analysis." *Can. Geotech. J.*, 20, 104–119.
13. Zhu, D. Y., Lee, C. F., Qian, Q. H., & Chen, G. R. 2005. "A concise algorithm for computing the factor of safety using the Morgenstern Price method". *Canadian geotechnical journal*, 42(1), 272-278.
14. Karimian, S. A. 2006. "Response of buried steel pipelines subjected to longitudinal and transverse ground movement" (T). University of British Columbia.
15. Jiao, G., Sotberg, T. and Igland, R.T. 1995. "SUPERB 2M statistical data-basic uncertainty measures for reliability analysis of offshore pipelines". SUPERB JIP Report No. STF70-F95212, Norwegian Marine Technology Research Institute, Trondheim, Norway.
16. Zimmerman, T.J.E., Cosham, A., Hopkins, P., and Sanderson, N. 1998. "Can Limit States Design be Used to Design a Pipeline Above 80% SMYS?" (OMAE98-902). In *Proceedings*

of the 17th International Conference on Offshore Mechanics and Arctic Engineering. Lisbon, Portugal.

17. ASCE Task Committee on Thrust Restraint Design of Buried Pipelines. 2014. “Research Needs and Recommendations for Testing Thrust Restraint of Buried Pipelines”. In Pipelines 2014: From Underground to the Forefront of Innovation and Sustainability (pp. 1805-1815).
18. Pipeline Research Council International (PRCI) (2017). “Guidelines for constructing natural gas and liquid hydrocarbon pipelines through areas prone to landslide and subsidence hazards.” Pipeline Research Council International.
19. Wijewickreme, D., et al., 2005. “Seismic vulnerability assessment and retrofit of a major natural gas pipeline system: a case history”. Earthquake Spectra, 21 (2), 539–567.
20. El Hmadi K. and O'Rourke M. Soil 1988. “Springs for Buried Pipeline Axial Motion Journal of Geotechnical Engineering”, Vol. 114, No. 11. ASCE
21. White D. J., Cheuk C. Y. and Bolton M. D. (2008). The uplift resistance of pipes and plate anchors buried in sand. Géotechnique 58, No. 10, 771–779.
22. Kulhawy, F. H., & Mayne, P. W. 1990. “Manual on estimating soil properties for foundation design” (No. EPRI-EL-6800). Electric Power Research Inst., Palo Alto, CA (USA); Cornell Univ., Ithaca, NY (USA). Geotechnical Engineering Group.

23. Liao, S. S., & Whitman, R. V. 1986. "Overburden correction factors for SPT in sand". *Journal of geotechnical engineering*, 112(3), 373-377.
24. Bolton M.D. 1986. "The strength and dilatancy of sands". *Géotechnique* 36, No. 1, 65-78
25. Phoon, K.K., and Kulhawy, F.H. (1999). "Evaluation of geotechnical property variability". *Canadian Geotechnical Journal*, 36: 625–639.
26. Cheuk C. Y., White D. J., and Bolton M. D. 2008 "Uplift Mechanisms of Pipes Buried in Sand". *Journal of Geotechnical and Geo-environmental Engineering*, Vol. 134, No. 2. ASCE.
27. Rowe, R. K., & Davis, E. H. (1982). The behavior of anchor plates in sand. *Geotechnique*, 32(1), 25-41.
28. Vanden Berghe, J. F., Cathie, D., & Ballard, J. C. 2005. "Pipeline uplift mechanisms using finite element analysis". In *Proceedings of the 16th International Conference on Soil Mechanics and Geotechnical Engineering* (pp. 1801-1804). IOS Press.
29. Meyerhof, G. G., and Adams J.I. (1986). The Ultimate Uplift Capacity of Foundations. *Canadian Geotechnical Journal*, Vol. 5, No. 4, pp. 225-244.

30. White, D. J., Barefoot, A. J., & Bolton, M. 2001. "Centrifuge modelling of upheaval buckling in sand". *International Journal of Physical Modelling in Geotechnics*, 1(2), 19-28.
31. Ghahremani, M., & Brennan, A. J. 2009. "Consolidation of lumpy clay backfill over buried pipelines". In *International Conference on Offshore Mechanics and Arctic Engineering* (Vol. 43475, pp. 313-320).
32. DNV-RP-F110 2007. "Global Buckling of Submarine Pipelines Structural Design due to high-temperature/High-pressure".
33. DNV-OS-F101 2007. "Submarine pipeline systems".
34. Zhao, Xu, Jing, Han, Zhao, Cao, Lv, and Song, 2019. "A Modification of Reference Strain Approach for Thin-Walled Submarine Pipelines under LargeScale Plastic Strain and Internal Pressure," *Thin-Walled Structures*, 140, pp. 182-194.
35. Nourpanah, N. and Taheri, F., 2010. "Development of a Reference Strain Approach for Assessment of Fracture Response of Reeled Pipelines," *Engineering Fracture Mechanics*, 77(12), pp. 2337-2353.
36. Rackwitz, R. 2000. Reviewing probabilistic soils modelling. *Computers and Geotechnics*, 26(3-4), 199-223.

37. Morgenstern, N.R., and Price, V.E. 1965. "The analysis of the stability of general slip surfaces. *Géotechnique*", 15(1): 79–93.
38. Janbu, N. 1954. "Application of composite slip surfaces for stability analysis". In *Proceedings of the European Conference on Stability of Earth Slopes*, Stockholm. Vol. 3, pp. 43–49.
39. Lowe, J., and Karafiath, L. 1960. "Stability of earth dams upon drawdown". In *Proceedings of the 1st Pan-America Conference on Soil Mechanics and Foundation Engineering*, Mexico City. Vol. 2, pp. 537–552.
40. Spencer, E. 1967. "A method of analysis of the stability of embankments assuming parallel interslice forces". *Géotechnique*, 17(1): 11–26.
41. Schittkowski, K. 1980. "Nonlinear programming codes: Information, tests, performance." *Lecture notes in economics and mathematical systems*, Vol. 183, Springer, New York.
42. Chen, Z. Y., and Shao, C. 1988. "Evaluation of minimum factor of safety in slope stability analysis." *Can. Geotech. J.*, 25, 735–748.
43. Boggs, P., & Tolle, J. 1995. "Sequential Quadratic Programming". *Acta Numerica*, 4, 1-51.

44. Zhu, D. Y., Lee, C. F., Qian, Q. H., & Chen, G. R. 2005. "A concise algorithm for computing the factor of safety using the Morgenstern Price method". Canadian geotechnical journal, 42(1), 272-278.
45. Li, C. C., & Der Kiureghian, A. 1993. "Optimal discretization of random fields". Journal of engineering mechanics, 119(6), 1136-1154.
46. Krige, Danie G. 1951. "A statistical approach to some basic mine valuation problems on the Witwatersrand". J. of the Chem., Metal. and Mining Soc. of South Africa. 52 (6): 119–139.
47. Yamazaki F, Shinozuka M. 1990 "Simulation of stochastic fields by statistical preconditioning". J Eng Mech;116(2):268–87.
48. Vořechovský, M. 2008. "Simulation of simply cross correlated random fields by series expansion methods. Structural safety", 30(4), 337-363.
49. McKenna, F., Fenves, G., Filippou, F., Mazzoni, S., Scott, M., Elgamal, A., & McKenzie, P. 2010. "OpenSees". University of California, Berkeley.

6 Summary and Conclusions

Upheaval Buckling considering soil spatial variability

The effects of the spatial variability of the soil friction angle on the UHB for onshore pipelines laydown over hill-type imperfections, have been investigated. The soil is characterized from common stochastic characteristics of natural deposits presented by Phoon ^[38]. The soil properties include the correlation length and exponential correlation structure. The expansion optimal linear estimation (EOLE) method proposed by Li and Der Kiureghian ^[28] is adopted to model the random field. For comparison, the friction angle is also assumed to be represented by a single random variable (i.e., a random field with an infinitely long correlation length), and a random field with independent, identically distributed (iid) random variables at every node (i.e., a random field with a zero-correlation length).

Steel pipes are model following the Ramberg-Osgood stress-strain relationship as Timoshenko beams in FE analysis. For simplicity, the residual stresses at the cold-formed bends are ignored. Equivalent force-displacement relationships are used to model the pipe-soil interaction according to Oil and Gas Pipeline System (CSA-2019) ^[14]. The acting forces; self-weight, internal pressure, and temperature are model as deterministic quantities.

Selected analysis cases were performed to investigate the effects of the correlation length, influence of the correlation function and the inherent variability of common geotechnical properties ^[38]. The variability of the critical UHB load is measured by means of numerical

simulation. The scope of the parametric analysis includes 252 parametric cases. The studied parameters are: pipe diameter, steel grade, imperfection size, operating internal pressure and soil. A result matrix was formed to fit an empirical equation to estimate the critical UHB load. Weak soil and strong granular soil conditions are considered. The variability of the friction angle has more relevance for pipelines with strong downward soil load, dominated by the static component. The dynamic component is less sensitive to the variability of the soil friction angle.

The spatial variability of the friction angle is significant for pipelines over narrow hill-type imperfections and less significant for smooth imperfection. This is applicable for all the imperfection types consider in the parametric analysis.

The correlation structure type has a marginal impact in the study cases. The type of correlation studied were bounded by the most rapid decrement as Triangular type and the slowest as a Bessel Second kind. This encompasses a wide range of possible correlation structures. Given the magnitude of the studied correlation length. The influence of the decrement in correlation as function of distance between random field FE points is relevant for soil correlation length similar or smaller than the imperfection size. The correlation length has some relevance if it less in magnitude in comparison with the total length of the hill type imperfection. It has marginal effects otherwise.

The most dominant deterministic parameters in the UHB problem were identified in order of relevance: the imperfection shape, the soil download force, the soil axial force and the pipeline mechanical properties. The dominant stochastic parameters of the friction angle, governing the

UHB variability are; variability of the soil, correlation and correlation structure. The inherent soil variability being the dominant source of uncertainty.

Ignoring the effects of the soil spatial of the soil friction angle may lead to overly conservative conclusions in the assessment of UHB for onshore pipelines by up to one order of magnitude in comparison to single random variable stochastic models.

Empirical equation for critical UHB force

The resulting empirical expression for the critical upheaval buckling force has a maximum absolute error less than 5% with respect to the deterministic FE parametric analysis. This represents a 50% increase accuracy with respect to similar equations^[2]. The proposed empirical equations yield conservative values to assess the variability of the critical buckling for all applicable cases. A pair of conservative variance reduction factors for the critical UHB empirical equation is proposed to account for the effects of the soil spatial variability in the upheaval buckling problem.

Cross-correlated random field

A robust approach to discretize multivariable random fields with valid cross-correlated structures is presented. This method is useful to characterize soil variables with probability distributions that are different from the normal or lognormal distribution. With correlation structures based on modified Bessel second kind decrement. This approach is based on the Matérn class of variogram to deal with empirical or measured correlation structures. The discretization of the random field is

achieved by linear coregionalization following loglikelihood approximations of the Bessel function parameters. A simply correlated random field model was used to investigate the effects of the spatial cross-correlation properties the soil, as a tri-variate $\mathbf{c}, \boldsymbol{\varphi}, \boldsymbol{\gamma}$ random field, on the UHB phenomena for onshore pipelines. The effects were established by variance comparison, between the response of single random field soil-pipe FE models. And the corresponding FE model, considering the cross- correlation a tri-variate soil.

The effect of simply cross-correlation structure, between soil properties, seems to have marginal effects for studied cases. The Gaussian simple cross-correlation structure of the field, seems to be of marginal relevance, for the cases studied. Assuming the soil properties have lognormal PDF, and normal correlation, and correlation structure. The studied cases are representative of a wide range of granular soil parameters close to dry condition. Although it is clear that other types of soil may be have different cross-correlated structure. The spatial variability of the soil is taken into account in a simplified manner. The soil pipe properties are assumed to have a Gaussian correlation structure and a simple cross-correlation by an exponential function. The difference between competing probabilities of tensile and compressive failures is given for a particular pipeline as a practical numeric example.

Pipelines along Unstable Slopes

A procedure to consider the soil variability impact on the failure probability of pressurized pipelines subjected to a two-dimensional soil movement is presented. From the deterministic FE model, a considerable difference between theoretical formulation and the numerical solution was

found. That could be due the fact that in the theoretical formulations the geometry of the pipe at the toe of the slope is not considered. Furthermore, it seems that some uplift soil resistance was assumed equal to the bearing capacity of the soil in the theoretical study case without any consideration about the embedment ratio. Yet the FE based reliability analysis remains conservative because the pipe wall may withstand significant deformation after the yielding point in tension or compression before rupture.

Strain concentration induced by the deformation of the pipe due to the initial geometry and extend of the failure surface are taken into consideration in the FE analysis. For a given pipeline, the failure probabilities conditional on a given ground movement magnitude (i.e. sliding magnitude) can be evaluated. The failure probabilities can be alternatively expressed as a function of time, if the probabilistic characterization of the average ground movement per unit time is known. The methodology can be incorporated in a reliability- or risk-based pipeline integrity management program to facilitate the maintenance decision-making regarding pipelines buried in unstable slopes. The analysis results suggest that the FE based approach have some practical advantages over the theoretical based solutions (the possibility to account for more realistic geometry). It seems that the spatial variability of the soil ultimate resistance tends to decrease the failure probability, because the tensile and the compressive strains at the stable-moving soil interface is governed by the relatively weaker soil on either side of the interface. The proposed procedure to estimate the pipe failure probability for a given imposed displacement can be easily extended to a variety of problems involvement additional external forces to the slope stability problem (e.g., seismic and water pressure) by adding to the lateral force equilibrium equations to identify the critical surface for the pipe-soil interaction reliability analysis due to landslides.

Recommendations for future research

The analyses performed clearly show that ignoring the spatial variability leads to overly conservative estimation in the variability of the predicted structural response. In the present, only the effects of friction angle, cohesion and density were explored. In reality, there are additional parameters that deserve attention. Further improvements can be categorized in three main areas: uncertainty models, geotechnical considerations, and structural models.

From the perspective of the mechanical stability of the pipelines, one can follow the same approach of developing empirical equations for particular steel pipelines by considering the residual stresses inherent to the manufacturing and construction processes. Also, it is not clear how much the stiffness of the pipeline is degraded in old corroded pipelines. Another interesting mechanism is the progression of UHB, as the vertical deformation may be a progression of cumulative minor events that involve remolding of the soil. In reality, the embedment or buried depth is also uncertain due to natural erosion, freeze and thaw cycles and the progressive displacement of the soil.

Geotechnical models to represent the soil as springs are characterized from natural soil properties. The same soil properties can be used to characterize a solid model of the soil to account for compatibility for deformations in the soil. The measurement of the soil natural variability effects on the variability of the pipeline response by using different geotechnical models can be investigated further in the future.

The uncertainty models presented are applied to simple and idealized soil parameters in the present work. It is not clear if the Gaussian random field discretization techniques are adequate for all soil types. Future work can be carried out to collect information about representative PDF, correlation structure and cross-correlation of the soil properties, which will be very useful to identify an adequate random field model.

Curriculum Vitae

Name: José Luis Espinosa Méndez

Post-secondary Education and Degrees: Autonomous University of Chiapas
Tuxtla Gutiérrez, Chiapas, México
2003-2007 B.S.

National Autonomous University of México
México DF., México
2009-2012 M.S.

The University of Western Ontario
London, Ontario, Canada
2013-2021 Ph.D.

Honours and Awards: The National Council of Science and Technology of the United Mexican States (CONACYT). PhD Scholarship 2009 to 2012

The Ontario Council on Graduate Studies of Canada (OCGS)
PhD Scholarship 2013 to 2021

The National Council of Science and Technology of the United Mexican States (CONACYT). PhD Scholarship 2013 to 2019

Related Work Experience: Research Assistance
II-UNAM Engineering Institute
Department of Applied Mechanics
2010- 2013

Teaching Assistant
The University of Western Ontario
2014-2019

Publications: Roberto Gómez Martínez, J. Alberto Escobar, Adrián Pozos and José Espinosa. 2012 “Control of the structural response of a tall slender monument with tuned mass dampers under wind forces”. XII National congress of structural engineering. Verona, Italy.